STRUCTURAL INVESTIGATIONS ON EXPERIMENTALLY AND NATURALLY PRODUCED SLICKENSIDES

A Thesis presented to the Faculty
of the State University of New York
at Albany
in partial fulfillment of the requirements
for the degree of
Master of Science

College of Sciences and Mathematics
Department of Geological Sciences

Thomas Michael Will

1987

Acknowledgements

This thesis was undertaken under guidance and supervision of Prof. Winthrop D. Means, SUNY at Albany. I am greatly indebted to him for his constant support, advice, and patience during the course of this work. I sincerely thank Prof. Christopher J. L. Wilson, Melbourne, Australia for many discussions on the subject and his help during the last stages of this work. I also want to say "thank you" to Prof. Herbert Vossmerbäumer, Würzburg, FRG under whose guidance I encountered geology, and who encouraged me to continue my studies in the United States.

A very special thanks to Diane Paton who helped me with all administrative and bureaucratic problems, and who got finally accustomed to my espresso. Andy Landor helped with technical advice.

This thesis would not have been completed without the moral support of my friends: Peter Hofmann, Matthias Ohr, Mark and Linda Jessell, Kay Stone, Antonio Teixell, and Mauricio Roma. Thanks to Christine for everything.

Financial support for this thesis was received through a fellowship from the "Studienstiftung des Deutschen Volkes".

Last but not least, I want to express my deepest gratefulness to my parents, for the many ways of help and support, and for their love.

STRUCTURAL INVESTIGATIONS ON EXPERIMENTALLY AND NATURALLY PRODUCED SLICKENSIDES

Abstract of
a Thesis presented to the Faculty
of the State University of New York
at Albany
in partial fulfillment of the requirements
for the degree of
Master of Science

College of Sciences and Mathematics
Department of Geological Sciences

Thomas Michael Will

1987

Abstract

This work has involved an experimental approach and a study of naturally produced slickensides.

The experiments, carried out on a pyrophyllitic rock, have been performed in order to define some extrinsic parameters that control surface and microstructural features. Normal stress, speed (i.e. strain rate), and amount of slip and total displacement were related to measureable surface features, such as length, and spacing between the developing ridges and grooves. Special attention was paid to a newly recognized type of slickenside lineation (Means, 1986). This lineation produced experimentally cannot be explained in terms of the traditional asperity ploughing or dissolution/precipitation models. It has the following distinctive features: (1) ridges and grooves are present, and occupy about the same amount of area of both hangingwall and footwall blocks, (2) ridges and grooves show a shallow U-shaped profile with planar bottom and top segments, (3) hangingwall and footwall blocks show complementary morphologies and fit perfectly into each other, (4) ridge and groove length can exceed the length of the slip displacement. A model is proposed to explain these features.

It could be demonstrated that slickensides are penetrative features. In both, the deformed samples and the

naturally produced slickensides, a strain-modified sub-surface zone of variable thickness is present. The microstructural features observed indicate a wide span of deformation processes ranging from brittle (intergranular cracks, open and refilled tension gashes, faulting) to ductile behaviour (undulose extinction, recrystallization).

A new slickenside definition is proposed.

Table Of Contents

List Of Tables

List Of Figures

1. Introduction

Slickensides are common features on fault planes and fold (flexural-slip folding) surfaces. It should be clear that the term slickenside refers only to planar structures and not to the linear features on slickensides. Following Fleuty (1975), the latter structures are named slickenlines.

In the classical view, slickensides are defined as "polished and striated surfaces that result from friction along a fault plane" (Billings, 1954, p.149). An almost identical definition is given by Gary et al. (1977, p.665). They define a slickenside as a "polished and smoothly striated surface that results from friction along the fault plane". The same definition can be found in a recent textbook on structural geology (Suppe, 1985, p.263). This repeated stressing that friction is the only process involved in the formation of slickensides is probably the reason that most geologists use the terms slickenside and slickenline only for features produced by abrasive scratching during frictional sliding.

During the work on this thesis it became clear that this view is oversimplified and mechanisms other than frictional polishing can be involved in the formation of slickensides. Thus, following Elliot (1976) I am using these terms in a more non-genetic way and consider slip-parallel features like the frequently occuring crystalline fibers and slickolites as

slickenlines in a broad sense.

Slickensides have been reported in various environments and geologic settings. They form on slip surfaces in hard rocks and are described in soft sediments and soils (Petit and Laville, 1986; Yaalon and Kalmar, 1978; respectively); they have been described from deep-sea drilling cores (e.g., Moore, 1980 and references therein); and are from glacially smoothed and commonly striated surfaces well known structures to glacial geomorphologists. Contrary to the general assumption that slickensides are a purely frictional phenomenon, Burg and Ponce de Leon (1985) mentioned slickenside striations on C-planes within a ductile shear zone in the Corcoesta granite pluton in northwest Spain. They did not discuss whether these slickensides had formed coevally with or post-dated the C-planes. However, if these slickenlines developed contemporaneously with the shear zone, then this described occurence indicates that slickensides and slickenlines can form under more ductile conditions than generally believed.

The general understanding of slickensides and slickenlines is still very poor. For this reason, slickenlines are commonly only used to infer the direction of the last incremental slip movement, and in connection with the fault surfaces for determining the orientation of the principal stresses (Angelier, 1979; Etchecopar et al., 1981; Rispoli and Vasseur, 1983).

The formerly used "smoothness-principle" (Willis and Willis, 1934, p.491) to infer the sense of displacement was unquestioned until 1958. However, the reliability of this criterion was questioned after experimental work (Paterson, 1958; Riecker, 1965; Norris and Barron, 1969; Gay, 1970; Lindström, 1974; Hobbs et al., 1976, p.305) and work on natural slickensides (Tjia, 1964, 1967, 1972; Petit et al., 1983, 1986). These authors showed that steps facing the movement of the opposite block occur. According to the terminology introduced by Norris and Barron (1969), steps are called incongruous when their risers (i.e. their steep sides) oppose the movement of the opposite block, and congruous when the steps face into the movement direction of the opposite wall.

Slickensides and slickenlines might reveal information on slip magnitudes (total as well as incremental), slip rates, the mode of sliding, stress magnitudes, depth, etc. However, those relationships have not yet been investigated.

In the course of this thesis, experimental and petrographic work was undertaken with some basic questions in mind. The primary goal was to improve the description and classification of surface and microstructural features of slickensides. Experiments were carried out in order to learn how some extrinsic parameters control surface and microstructural features of slickensides. For example, how do slickensides and slickenlines develop with time and

displacement? Does their morphological character vary with changes in some of the extrinsic parameters, such as the amount of displacement, the sliding mode, normal stress, shear strain, shear strain rate, etc.? Is it possible to use slickensides and/or slickenlines as indicators of seismic (stick-slip sliding) versus aseismic (stable sliding) slip on a fault plane? If this were feasible slickensides and slickenlines might ultimately provide a powerful tool for the prediction of earthquakes. Is it possible to correlate petrographic and microstructural observations with morphological features seen in hand samples? Is it possible to classify slickensides according to a dominant deformation mechanism?

In general, the ultimate goal of the ongoing slickenside research at Albany is to improve our basic understanding of the significance of slickensides and of the processes associated with their geological origin.

Before giving some considerations to the questions raised above, the most commonly found fault plane markings are described in the following chapter.

2. Description of features on slickensides and current ideas about their origin

Surface features or markings on slickensided surfaces, called "tectoglyphs" by Dzulynski and Kotlarczyk (1965), can be described in a genetic or a purely descriptive way.

By means of descriptive terms three categories: linear, curvilinear, and planar features on slip surfaces could be distinguished. Linear features include scratches, elongated bodies of material, crystalline fibers, and slickolites. Chatter marks, crescentic fractures, and similar features fall into the second category. Polished and mineral coated surfaces are classed as planar features.

In this chapter, different fault plane markings are listed and discussed in terms of genetic ideas employed by previous workers.

2.1. Scratch lineation and friction cracks

Elongated depressions in a fault plane are called scratches, striations, furrows, and grooves (fig. 1a). The order of these terms is sometimes used to indicate that a striation is more prominent than a scratch, while a furrow is more prominent than a striation etc. For instance, Willis and Willis (1934, p.438) describe a scratch as "a mere scratch, lacking significance", whereas a groove is "a broad depres-

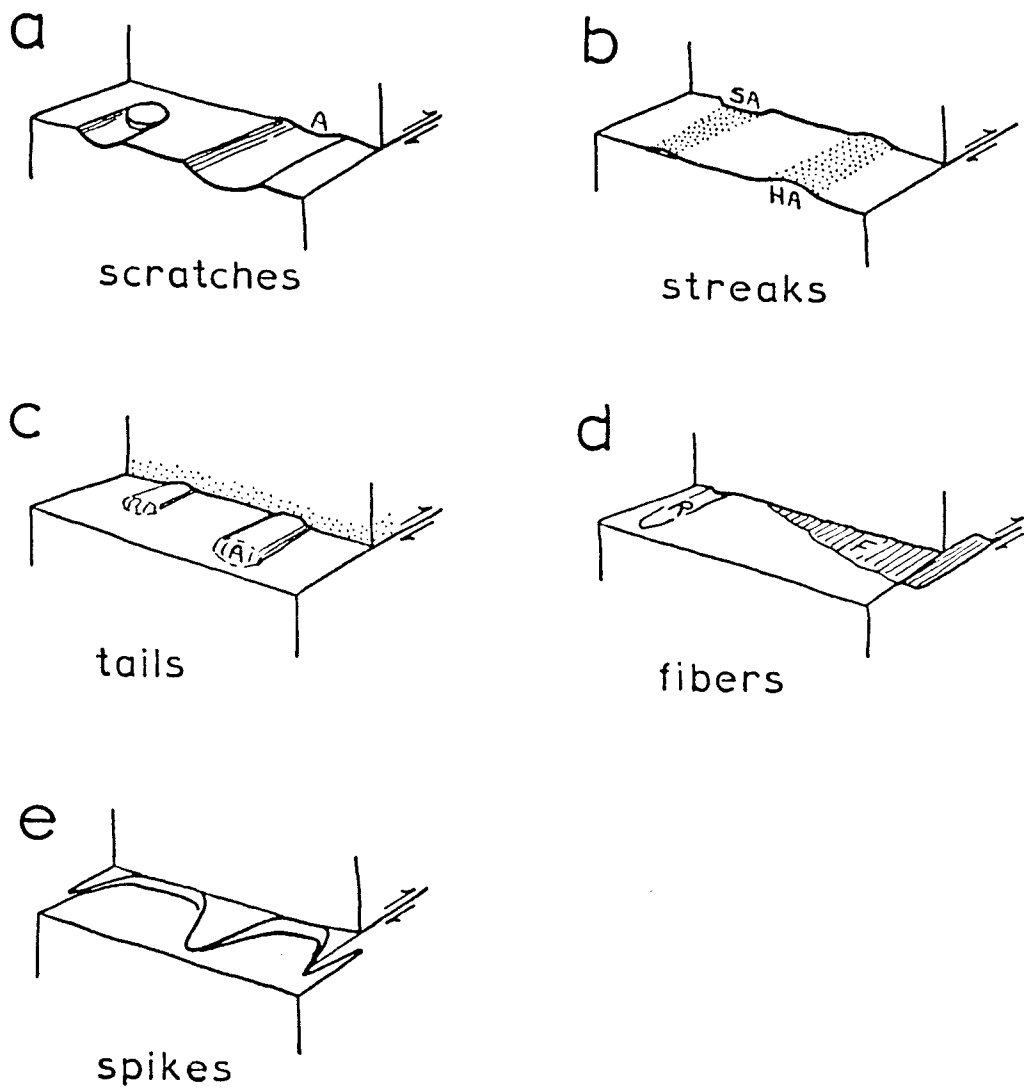

Figure 1. Different types of slickenside lineations (from Means, 1987, figure 1). A - asperity, SA - Soft asperity, HA - Hard asperity, R - Rods, F - Fibers.

sion, ..., generally rounded on the bottom and often without definite margins". All of these features lie parallel to the slip direction, therefore indicating the slip direction. They are believed to be formed by frictional sliding (c.f., definitions cited above), when an asperity, which can be any kind of protuberance (e.g. a mineral edge), moves relative to a surface and scores it. This process may embrace brittle and/or plastic deformation mechanisms (Engelder, 1978). If the ploughing tool is still preserved at one end of a groove it points into the movement direction of the surface not containing the groove (Tjia, 1964). These grooves were called slickenside prod marks by Dzulynski and Kotlarczyk (1965).

During frictional sliding experiments (e.g., Engelder, 1974, 1978; and references therein) microscopic grooves, called "wear grooves" (Engelder, 1974), are frequently observed. Engelder (1974) described carrot-shaped wear grooves whose tip ends point into the displacement direction of the surface containing the grooves. In his experiments the wear grooves were only produced during seismic stick-slip sliding. The length of the wear grooves was always less or equal to the length of one slip increment regardless of the total slip displacement of the experiment. Combining the experimental observations he concluded "...slip surfaces with wear grooves considerably shorter than total slip are seismic". On the other hand, Coulson (1970) finds wear grooves only during stable sliding, while LaFountain et al. (1975)

describe them as being produced during both stick-slip and stable sliding experiments. In any case, the term "wear groove" has genetic implications, indicating seismic slip (Engelder, 1974) or aseismic slip (Coulson, 1970), and should not be applied unless the origin of the grooves is clear.

Curvilinear fault plane markings include features such as pluck marks, chatter marks, crescentic fractures, and lunate fractures (c.f. figures 1 and 3 in Harris, 1943). All of these features are called friction cracks by Harris (1943). They lie, like fracture steps, at a high angle to the displacement vector on the slickensided surface and are a result of friction during faulting. More detailed description and discussion of these markings can be found in Preston (1921), Willis and Willis (1934, pp.489-492), Harris (1943), MacClintock (1953), Tjia (1968, 1972), and in some textbooks on glacial geomorphology (e.g., Embleton and King, 1975, pp.187-191; and references therein).

2.2. Streak lineation

Elongated bodies of very fine grained, comminuted gouge material on a slip plane are called debris streaks in this thesis. Debris streaks form when a weak asperity slides over a harder surface, thus wearing down and leaving behind a track of piled-up material parallel to the slip direction (fig. 1b). This mechanism, called debris streaking by

Means (1987), can be considered to be counterpart to an asperity ploughing mechanism.

Debris streaks can also be formed by another process. A particle or rock fragment that is locked up at the sliding interface forces debris material to be piled-up on its up-slip end. Elongated, slip-parallel ridges of debris or gouge material, called spurs (Willis and Willis, 1934, p. 488), are the result. This process is similiar to the mechanism sometimes invoked for the formation of drumlins. According to Tjia (1968) spurs are "ridges gently rising in the direction into which the opposite wall moved". Spurs are shorter than trails (Tjia, 1967).

2.3. Erosional sheltering lineation

This term was employed by Means (1987) to account for elongated ridges of host rock material on a slip surface (fig. 1c). These features, called tails by Means (1987) or trails by Willis and Willis (1934, pp. 488-489), were already recognized by Chamberlin (1888) on glacially striated surfaces as described in Willis and Willis (1934, p.489). Tjia (1968) defines them as "ridges which are protected by a protuberance at the end facing into the direction from where the adjoining wall originated". Trails can be formed when a hard particle is attached to one of the sliding surfaces. This hard particle protects the material on its down-slip

side from erosion, while the material not on the down-slip side will become eroded and removed. The final appearance of this surface typically shows elongated ridges of the host rock material with a hard particle at the up-slip end. The terms down-slip and up-slip side refer to the movement direction of the block not containing the trails, and are analogous to the terms downstream and upstream in reference to rivers.

2.4. Crystalline fiber lineation

Many fault surfaces contain elongated crystalline fibers as indicated in figure 1d. The fibrous material is commonly quartz or calcite, but chlorite, epidote, and occasionally potassic feldspar can also occur. According to Durney and Ramsay (1973), these lineations form by growth of fibrous crystals out of a fluid phase. The fibers grow parallel to the local displacement direction into dilating voids. This leads to a strong crystal-shape preferred orientation parallel to the displacement vector. Such fibrous steps are called accretion steps by Norris and Barron (1969).

The processs responsible for crystalline fiber growth is described as "pressure solution slip" by Elliot (1976). It implies dissolution of asperities (or infiltration by fluids of exotic origin) on the slip plane followed by a diffusive mass transfer of the dissolved material onto accretion steps

during shearing. Sibson (1986) suggests that the presence of crystalline fibers is diagnostic of aseismic pressure solution slip, i.e. very low slip rates, and that this mechanism commonly operates under conditions of very low effective confining pressure.

2.5. Slickolite lineation

Slickolites are similar to stylolites, however in slickolites the individual columns and spikes point in a direction subparallel rather than subnormal to the slip plane (fig. 1e) as they do in stylolites.

First described by Bretz (1940) slickolites are "essentially slickensides, but not abrasional in origin. They are made by differential solution along minor fault planes in calcareous rocks and repeatedly are accompanied by other evidence of displacement" (Bretz, 1950). Their origin seems to be opposite to that of crystalline fibers. Slickolites are produced by local dissolution, whereas crystalline fibers are formed by local precipitation. For this reason, slickolite formation is accompanied by a volume decrease, and crystalline fiber growth by a volume increase of the rock system under consideration.

Both crystalline fibers and slickolites can occur together on the same fault surface provided that this surface is undulating (see Mattauer, 1973, p.349).

2.6. Ridge-in-groove type lineation

Slickenside lineations of this type were first described in shales and mudstones and from experimentally sheared paraffin wax (Means, 1986).

This newly recognized type of slickenside lineation has some very distinctive features as shown in figure 2. (1) ridges and grooves are slip-parallel and both occupy about the same amount of area on both the hanging and footwall blocks. (2) Ridges and grooves commonly show a shallow U-shaped profile with planar bottom and top segments. These segments are connected by slip-parallel, planar surfaces dipping between 5^{o} and 20^{o} with respect to the average fault surface. (3) Hanging and footwall blocks show complementary morphologies. This means that hanging and footwall blocks fit perfectly into each other, i.e. a ridge on the hangingwall block fits perfectly into a groove on the footwall block, and vice versa. This characteristic feature was called "nesting" by Means (1986, 1987). (4) The length of individual ridges or grooves can exceed the length of the slip displacement. In this work, these characteristics will be explained more fully. The origin and deformation mechanism(s) involved in the formation of this peculiar type of slickenside lineation are not yet understood. It seems to be clear, however, that none of the mechanisms described and discussed above can be

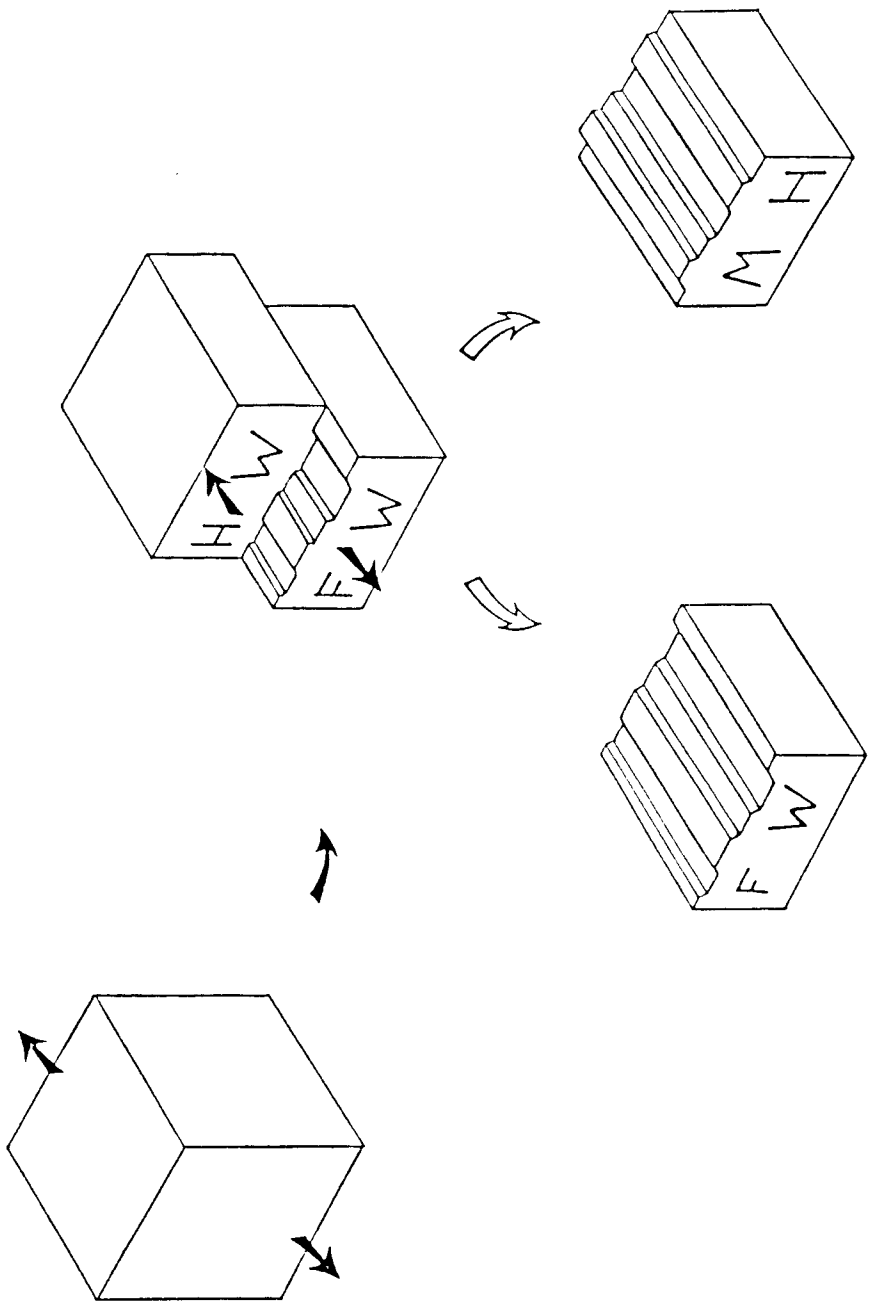

Figure 2. Slickenside lineation of the ridge-in-groove type. Nesting occurs between the footwall and hangingwall blocks.

used to explain this type of lineation and its features.

Asperity ploughing is an unlikely mechanism since there is no way to explain why the hanging and footwall sides should match after the frictional sliding process has ceased. Another argument against a frictionally dominated asperity ploughing mechanism is the common lack of abraded wear or gouge material on the ridge-in-groove type bearing slickenside. When an asperity becomes worn down during the frictional sliding process fault gouge or debris material is expected to be produced through this abrasive sliding process. In order to provide asperities either a rough pre-sliding fracture or joint surface must have been present, or cracks must propagate in front of the shearing material. In either case, a rough surface containing asperities will be created, and consequently gouge material can be produced during the future sliding process. This might imply that the ridge-in-groove striation indicates shearing without fracturing or cracking as a precursory process, and therefore that sliding took place in an initially undisturbed rock. This view is supported by evidence from the wax-shearing experiments of Means (1986, 1987) and shearing of pyrophyllitic clay (this study).

Dissolutional and/or precipitational processes are ruled out by the fluid-absent wax-shearing experiments of Means (1987). Furthermore, the common lack of crystalline fibers or slickolites in experimentally deformed materials and

naturally produced slickensides of this type seems to support the assumption that dissolutional and precipitational processes are not responsible for this type of slickenside lineation.

Different kinds of surface features described here can occur together on the same slickenside. This might indicate that different mechanisms are active at different or the same time. With the exception that crystalline fibers and slickolites can form coevally on the same fault plane (Mattauer, 1973, p.349) there is no further evidence to confirm the latter idea.

3. Experimental work

From field observations the structure and configuration of a rock body can be observed and described. Direct observation of motion within this body cannot be made nor can the processes by which this motion and structure was achieved be observed. In order to understand the dynamic and kinematic history of a deformed rock body experiments are helpful. During an experiment we are able to measure the incremental changes in the structure of a body and relate these changes to the known motion. Thus, experiments may provide us with insight into the deformation history, and the processes responsible for the structural features we observe in naturally deformed materials. Nowadays, probably nobody will question the importance of experimental work. Experimentally obtained results and experimentally based models provide field workers with answers to many questions.

Faulting, and especially the origin and development of slickensides and slickenlines on slip surfaces, have not received much experimental attention in the past. For this reason, very little is known about the origin and development of structures on and below slickensided surfaces in rocks. The basic idea behind the experimental work was to learn from experiments whether some measureable experimental parameters, such as length of displacement, strain rate, normal stress, etc., control surface and microstructural features of

slickensides.

At some future date, further experiments of this kind might enable field geologists to use slickensided surfaces as dynamic and kinematic indicators on naturally occuring fault and fold surfaces.

All experiments were carried out using a pyrophyllitic rock or pyrophyllitic clay.

Pyrophyllite belongs to the clay mineral group. It is a very soft mineral with a Mohs hardness of 1-2 (Hurlbut and Klein, 1977, p.404). Like micas, pyrophyllite has a layered structure in which a sheet of octahedrally coordinated Al-ions is sandwiched between two sheets of linked SiO_4-tetrahedra (Deer et. al., 1976, p.225). Figure 3 shows a photomicrograph taken from a thin section of this undeformed material. The photomicrograph reveals a random orientation of the individual minerals in this rock. Pyrophyllite was quarried at Guilford and Orange Counties, North Carolina (Hurlbut and Klein, 1977, p.404).

The material I used was purchased from the American Lava Company under the trade name "Lava Grade A" and probably comes from one of these localities.

Pyrophyllite is not a material that occurs very frequently in nature; however, it was used because it is inexpensive and could be easily deformed with the available equipment. I am only aware of one paper published that deals with deformational experiments using pyrophyllite: Means and

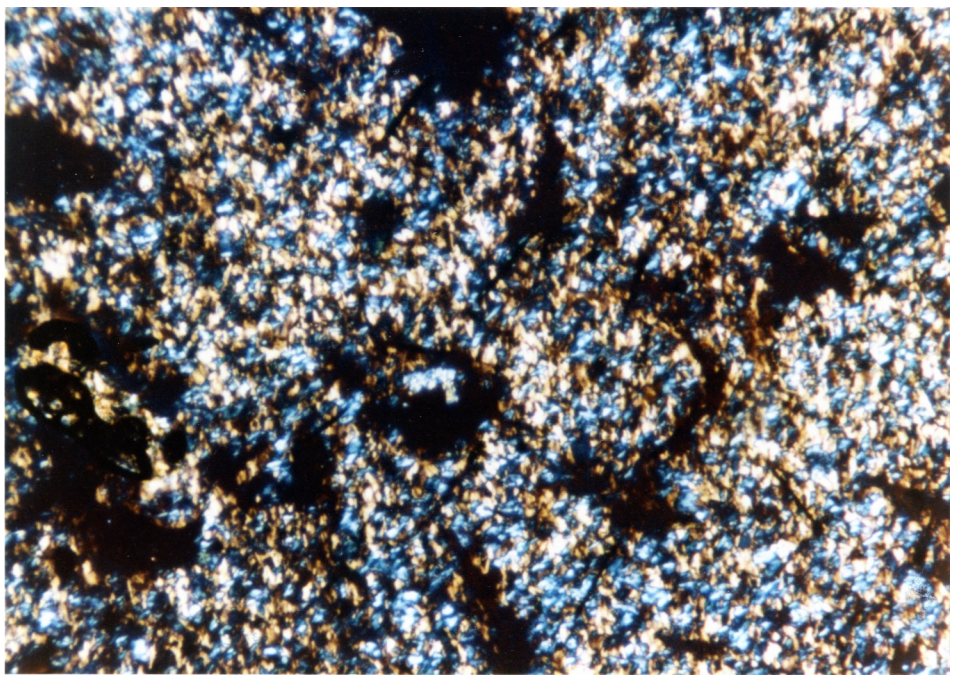

Figure 3. Photomicrograph of undeformed pyrophyllite. No preferred orientation of the pyrophyllite grains is visible. Field of view is 0.85 mm wide, crossed polarizers, gypsum plate.

Rogers (1964). Experimental results on mineral or rock analogs are, of course, limited in their direct application to naturally occuring deformation products and structures. However, it is often still possible to gain insight into the dominant deformation mechanisms active during an experiment, and to apply this knowledge to naturally occuring rocks and their structures.

3.1. Deformation apparatus, types of experiments, and sample preparation

Three different types of experiments were made: triaxial compression, twist, and shear experiments. All of these experiments were carried out at room temperature.

3.1.1. Hydraulic press

All experiments were performed using a Carver Laboratory Press, Model C. This hydraulic press is driven by an electric motor which is connected to a speed reducer. Two different motors, a "slow speed" and a "fast speed" motor, were used. The speed reducer box is supplied with different gears which make it possible to run experiments under different strain rates. Table I shows the different transmission settings and the corresponding velocities in inches per hour and meters per second for both the fast and slow speed motors. These are

Table I. Transmission settings on fast- and slow-speed motor and the corresponding velocities in inches per hour and meters per second.

Transmission setting	velocity [inch/hr]	velocity [m/sec]
Fast-speed motor		
5	8.76	6.18×10^{-5}
10	4.38	3.09×10^{-5}
25	1.75	1.24×10^{-5}
50	0.876	6.18×10^{-6}
100	0.438	3.09×10^{-6}
Slow-speed motor		
1	0.665	4.70×10^{-6}
2.5	0.266	1.88×10^{-6}
5	0.106	7.52×10^{-7}

the velocities with which the upper platen moves downwards with respect to the lower platen.

The press is equipped with two gauges. The upper dial is connected to the upper platen and measures the displacement between the moving upper and the stationary lower platen. The second gauge measures the force applied vertically on the sample and the confining pressure medium.

3.1.2. Twist experiments

Twist experiments were carried out in order to study the effects of normal stress on developing features on the artificially produced slip planes.

Three-quarter inch cylinders of solid pyrophyllite were drilled out of a larger block of pyrophyllite and subsequently sliced into approximately 5-8 mm thick disks by using a low-speed saw. In order to obtain a high degree of contact area, the surfaces of the disks were smoothly polished using 600 and 1000 grits. With 5-minute epoxy as an adhesive, a disk was glued on both the upper and lower pistons. Marker lines were drawn onto the edges of the two disks (fig. 4). A bronze cylinder was pushed over the shaft of one piston and sample. The second piston and sample were carefully put on top of the first sample, and finally the bronze cylinder was gently pushed over both samples (fig. 4).

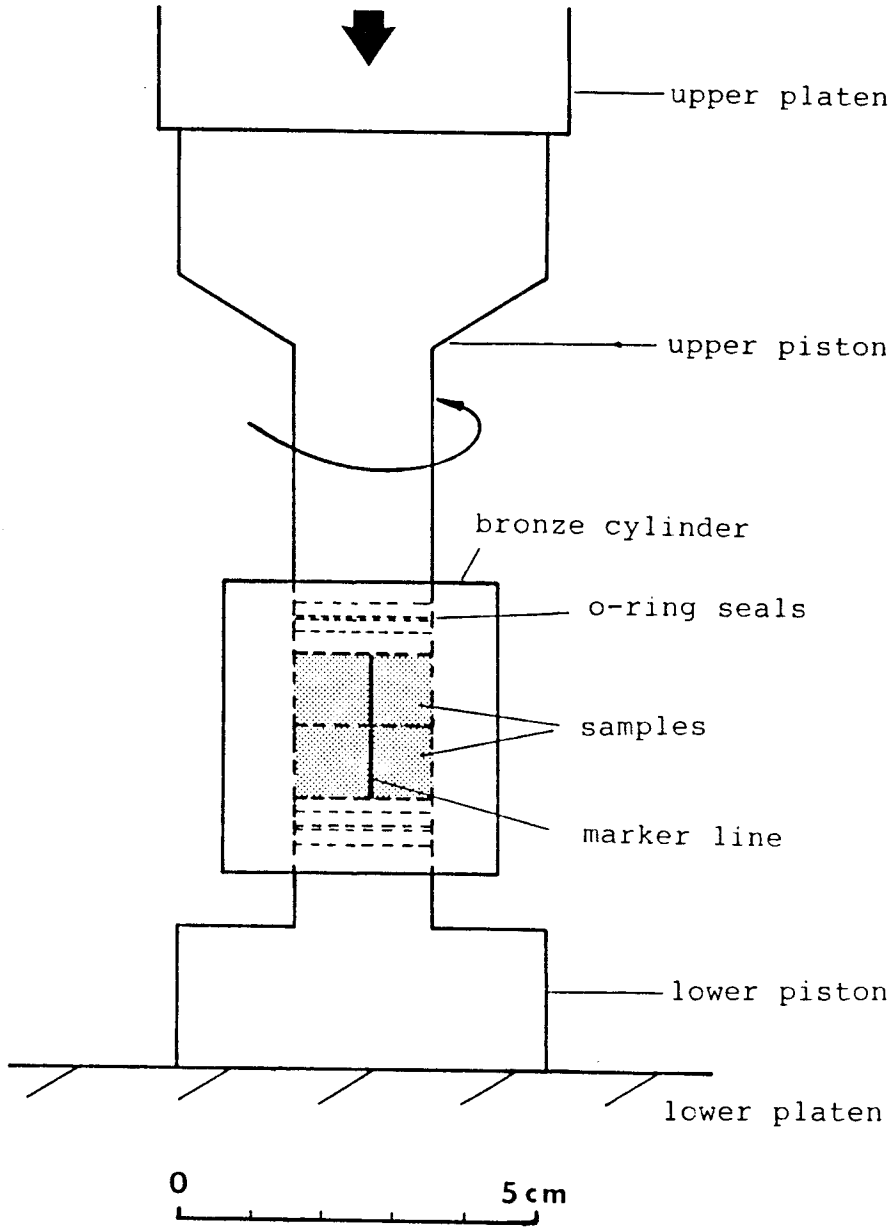

Figure 4. Experimental set-up for the twist experiments.

Using this technique, no material could be lost during an experiment. Figure 4 shows a sketch of this experimental set-up assembled on the press. The upper piston was rotated by hand with respect to the lower piston using a pipe-wrench.

After rotation, the samples were carefully unloaded, the assembly was dismounted from the press, the cylinder carefully removed, and the displacement determined by measuring the distance between the offset marker lines.

Even though this type of experiment is simple, some problems arose. The bonding between the pistons and the pyrophyllite disks was sometimes not strong enough to accommodate the torque applied by the pipe-wrench. As a result, shearing occurred at the steel-pyrophyllite interface, commonly within the adhesive material, and not at the pyrophyllite-pyrophyllite interface. Since the rotation was carried out by hand two additional problems arose: (i) maintaining constant angular velocity, and (ii) producing constant stable sliding conditions during an experiment. In order to overcome these two difficulties we tried to build a mechanically driven rotation device, but the right-angle drive used was too weak to transmit the torque from the speed reducer to the lower piston and to overcome the friction between the two pyrophyllite blocks.

3.1.3. Double-shear experiments

All of the experiments with the double-shear jig (fig. 5) were carried out at room temperature conditions.

Compared to standard shear-box experiments this jig (fig. 5) has the advantage that it is small in size and does not need much material, and two samples can be deformed at the same time. The two rectangular sample holes have the following dimensions: 2cm x 1cm x 1.27cm. The two holes are loaded with the experimental material and two steel or glass plates are tightly clamped on the front and back sides of the deformation apparatus. This ensures that no material will leak out during a run. The loaded jig was put onto the lower platen of the press. When the upper platen of the press moved down, the plunger of the jig was pushed down at a constant rate.

Experiments on the solid pyrophyllitic rock were not very sucessful for the following reasons. In the first attempts to produce slickensided surfaces in this set-up, I used single solid blocks of pyrophyllite in each hole. Under the given experimental conditions no shear planes developed but the material fractured.

Other attempts were made by using two smaller blocks (each one 2cm x 0.5cm x 1.27cm in size) in each sample hole. The problem with this set-up was that I was not able to obtain samples of a sufficiently precise shape. Openings and

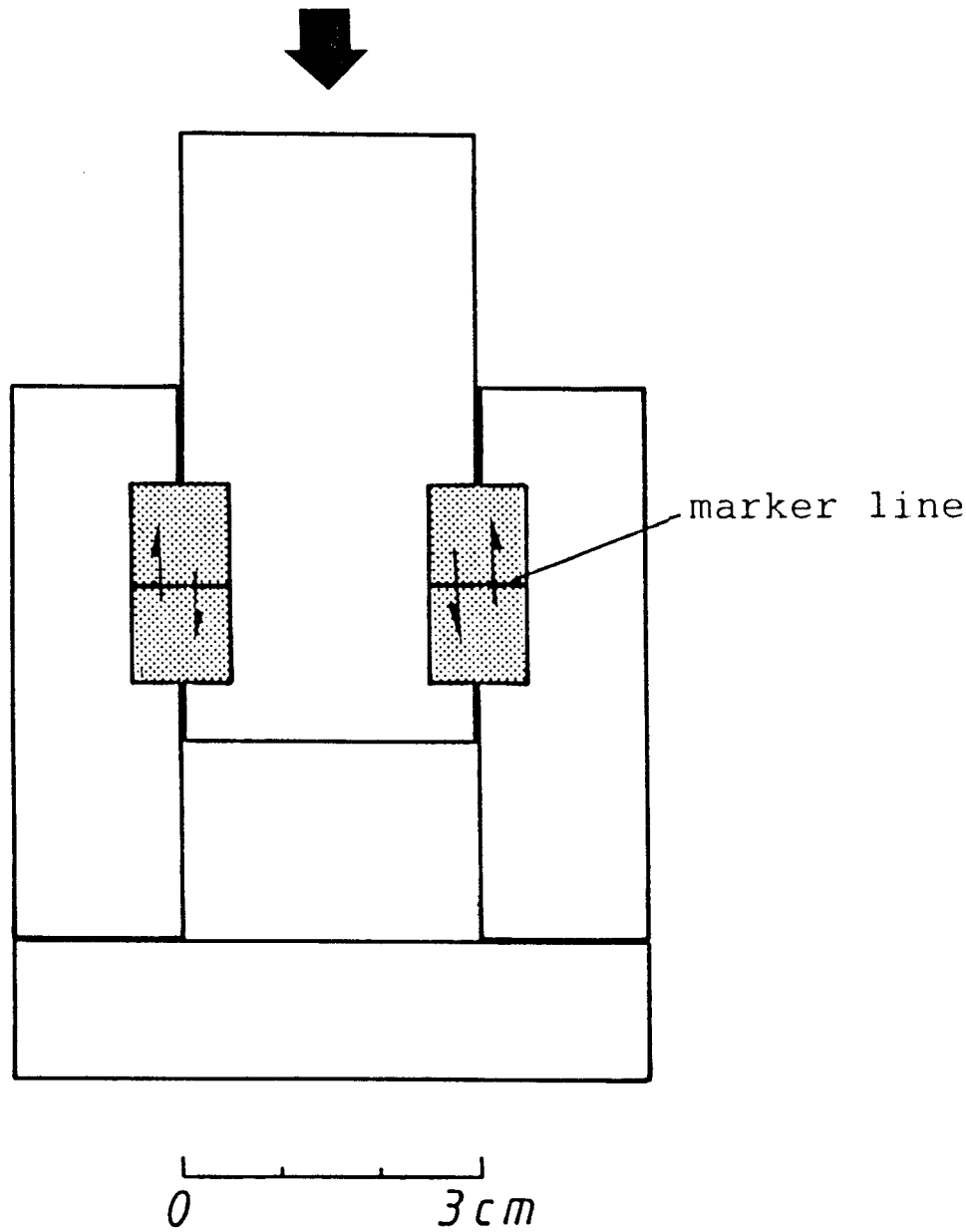

Figure 5. Double-shear jig.

small voids occurred between the two blocks, and therefore, the area of actual contact was too small to obtain markings on the sliding surface as a whole. Only few scratches and grooves developed on the slip plane, as shown in figure 6.

For these reasons, shearing experiments on the solid pyrophyllitic rock are not discussed further.

In order to obtain slickensided surfaces during shearing another type of sample was required. Instead of using solid pyrophyllite, pyrophyllitic clay was used. For this purpose, the pyrophyllitic rock was ground with sandpaper into a powder. The grain size of this pyrophyllite powder was determined using standard sieves. The amount of material of one grain size fraction was weighed and the grain size distribution (Table II) obtained.

Table II. Grain size distribution of pyrophyllite powder.

Grain size [μm]	Frequency [%]
> 105	4
53 - 105	12
38 - 53	43
< 38	41
	100

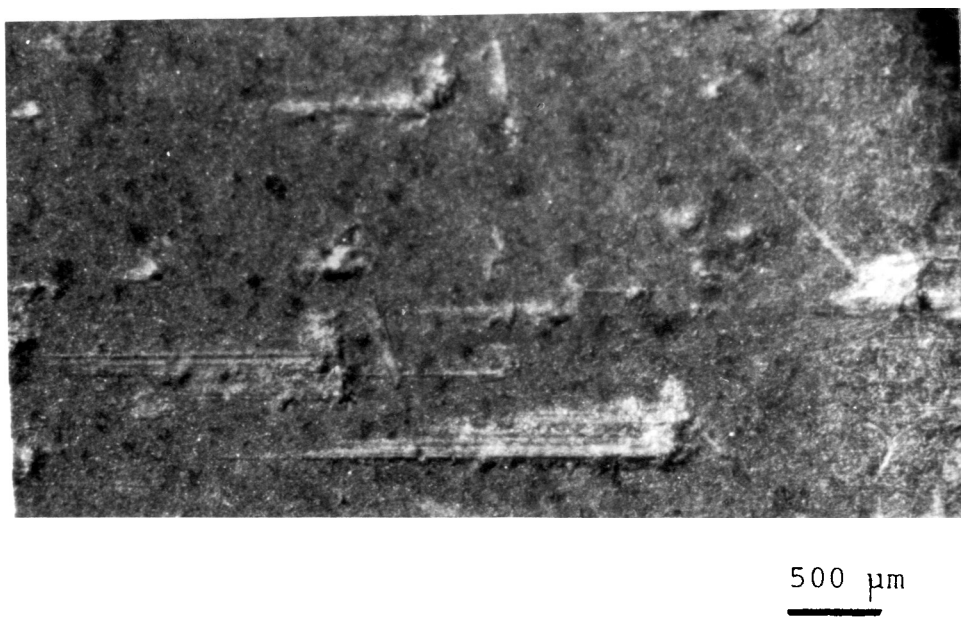

Figure 6. Scratches on solid pyrophyllite. Experiment PS-015. The upper, removed block moved to the right, field of view is approximately 5 mm wide.

In photomicrographs (e.g. figures 20, 21, 22), however, the grain size of most of the pyrophyllite grains appears to be at the order of 10 µm. It might be that pyrophyllite grains adhered to each other during the estimation of the grain size by means of the standard sieves. This could have obliterated the true grain size distribution of the pyrophyllite powder.

Next, a small amount of water was added to the pyrophyllite powder. The amount of water added was approximately 20% by weight of the whole mixture. Powder and water were thoroughly mixed until a stiff pyrophyllitic clay was produced. The grey pyrophyllitic clay could now be loaded into the jig holes. No pre-cut surface was made. As indicated in figure 5, horizontal white talcum filled marker lines were scratched on the front and back faces of the material. These marker lines ensured that the total as well as the slip displacement could be accurately measured (c.f. fig. 10).

Shearing of this material in this set-up produced beautifully striated slickenside surfaces (fig. 7) and so this technique was used for all quantitative investigations described below.

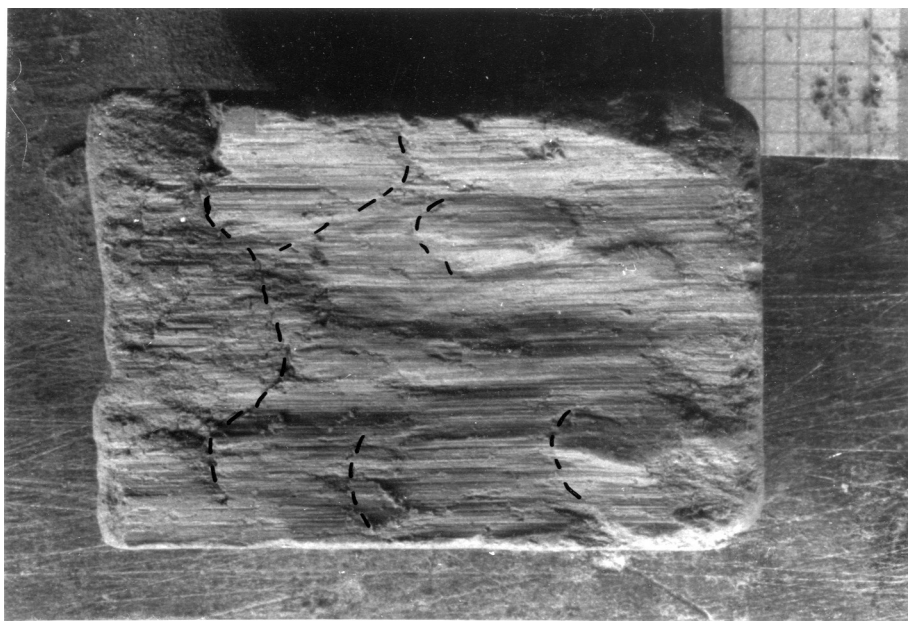

Figure 7. Striated slickenside surface in pyrophyllitic clay. Upper, removed block moved to the right with respect to the block shown. Stipled lines indicate "transverse structures". Experiment PS-014-LL, slip displacement 5.4 mm, marker grid in mm.

3.1.4. Triaxial compression experiments

The triaxial experiments were done in order to test whether it is possible to produce good striated surfaces in pyrophyllite in axially symmetric compression.

In these experiments rectangular blocks of solid pyrophyllite were used. The length and width dimensions of a block were made approximately equal (4-5 mm) so that its upper and lower faces were squares. The height of the block always exceeded its length by a factor of two or three. A pre-cut surface was made by three-point loading in a vise. The obtained fracture surface made angles of between 30°-50° with the long axis of the sample.

The prepared sample was placed into the cylindrical opening (3/4 inch in diameter) of a thick-wall steel cylinder. Molten paraffin wax was carefully poured into this opening. The wax serves as a confining pressure medium. The thick-wall steel cylinder has two horizontally oriented cylindrical holes (fig. 8). These two holes run from the outside of the cylinder to its center. As the upper piston, driven by the upper platen, advances relative to the lower platen, the wax becomes more and more compressed and exerts a steadily increasing confining pressure on the steel walls and the sample. The confining pressure on the sample becomes constant when the wax starts to extrude out of the two holes. By changing the confining pressure medium, for instance using

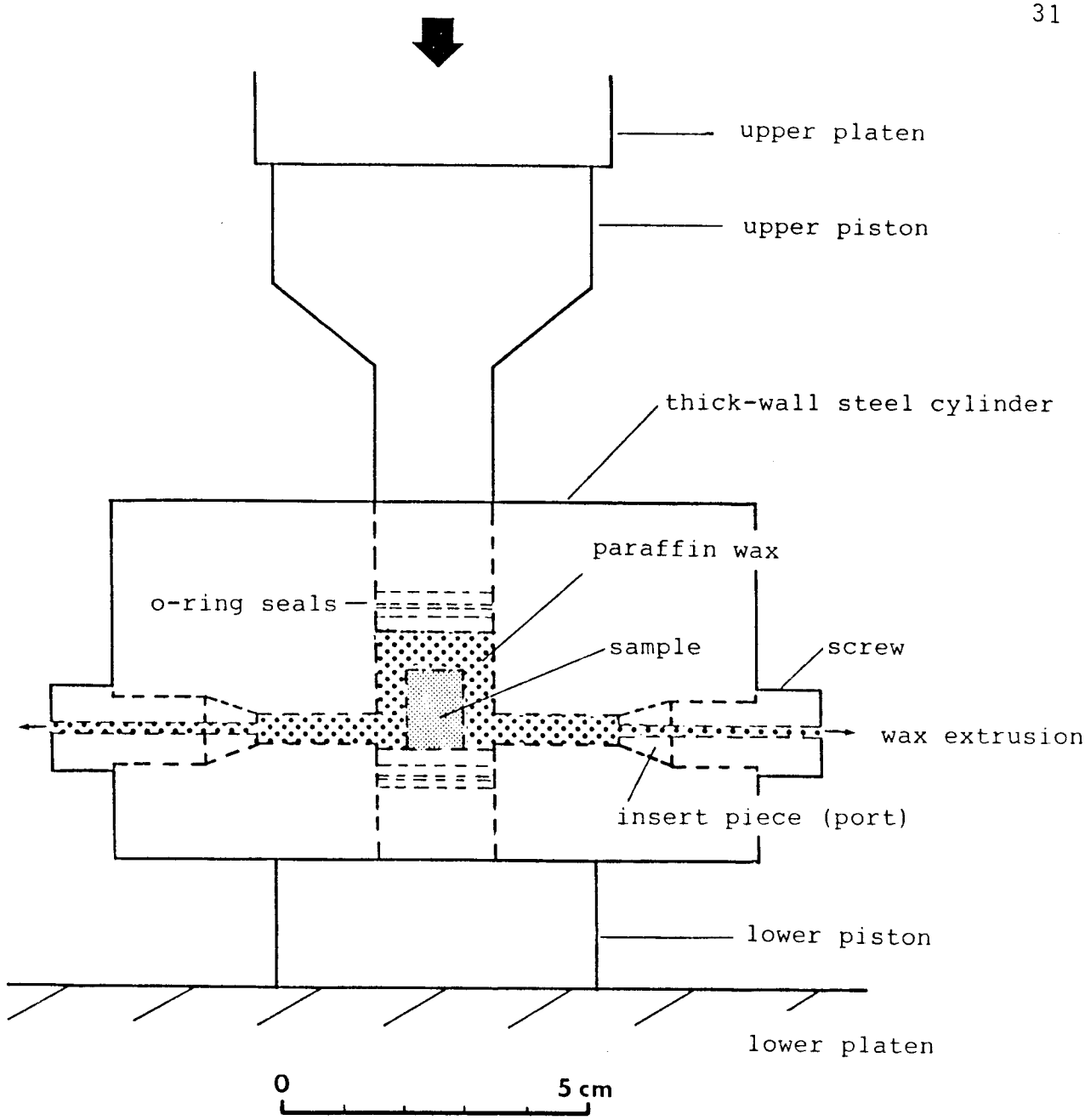

Figure 8. Experimental set-up for the triaxial compression experiments.

lead instead of wax, or changing the diameter of the two extrusion holes with insert pieces, different magnitudes of confining pressure can be obtained. Figure 8 shows a sketch of the ready-to-deform sample within the cylinder, mounted on the press.

The triaxial compression experiments yielded striated slip surfaces in pyrophyllite. The confining pressure and the strain rate were 300-400 bars and 10^{-4} to 10^{-5} sec^{-1}, repectively. However, systematic investigations using this type of experiment were not undertaken. The experimental set-up of the twist and double-shear experiments described above was simpler, so that these types of experiments were preferred over the triaxial compression test. For the benefit of future workers, a program was written, which calculates the stresses, the longitudinal strain, and the strain rate produced during a triaxial compression experiment. This program is described in Appendix A.

3.2. Shearing of pyrophyllitic clay

In these experiments performed using the double-shear jig lineations of the ridge-in-groove type were produced. No external normal stresses were applied on the slip plane. However, whether normal stresses were acting on the sliding surfaces during shearing is not known. Posssible causes of non-zero normal stress on the sliding surface might be a collapse of pore space in the pyrophyllitic clay during shearing, or an undulating fault plane with fault plane segments inclined to the overall shear direction.

3.2.1. Terminology

The labels on the sheared samples in figure 9 refer to the terminology of sample description used throughout this thesis. L and R means left or right sample, and LL, LR, RL, and RR stand for the "left-left", "left-right", "right-left", and "right-right" "half-samples", respectively.

Figure 10 explains how the total displacement, d_t, the slip displacement, d_s, and the shear strain can be measured using the marker line.

Table III summarizes the experimental data.

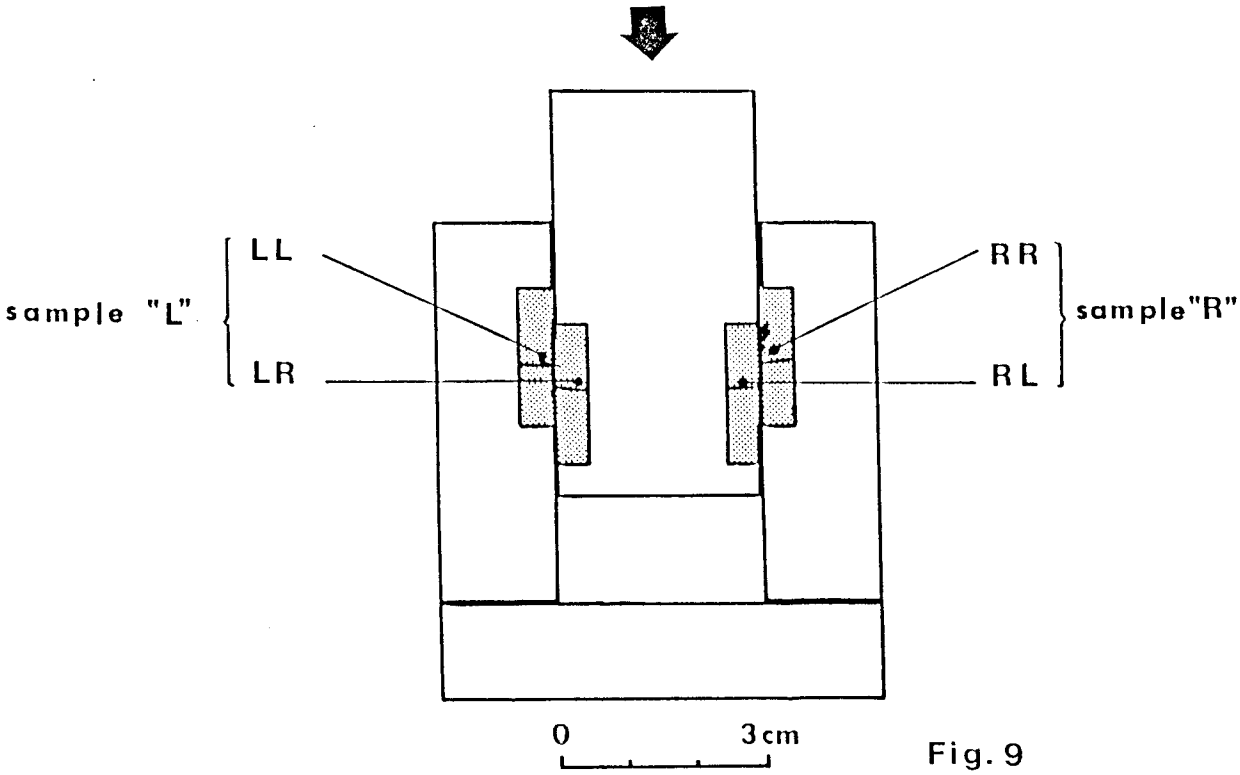

Fig. 9

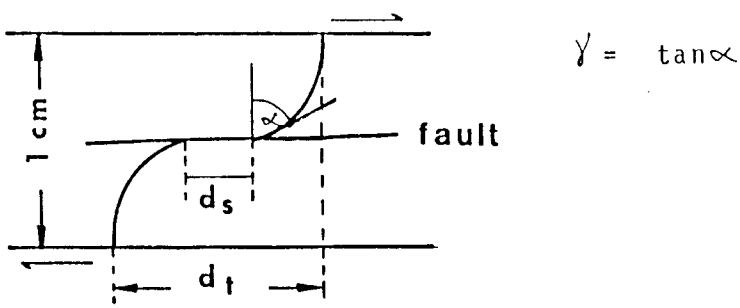

Fig. 10

Figure 9. Sample terminology as explained in the text.

Figure 10. Measurement of slip displacement (d_s), total displacement (d_t), angular shear (α), and the shear strain (γ).

Table III. Shearing of pyrophyllitic clay - experimental data.

Experiment	speed [m/s]	slip displacement [mm]	total displacement [mm]	mean* spacing [mm]
PS-012-L	3.09×10^{-5}	?	7.52	?
PS-012-R	3.09×10^{-5}	5.41	7.42	0.125 (5)
PS-013-L	3.09×10^{-6}	5.59	7.72	0.113 (2)
PS-013-R	3.09×10^{-6}	?	7.67	?
PS-014-L	3.09×10^{-7}	?	5.38	0.135 (5)
PS-014-R	3.09×10^{-7}	?	5.56	?
PS-041-L	3.09×10^{-5}	3.53	2.18	0.072 (5)
PS-041-R	3.09×10^{-5}	?	2.18	0.106 (1)
PS-042-L	3.09×10^{-6}	?	3.18	0.120 (1)
PS-042-R	3.09×10^{-6}	1.75	3.48	0.141 (1)
PS-046-L	3.09×10^{-6}	0.66	2.36	0.115 (2)
PS-047-L	3.09×10^{-6}	?	?	0.101 (4)
PS-047-R	3.09×10^{-6}	2.79	3.56	0.093 (1)
PS-048-L	3.09×10^{-5}	1.35	4.17	0.101 (2)
PS-048-R	3.09×10^{-5}	2.08	4.06	0.098 (6)
PS-049-L	4.70×10^{-6}	4.95	6.93	0.114 (3)
PS-049-R	4.70×10^{-6}	5.18	7.06	0.125 (1)
PS-050-L	3.09×10^{-6}	4.11	6.05	0.093 (5)
PS-050-R	3.09×10^{-6}	5.00	6.35	0.093 (2)
PS-051-L	3.09×10^{-6}	7.54	8.71	0.073 (6)

Experiment	speed [m/s]	slip displacement [mm]	total displacement [mm]	mean* spacing [mm]
PS-051-R	1.18×10^{-6}	3.99	7.54	0.080 (3)
PS-052-L	7.52×10^{-7}	5.26	8.84	0.075 (5)
PS-052-R	7.52×10^{-7}	6.63	8.76	0.103 (2)
PS-054-L	4.70×10^{-6}	2.55	6.00	0.088 (5)
PS-054-R	4.70×10^{-6}	3.67	6.11	0.076 (4)
PS-055-L	4.70×10^{-6}	0.94	2.52	0.073 (3)
PS-055-R	4.70×10^{-6}	1.04	2.64	0.087 (6)
PS-056-L	4.70×10^{-6}	3.70	4.86	0.082 (5)
PS-056-R	4.70×10^{-6}	2.69	5.19	0.095 (4)
PS-057-L	4.70×10^{-6}	2.55	4.59	0.080 (7)
PS-057-R	4.70×10^{-6}	2.04	4.29	0.069 (8)
PS-058-L	4.70×10^{-6}	?	?	?
PS-058-R	4.70×10^{-6}	7.77	10.10	0.061 (3)
PS-059-L	4.70×10^{-6}	5.49	8.73	0.071 (3)
PS-059-R	4.70×10^{-6}	3.65	8.75	0.067 (5)
PS-060-L	4.70×10^{-6}	7.21	10.10	0.063 (4)
PS-060-R	4.70×10^{-6}	7.26	10.10	0.056 (5)
PS-061-L	4.70×10^{-6}	1.37	5.96	?
PS-061-R	4.70×10^{-6}	3.75	4.95	?
PS-062-L	4.70×10^{-6}	4.69	5.31	?
PS-062-R	4.70×10^{-6}	3.07	6.53	?
PS-063-L	1.24×10^{-5}	5.00	7.65	0.100 (4)
PS-063-R	1.24×10^{-5}	4.50	6.40	0.088 (6)

Experiment	speed [m/s]	slip displacement [mm]	total displacement [mm]	mean* spacing [mm]
PS-064-L	6.18×10^{-6}	5.55	7.56	0.102 (4)
PS-064-R	6.18×10^{-6}	3.91	7.82	0.092 (6)
PS-065-L	4.70×10^{-6}			
PS-065-R	4.70×10^{-6}			
PS-066-L	4.70×10^{-6}	sliding interrupted and started		
PS-066-R	4.70×10^{-6}	again several times		
PS-067-L	4.70×10^{-6}			
PS-067-R	4.70×10^{-6}			
PS-068-L	4.70×10^{-6}	1.94	7.27	?
PS-068-R	4.70×10^{-6}	5.21	8.12	?
PS-069-L	4.70×10^{-6}	2.45	2.45	?
PS-069-R	4.70×10^{-6}	3.98	3.98	?

(*) The mean spacing is the average horizontal distance between two grooves or two ridges on a pair of sliding surfaces. The number in parenthenses gives the number of profiles measured on the sliding surfaces. For further explanation see text.

3.2.2. Experimentally produced slickenside lineations of the ridge-in-groove type

In these experiments, lineations of the ridge-in-groove type were produced. As outlined above, this type of lineation has the characteristic feature of hangingwall ridges fitting perfectly into footwall grooves, and vice versa. This nesting property could be proved using the technique described below.

After an experiment the samples were carefully removed from the jig and opened up like a book (figure 11a). Both footwall and hangingwall surfaces were photographed as indicated in figure 11a; the footwall block from the left, and the hangingwall block from the right side. For every exposure the same light source was used, and the surfaces were illuminated at the same angle. Surface segments with normals that bisect the angle between the light and the camera will be most brightly illuminated in the photograph. Surface segments inclined away from this position reflect light less brightly, and hence will become darker on the final photograph.

The negative or the print of one of the sliding surfaces was reversed. If two surfaces nest, then the reversed print and the original of the opposite wall should be identical. I preferred to reverse already developed prints, because it is not only easier to do but gives also a much better quality of reversed prints. An undeveloped sheet of photographic paper

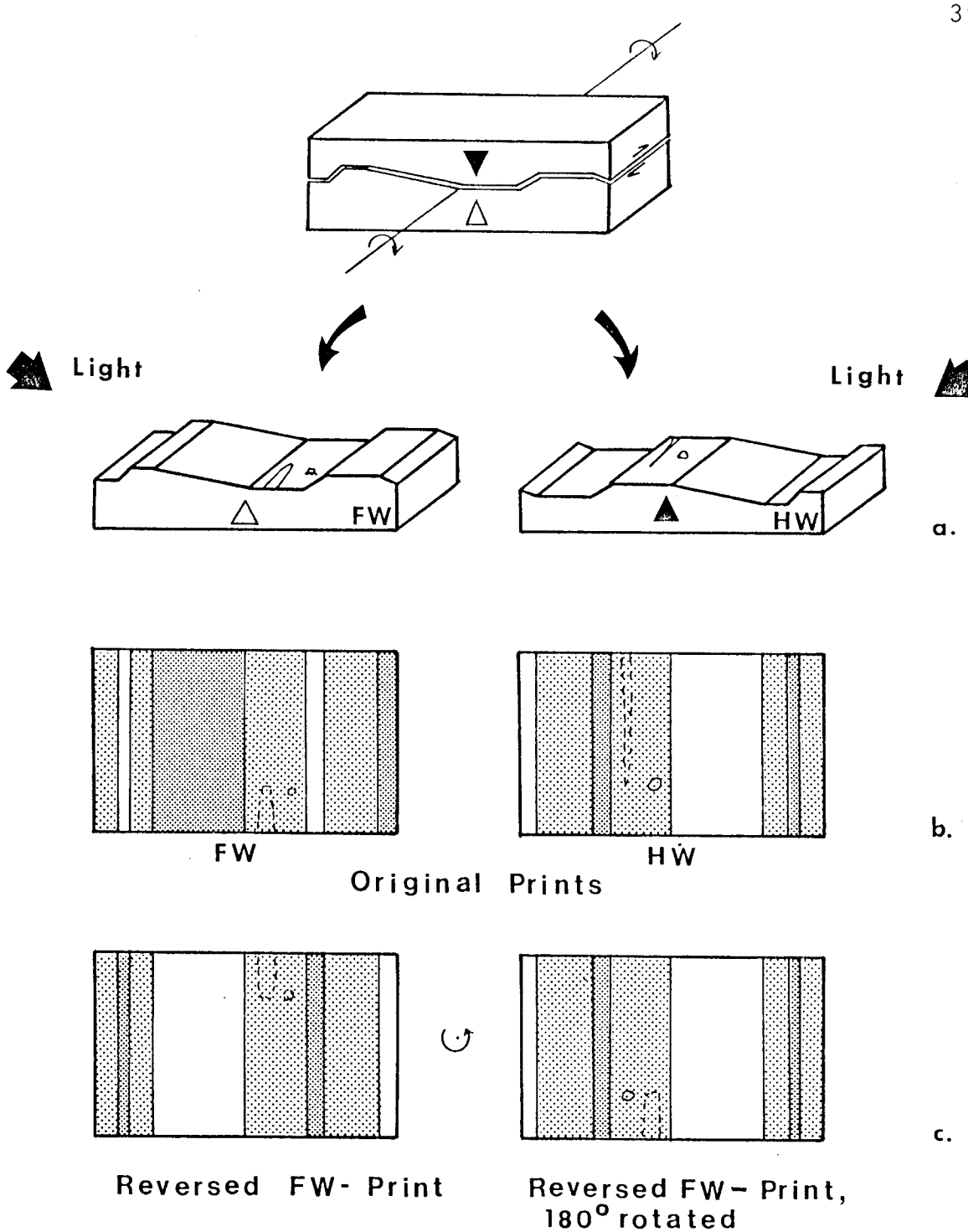

Figure 11. Reversed print technique. The opened up hangingwall (HW) and footwall (FW) blocks are lit as indicated by the arrows in (a). (b) Resulting distribution of dark and light stripes. (c) Reversed print of the footwall surface (left), reversed footwall surface print, 180° rotated (right). If two surfaces nest, then this reversed print is identical with the original print of the hangingwall surface. In addition, the sketch shows that striations of an abrasional origin (dashed lines) do not nest, and therefore are not identical on the original print of the hangingwall surface and the reversed print of the footwall surface.

is placed under the developed print with the two emulsion sides in tight contact with each other. All the dark areas on the original print now become bright on the reversed print, and vice versa. This is schematically illustrated in figure 11c. If the two surfaces have complementary morphologies and therefore do nest, the original from one side should be identical with the reversed print from the opposite side. This technique makes it possible to compare identical pictures with each other. This is demonstrated in figures 12 and 13. Figure 12a shows the original prints of the sliding surfaces PS-051-LL and PS-051-LR. PS-051-LL was reversed, and figure 12b documents the striking similiarity between the reversed print of PS-051-LL and the original print of PS-051-LR. Not only are the large-scale features identical on both pictures, but so are the small-scale features, as demonstrated in figure 13, which shows a detailed view of the sliding surfaces along a common profile line. Note that even most of the smallest and faintest lineations can be traced from one photograph to the other.

After demonstrating that this particular type of slickenside lineation develops under the given experimental conditions in this material, several parameters which might influence the morphology of the ridges and grooves on the slip plane were investigated.

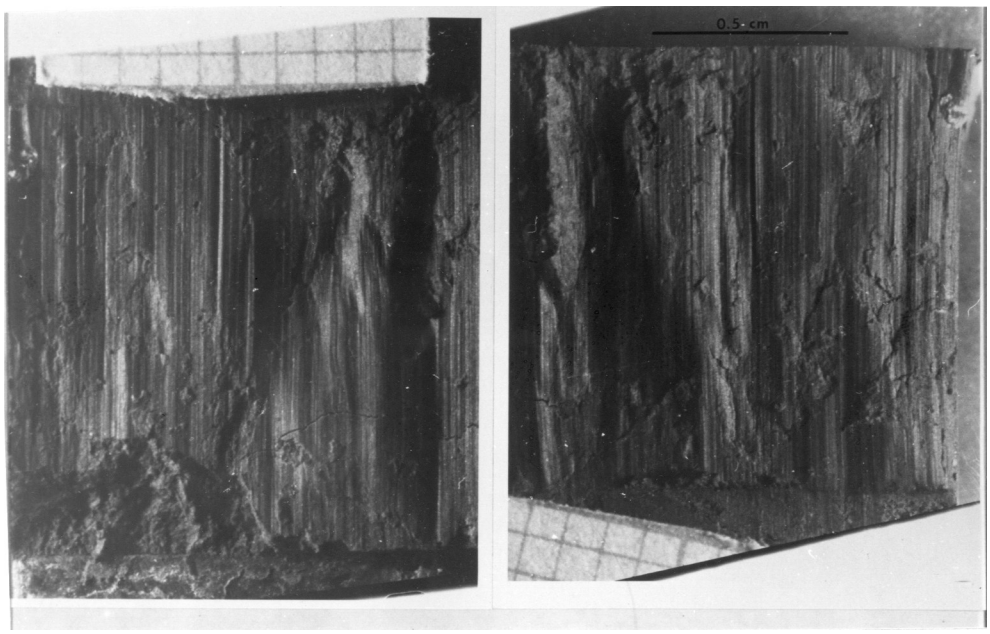

a

PS-051-LL original PS-051-LR original

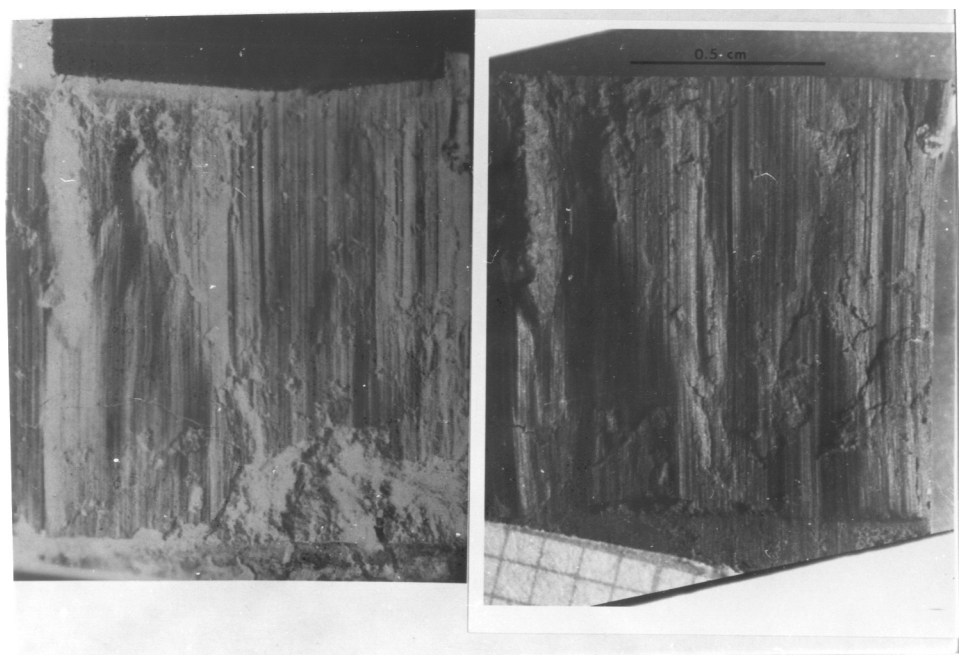

b

PS-051-LL reversed PS-051-LR original

Figure 12. (a) Sliding surfaces of PS-051-LL and PS-051-LR after slip displacement of 7.5 mm. (b) Nesting is demonstrated by the close match of the reversed print of PS-051-LL (left) and the original print of PS-051-LR (right). Marker grid is in mm.

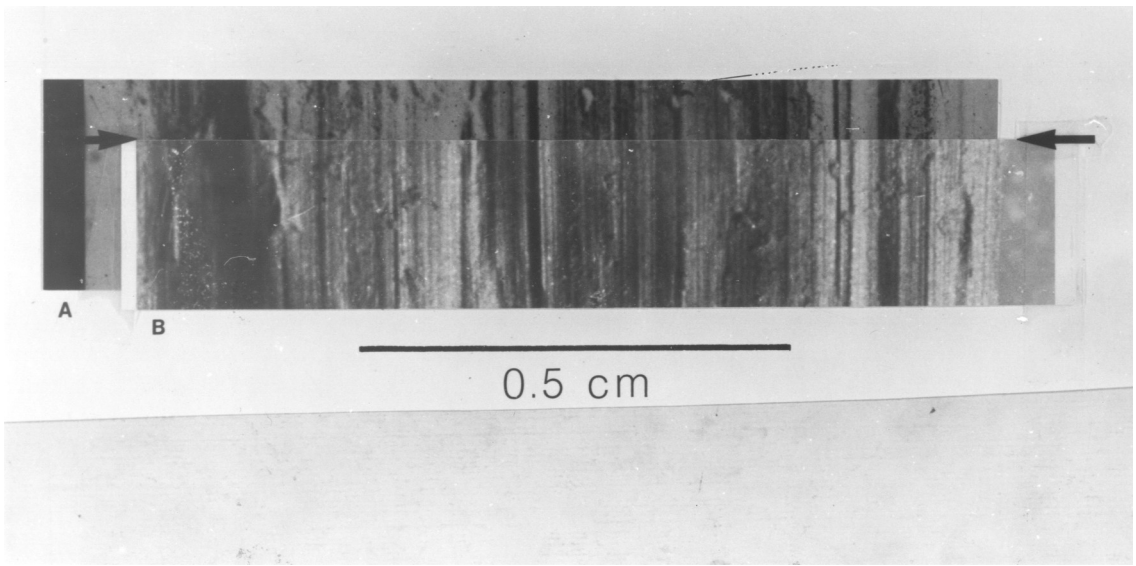

Figure 13. Profile along a common profile line (between arrows) of the sliding surfaces of figure 12b. A is the reversed print of PS-051-LL, B the original print of PS-051-LR. Almost all of the striations can be traced from one photograph to the other and indicate a "small-scale" nesting.

3.2.3. Influence of slip displacement and speed on reflection spacing

Photographs of the sliding surfaces were used to determine the distance between two adjacent planar surface elements. Throughout the further description, this feature is called reflection spacing or simply spacing. Various profiles were taken perpendicular to the sliding direction, and either the number of the bright stripes or of the dark stripes were counted. Each profile was taken across a planar part of the sliding surface, in order to obtain comparable data. The number measured was divided by the actual profile length on the surface, and a mean spacing value calculated. Measurements were taken from both sliding surfaces (e.g., from PS-056-RL and PS-056-RR) and subsequently combined (e.g., to PS-056-R). In order to obtain a statistically more reliable value the mean spacing values of the individual profiles were added and divided by the number of measured profiles on the two sliding surfaces. This value corresponds to the average reflection spacing on a pair of sliding surfaces and is given in Table 3; the number in parenthenses is the number of profiles.

The graph in figure 14 plots spacing versus slip displacement at a constant speed of 4.70×10^{-6} m/sec. In this diagram, the dots correspond to the calculated mean spacing values. The bars indicate the observed range in the

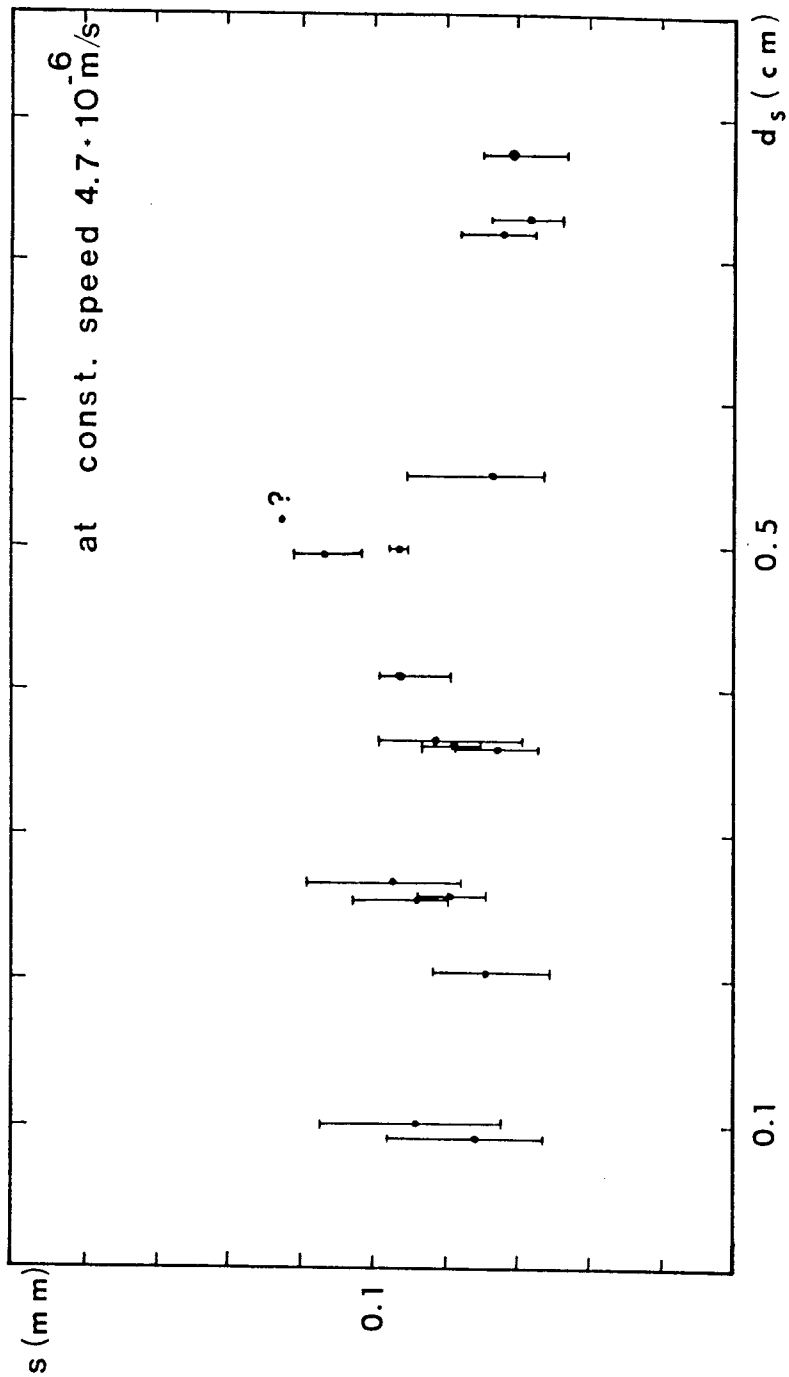

Figure 14. Spacing, s versus slip displacement, d_s.

spacing value. The diagram shows that the spacing does not change significantly with displacements greater than 0.1 mm. Data could not be obtained at slip displacements less than 0.1 mm, since the samples could not be opened up along the sliding surface, but broke apart. However, since no grooves and ridges develop at zero displacement, the origin of the coordinate axes might be part of a curve plotted through these data points. This would imply that there is a steep increase in the spacing value at very low displacements, while the spacing does not seem to be very sensitive to the amount of displacement at higher displacements. If, however striations originated with a finite distance from each other such an implication would no longer be valid.

The same general trend as in figure 14 can be seen when the spacing values are plotted versus the speed or the shear strain rate, respectively, with which the blocks slid past each other (figure 15). These experiments were carried out at a constant slip displacement of approximately 5.25 $\pm$ 0.25 mm. If the origin of the coordinate system is part of a graph plotted through the data points, a steep increase in spacing at low speeds would be followed by some type of steady-state behavior at intermediate and higher speeds. But, as long as the possibility exists that striations originate with a finite spacing, this implication cannot be proved.

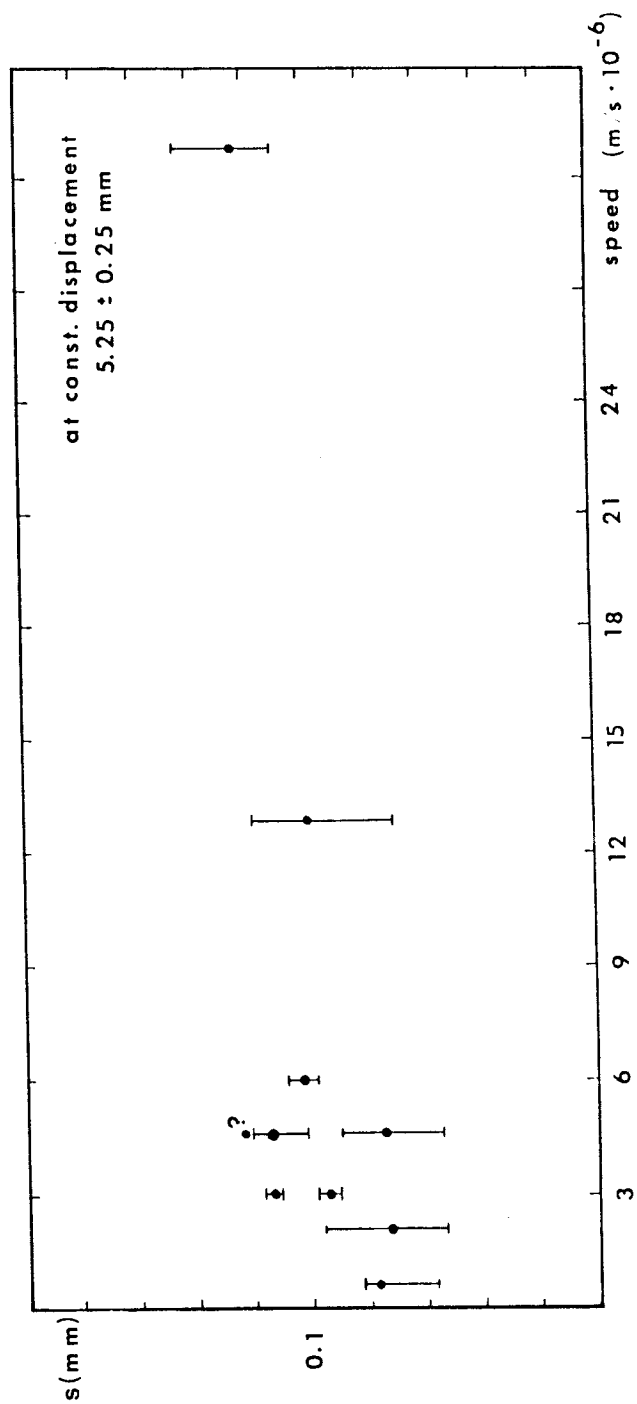

Figure 15. Spacing, s versus speed.

3.2.4. Striations longer than the displacement

Figure 16 demonstrates a very surprising feature observed during the experiments. The scale bar on the left indicates the slip displacement measured on the slip surface. Adjacent to it, between the two arrows, a groove much longer than the slip displacement, is clearly visible. This groove runs very continuously, without any offset or truncation parallel to the slip direction. This "excess-length" feature is in contrast to Engelder's (1974) carrot-shaped wear grooves which were equal in length or shorter than the slip displacement.

The length of several of these "excess length" ridges and grooves were measured on sliding surfaces produced during different experiments. The result is given in figure 17. This diagram plots the length/slip displacement ratio versus the slip displacement. This graph indicates an approximately exponential decrease in excess length with increasing slip displacement and is asymptotical to 1 on the vertical axis. All experiments were carried out at the same speed of 4.70×10^{-6} m/sec.

If further measurements of this kind are made, then the slip displacement should be recorded more carefully by using more than one marker line on the outer faces of the sheared material. This would lead to a better correlation between the ridge and groove lengths, especially when measured close to

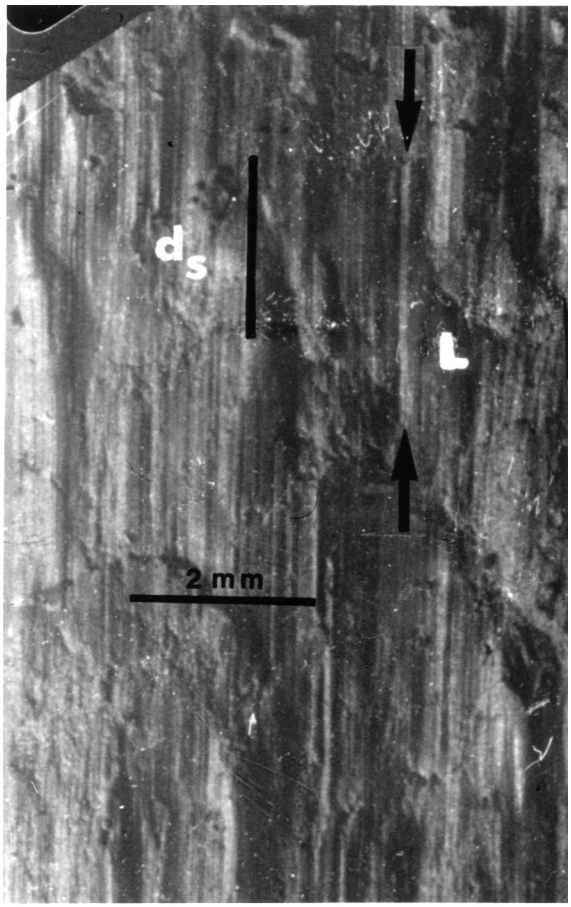

Figure 16. Demonstration of the "excess-length" feature (see arrows). The upper, removed block moved down with respect to the sample shown. Experiment PS-056-RL, slip displacement 2.7 mm.

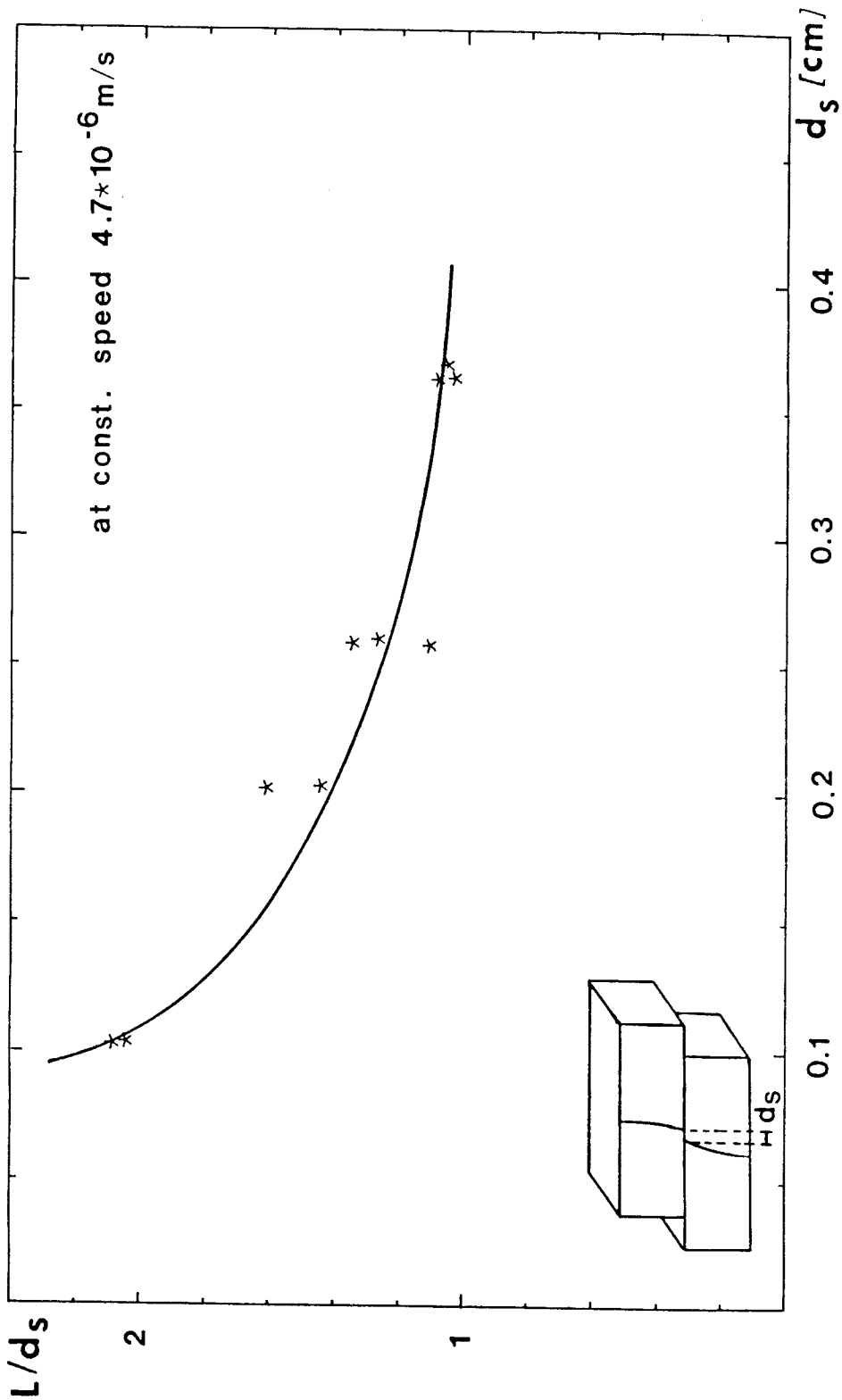

Figure 17. Ridge and groove length / slip displacement ratio versus slip displacement.

the margins of the sliding surface, and the slip displacement in the measured area.

3.2.5. Microstructural and SEM observations

Thin sections of the pyrophyllitic clay were made by using the "Spurr low-viscosity embedding media" (Polysciences, Inc.).

The photomicrograph of figure 18 shows the fabric of an undeformed reference sample. After inserting the gypsum plate, domains of dominantly yellow and blue colors can be recognized in an otherwise randomly colored matrix. But no overall preferred alignment of phyllosilicates is visible in the undeformed sample. This changes with shearing. Figures 19 and 20 show a strain-modified fabric produced by shearing. Short slip planes inclined to the main sliding surface as well as the main sliding surface can be identified due to the preferred orientation of phyllosilicates along these planes. The short slip planes are called "second-order" slip planes in the following description.

The orientation of these "second-order" planes corresponds to that of R-shears (for example, Tchalenko, 1970), or to that of an extensional crenulation cleavage (Platt, 1979; Platt and Vissers, 1980) or shear bands, C', respectively. The terms extensional crenulation cleavage and shear band are used interchangeably. In order to emphasize

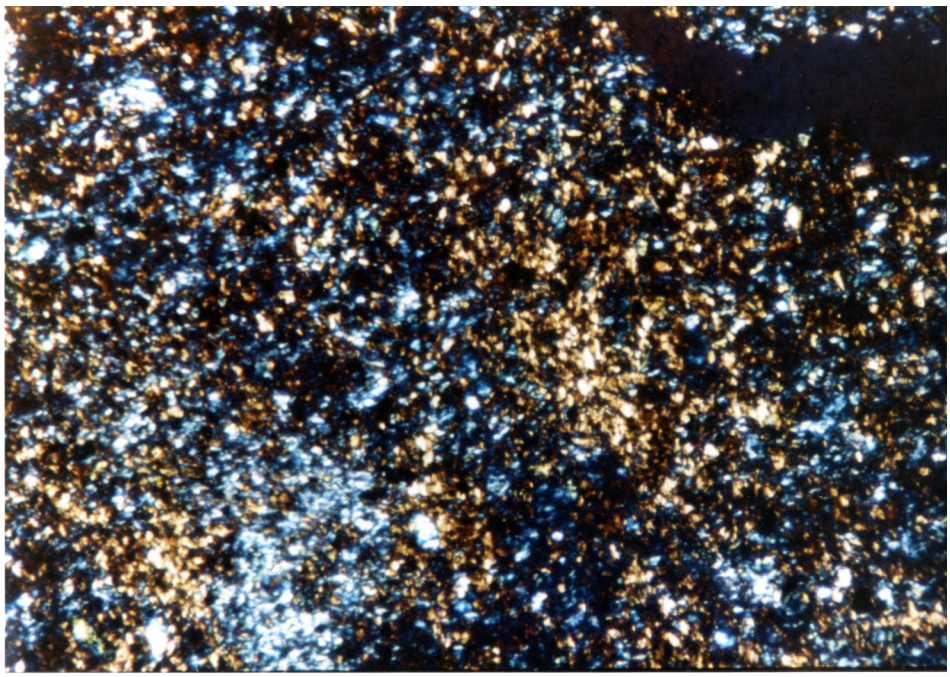

Figure 18. Photomicrograph of an undeformed pyrophyllitic clay sample. Randomly oriented pyrophyllite grains are visible. Field of view is 0.86 mm wide, crossed polarizers, gypsum plate.

the ductile behaviour of the pyrophyllitic clay during the first increments of deformation, I describe these slip planes as shear bands rather than R-shears. For the same reason, the main sliding surface is described as a C-plane. This choice of terminology is more a personal matter of taste, and it would be also justified to describe the slip planes as R-shears, and the main sliding surface as a P-shear. Whether phyllosilicates align in a S-plane foliation could not be proved for certain.

Figure 19 shows the distribution of shear bands along the sliding surface of experiment PS-056-RL after a total displacement of 5.2 mm. "Transverse structures" could be observed in some cases (c.f. figure 7). These transverse features might be the surface expression of shear band traces. In a view parallel to the overall sliding direction (figure 20), it can be seen that the (001) traces of the phyllosilicates in the shear bands are slightly oblique to the shear band boundaries, dipping at a shallower angle than the boundary of the shear band. The thickness of the strain-modified zone can vary along the sliding surface. However, there is not enough information to correlate the thickness of the strain-modified zone with specific positions at the sliding surface. Figure 21 shows a view perpendicular to the slip direction. Again, a strain modified fabric can be recognized by the alignment of the phyllosilicates in bands across the field of view in otherwise randomly oriented

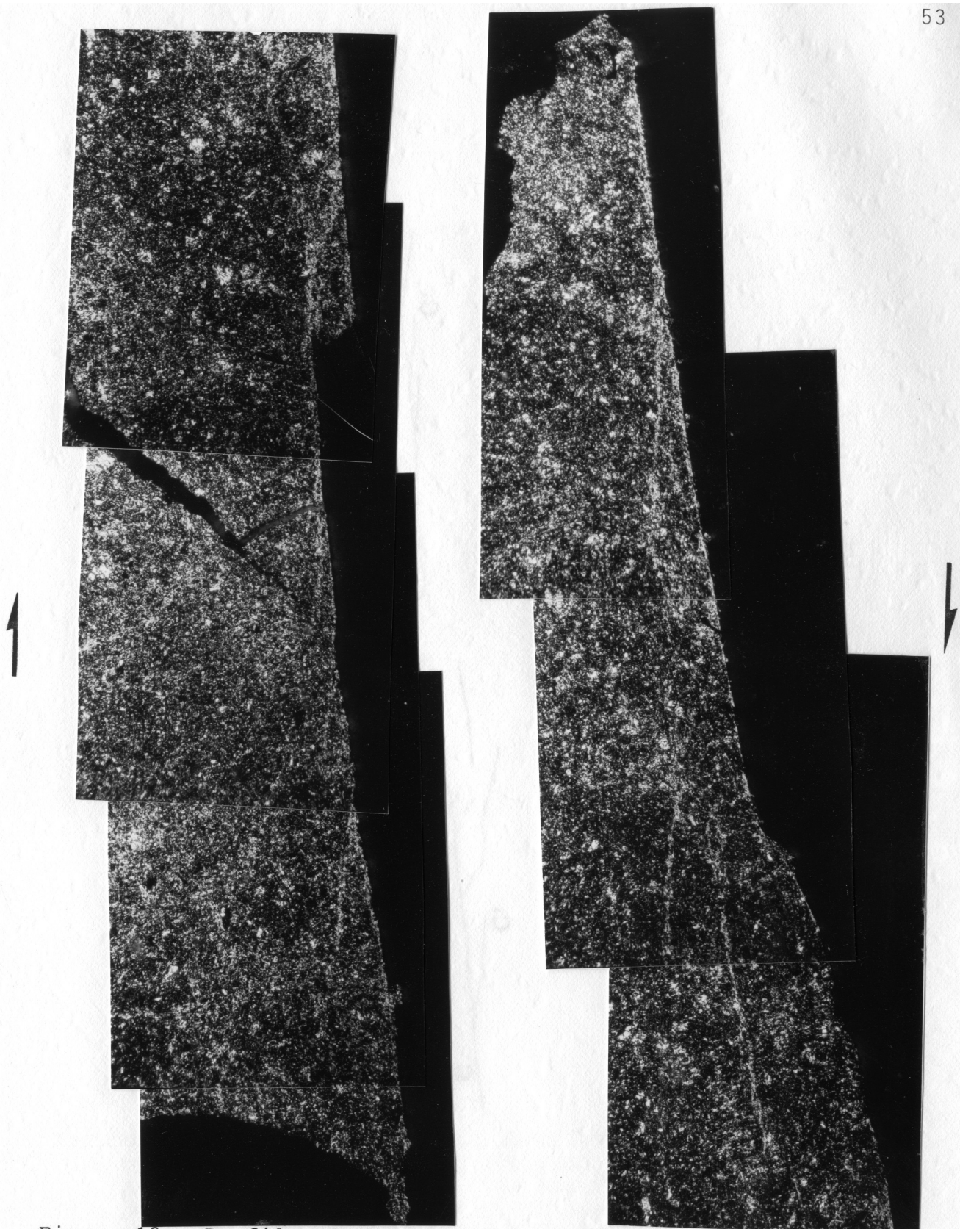

Figure 19a. Profile along the sliding surface of experiment PS-056-RL. Total displacement 5.2 mm. Several shear bands, C', are visible running at an acute angle of approximately 20° to the main sliding surface, C. Sense of shear is dextral. Field of view is 8 mm wide.

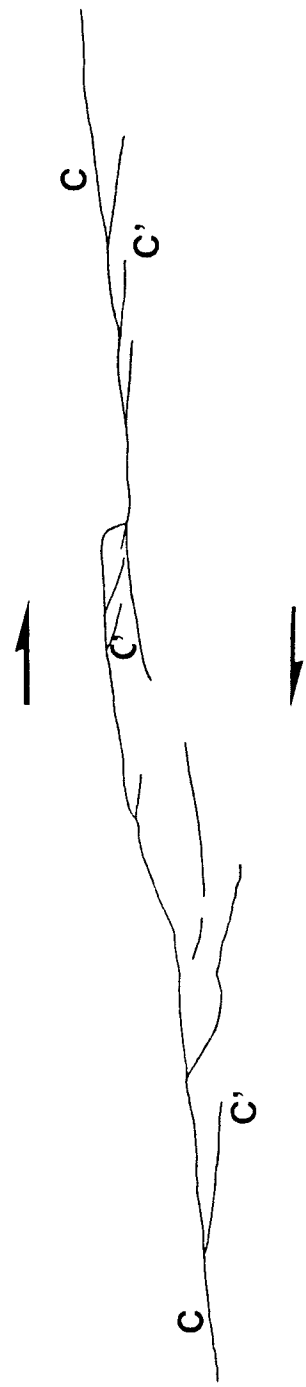

Figure 19b. Shear bands and main sliding surface as traced from figure 19a.

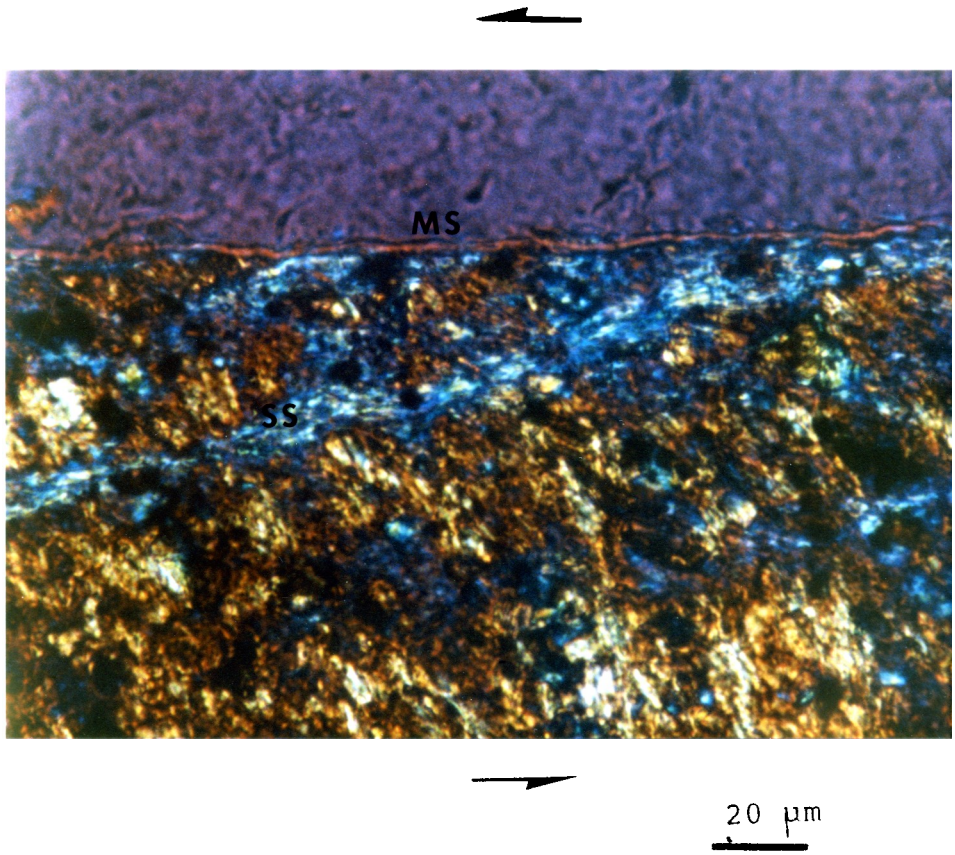

Figure 20. Shear induced strain modified fabric in pyrophyllitic clay. MS is the main sliding plane, SS are second-order slip planes. The material on top of the main sliding plane is epoxy. The sense of shear is sinistral. Field of view is 0.20 mm wide, crossed polarizers, gypsum plate. Experiment PS-056-RL.

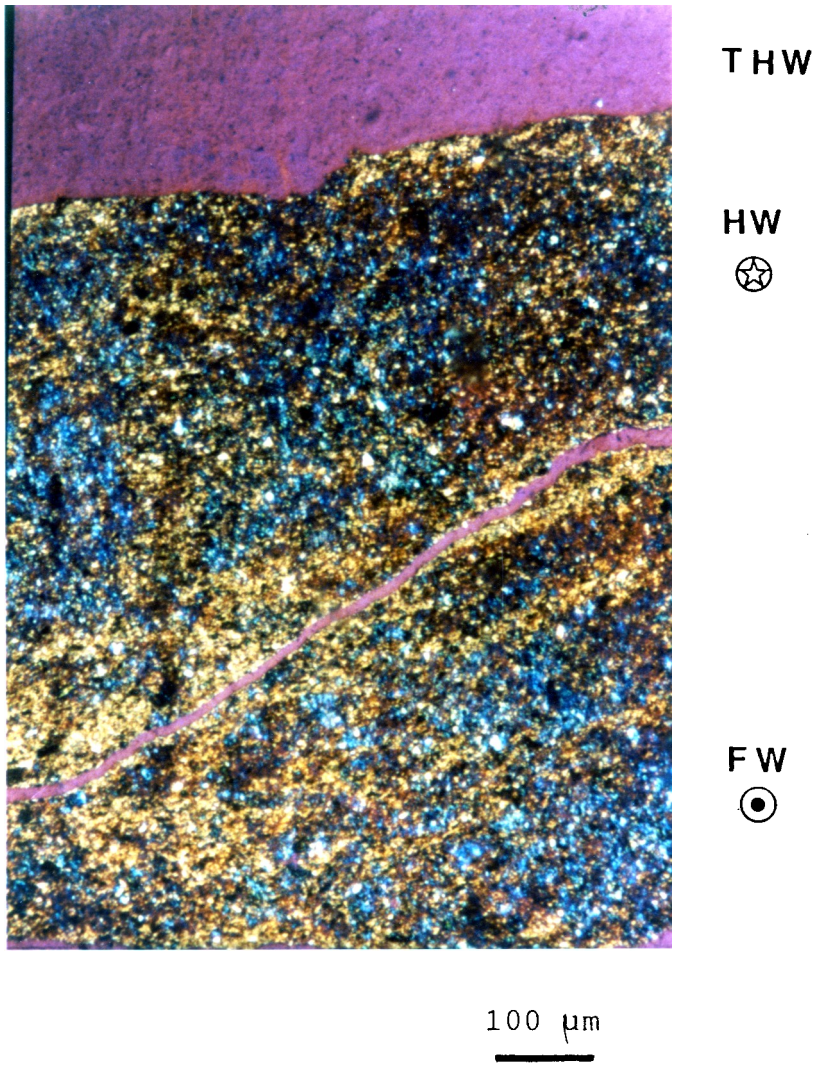

Figure 21. View perpendicular to the slickenside and the sliding direction. A strain modified fabric is visible. Yellow bands of phyllosilicates run across the field of view (0.86 mm). Hangingwall (HW) and footwall (FW) are present. FW moved towards the viewer. The top of the hangingwall (THW) is also striated. The purple material above THW is epoxy. Crossed polarizers, gypsum plate. Experiment PS-068-LL.

pyrophyllite grains. This photomicrograph shows that several of those aligned phyllosilicate shear bands are present. Each individual band is interpreted as a C'-plane, being part of a larger C'-zone. The orientations of the long axes of the phyllosilicates were measured in the individual shear bands. The (001) traces vary between 0^{o} and 40^{o} with respect to the shear band boundaries. This variation in orientation probably reflects the influence of the inherited random phyllosilicate orientation from the starting material.

The C-plane appears to be straight under low magnification (figure 21). Under high magnification, figure 22, the "straight" segments show minor ridges and grooves. These minor undulations can be caused by slightly misoriented phyllosilicates, which are in some cases oriented sub-parallel to the morphology of the ridges and grooves. These very small-scale (sometimes smaller than 10-20 μm) ridges and grooves are very likely candidates for the fine striations observed in SEM micrographs (figure 23).

A SEM-photomicrograph (figure 24) revealed a striated fault plane paralleling the C'-plane orientation within the sample. The presence of striations on the main sliding plane and this fault plane segment indicates that both surfaces are slip planes.

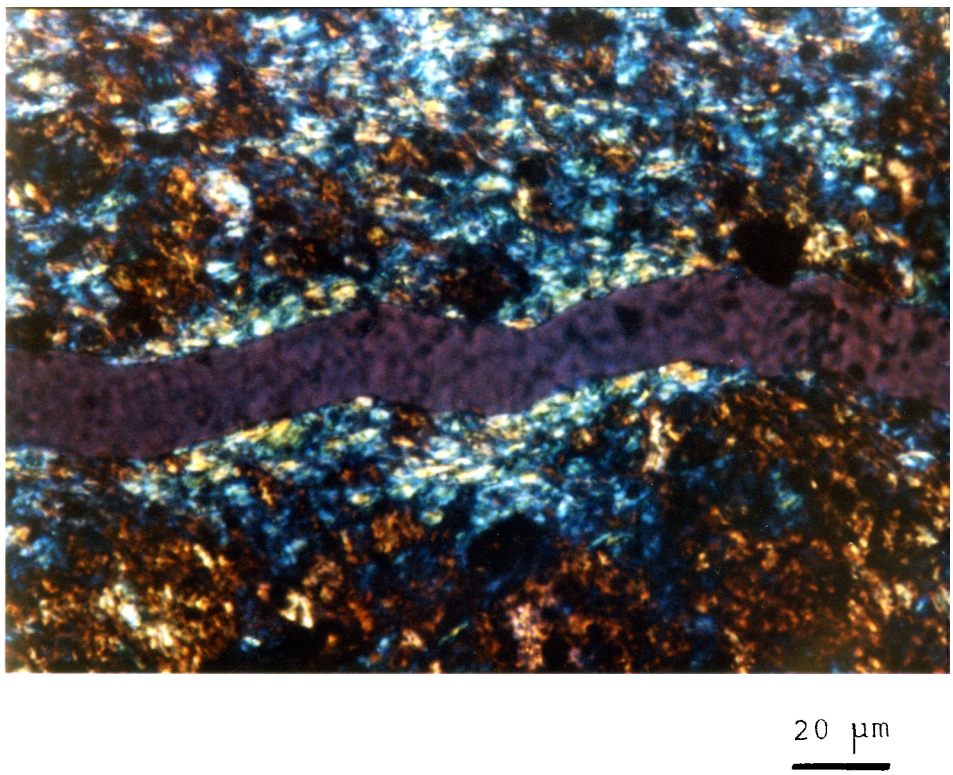

Figure 22. View perpendicular to striation. Minor ridge-in-groove type undulations are present. The footwall block (FW) moved towards the viewer, HW is the hangingwall block. Field of view is 0.20 mm wide, crossed polarizers, gypsum plate. The purple material is epoxy. Experiment PS-068-LL.

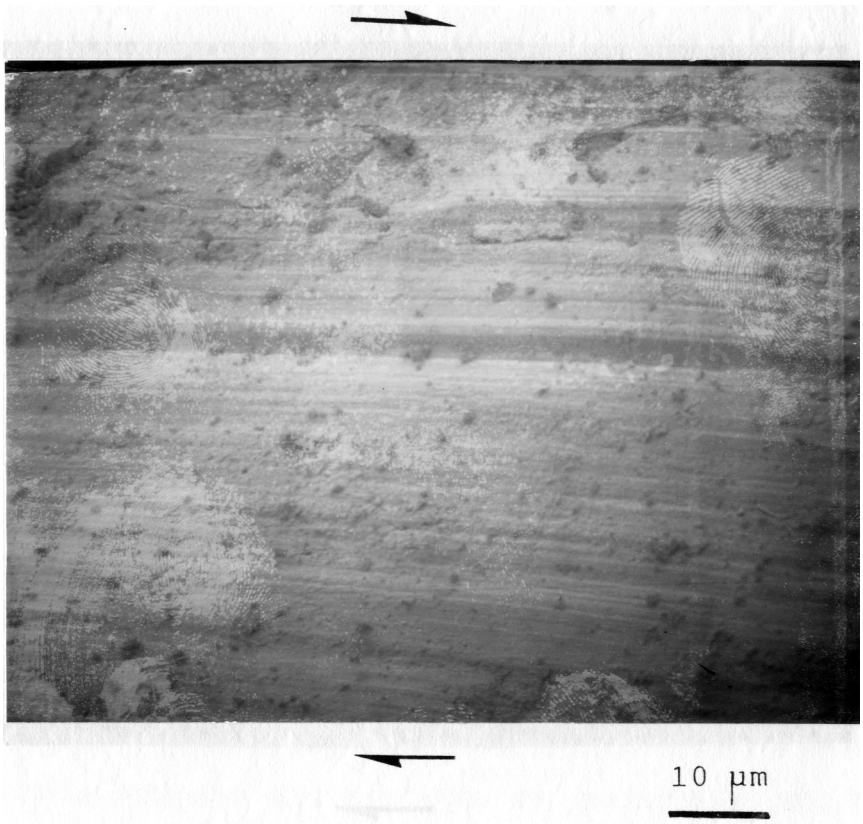

Figure 23. SEM-micrograph of slickenside. Ridges and grooves of different wavelengths and amplitudes are present. The hangingwall block moved to the right. Field of view is approximately 0.1 mm wide. Experiment PS-051-LR.

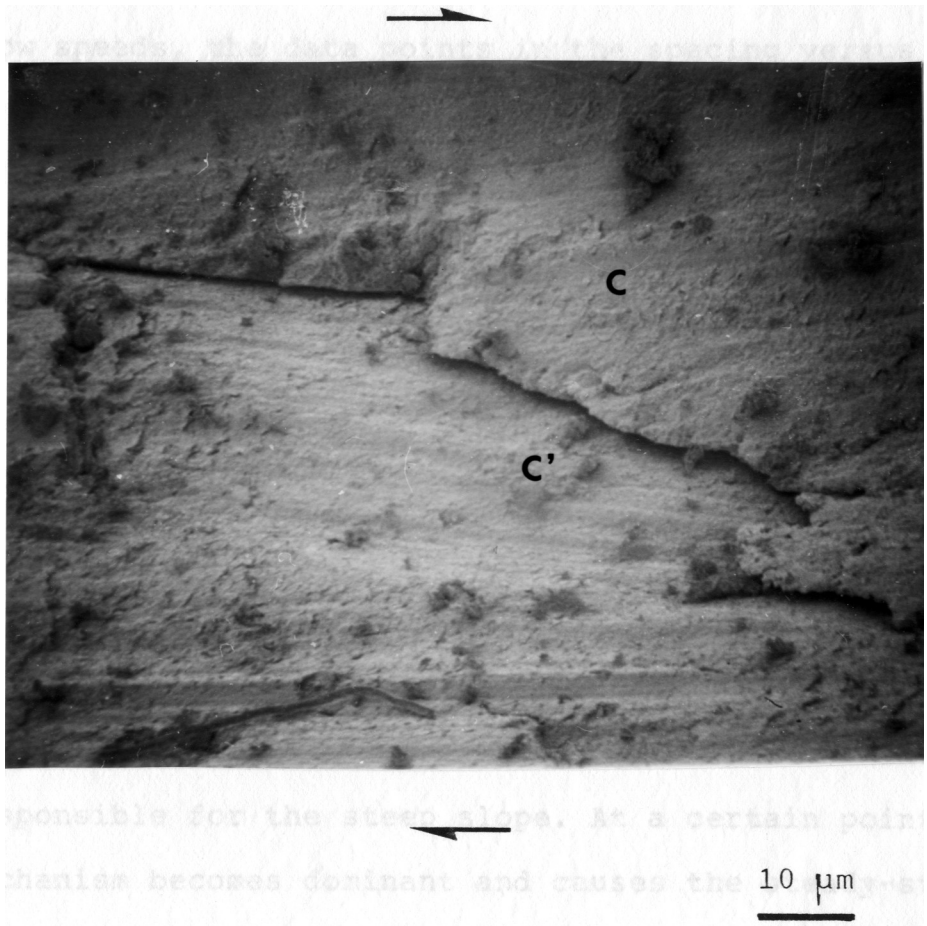

Figure 24. Striated slip planes in C- and C'-plane orientation. SEM-micrograph. The hangingwall block moved to the right. Field of view is approximately 0.1 mm wide. Experiment PS-051-LR.

3.2.6. Discussion

Due to the lack of data at low slip displacements and slow speeds, the data points in the spacing versus slip displacement or speed diagrams, respectively, can be fit by different mathematical functions. One is a continuous function which has first derivatives at every point along the function. Another possible function would also be a continuous function but without first derivatives at every point. The different functions are shown in figures 25b and 25a, respectively.

Possible ways to interpret these graphs are the following. If figure 25a is correct, a two-stage process could lead to the experimental results obtained. At low slip displacements or low speeds one process is dominant and is responsible for the steep slope. At a certain point another mechanism becomes dominant and causes the steady-state behavior. A single stage process based on an asperity ploughing model could also be imagined (figure 25b). An asperity approaches the surfaces, contacts it, and starts to score into it. This necessarily leads to an increase in groove width until the width of the groove is the same as the diameter of the ploughing tool. However, an asperity based model must be ruled out in this case. These surfaces are nesting surfaces, and an asperity ploughing model cannot be used to explain this property. Furthermore, an asperity model

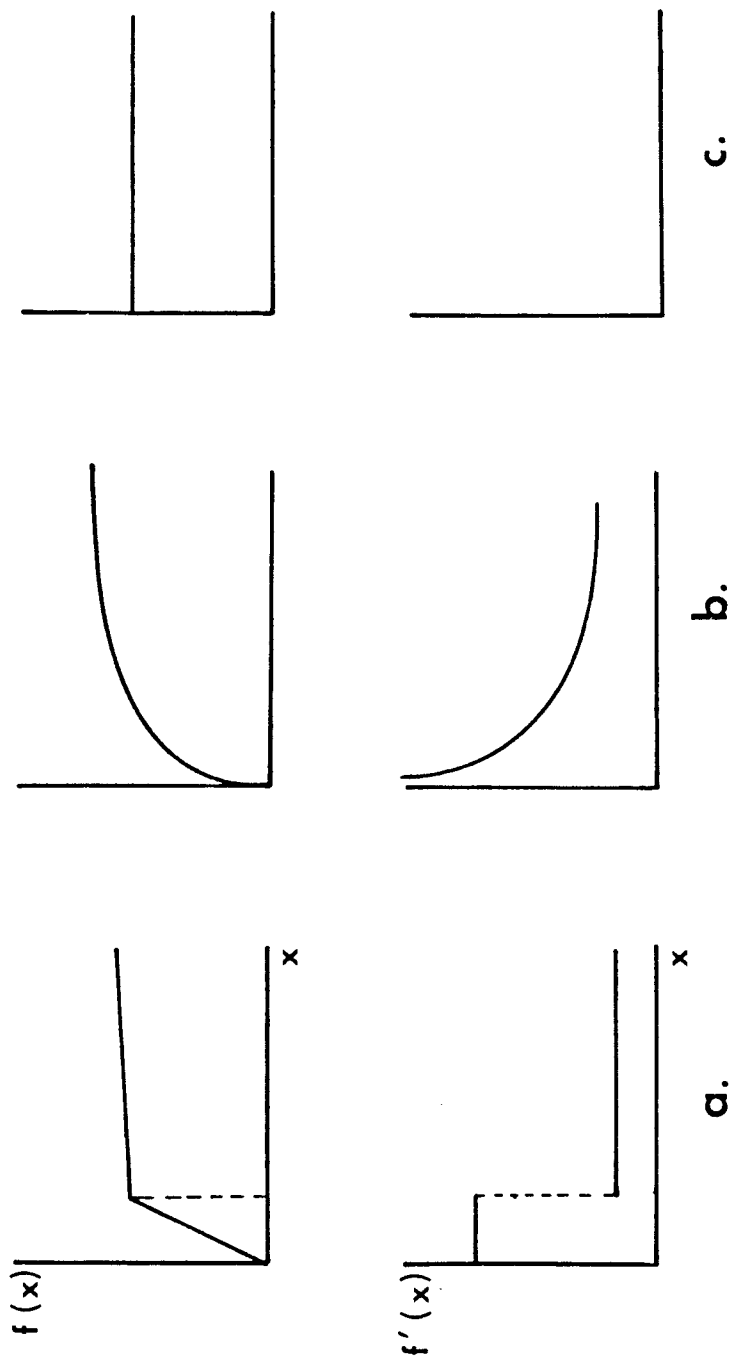

Figure 25. Different mathematical functions which fit the data points in spacing versus slip displacement, or speed diagrams.

explains the formation of grooves, but not the formation of ridges of similar shape and area distribution on the same surface.

It even is possible to speculate that the spacing between ridges or grooves might be insensitive to the amount of displacement, even at very small displacements. This possibility is shown in figure 25c.

Not only is the interpretation of data ambiguous but there is another fact which could have influenced the spacing values measured. SEM micrographs (figures 23 and 24) revealed numerous very fine striations, normally invisible under an optical microscope. In order to establish a relationship between the spacing value and the experimental parameters, these fine striations must be taken into account. This can be done by using SEM facilities.

After demonstrating the unusual excess length property in the pyrophyllitic clay samples I wanted to be sure that there are no variations in displacement across the slip plane, since this could simulate this feature. For this purpose, a planar marker was used. The samples were prepared in the usual way, except that a cut across the sample was made and subsequently filled with talc powder. Using this technique, a marker line perpendicular to the future slip direction was produced on the future slip plane. The different behaviors expected of the marker line at homogeneous or heterogeneous displacement across the slip plane are shown in figures 26a

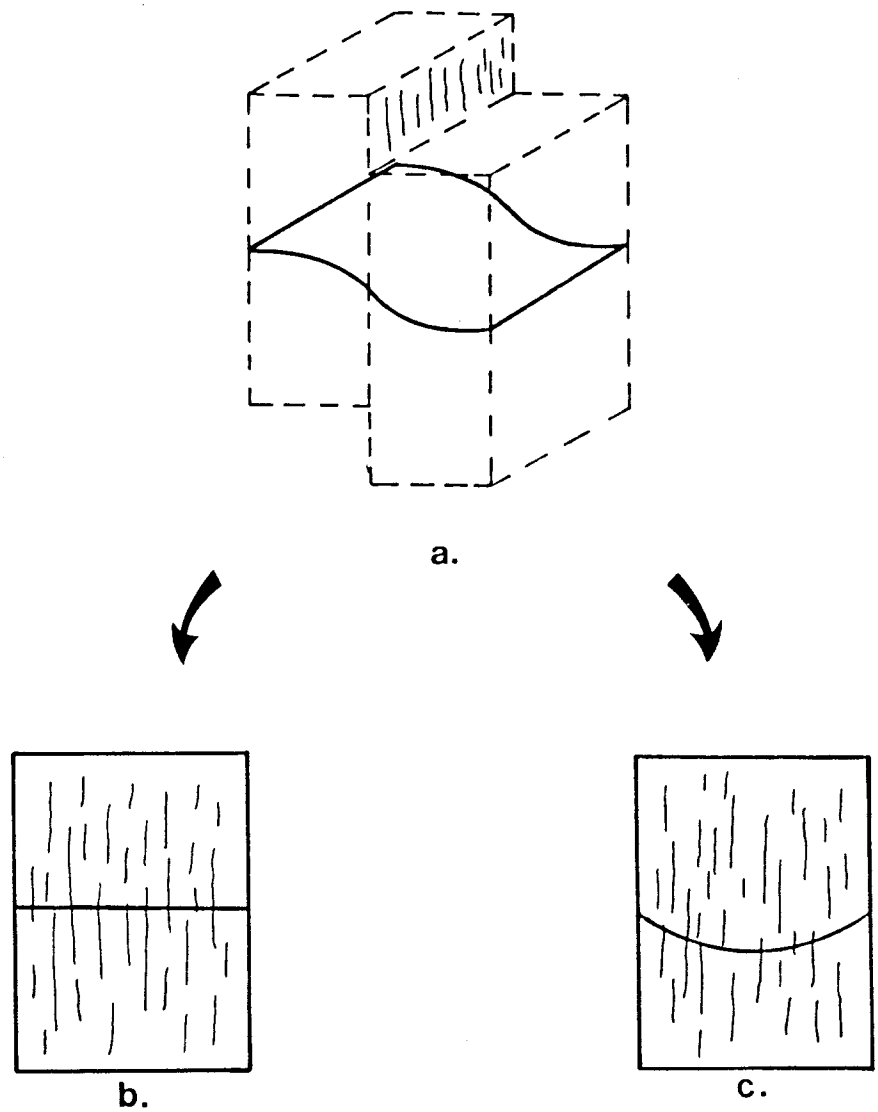

Figure 26. Different marker line responses to a homogeneous slip displacement (b), and a heterogeneous slip displacement (c) on sliding surface. (a) shows the orientation of the marker plane.

and 26b, respectively. Figure 27 shows the marker of PS-061-RL after a slip displacement of 3.75 mm. This marker line was not bent, but remained more or less straight during slip, and thus indicated an equal displacement across the whole width of the sliding surface. There is, however, a heterogeneity in strain distribution along the long edge of the sample (figure 28). In the experiments PS-066 and PS-067 a marker grid instead of a single marker line was scratched on the outer faces of the samples. As shown in figure 28, the dislocation of the marker grid indicates different responses of the pyrophyllitic material to increasing shear strains at different positions along the sample. More than one slip plane is present. In these two experiments the marker lines nearer to the edge of the sample were already offset while the marker lines at the center were still only bent, without offset. Figure 29 shows the outer face of the sample PS-056-R containing a main sliding surface and small shear bands in a C'-orientation, running at a shallow angle to the main plane. It was possible to recognize the order in which the main sliding surface and the shear bands formed. The shear bands always formed first and nucleated especially at the two edges of the samples. With further displacement, parts of these shear bands linked up to build the main sliding surface.

These observations, combined with those obtained from thin sections, can be used to propose a model for the origin of the ridge-in-groove type lineation, as follows.

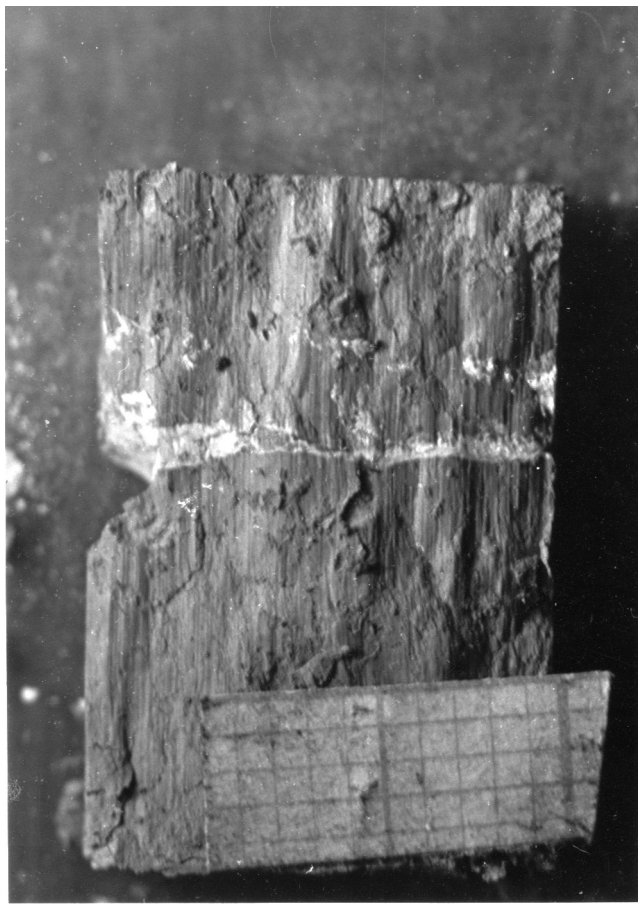

Figure 27. Trace of marker plane on slickenside as obtained in experiment PS-061-RL, indicating a rather homogenous slip displacement on the slickenside. The upper, removed block moved up with respect to the sample shown. Scale grid is in mm.

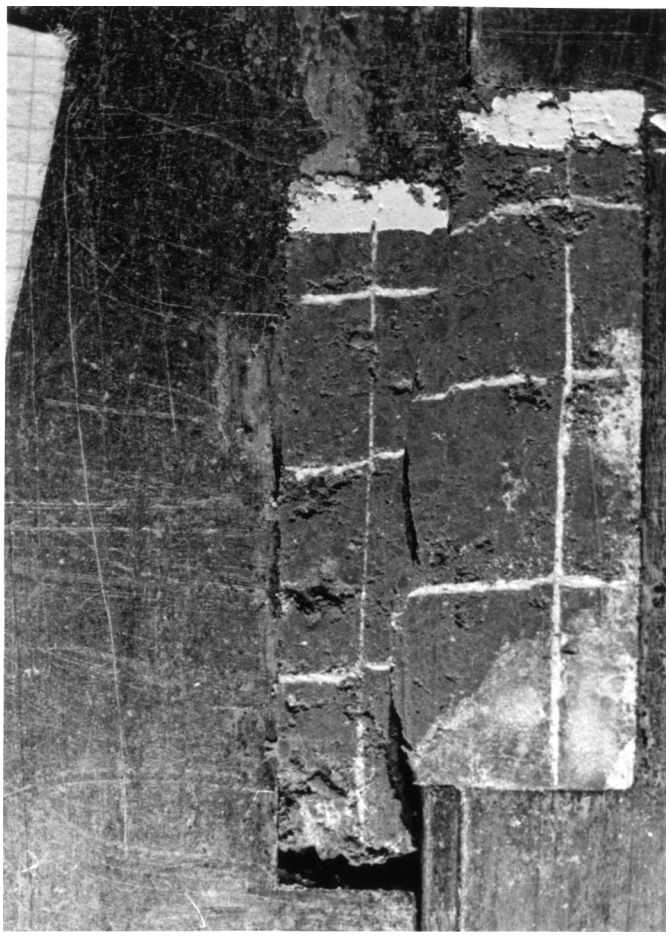

Figure 28. Different offset of the marker lines at the sliding surface. Note the void formation. Scale in mm. Experiment PS-067-R.

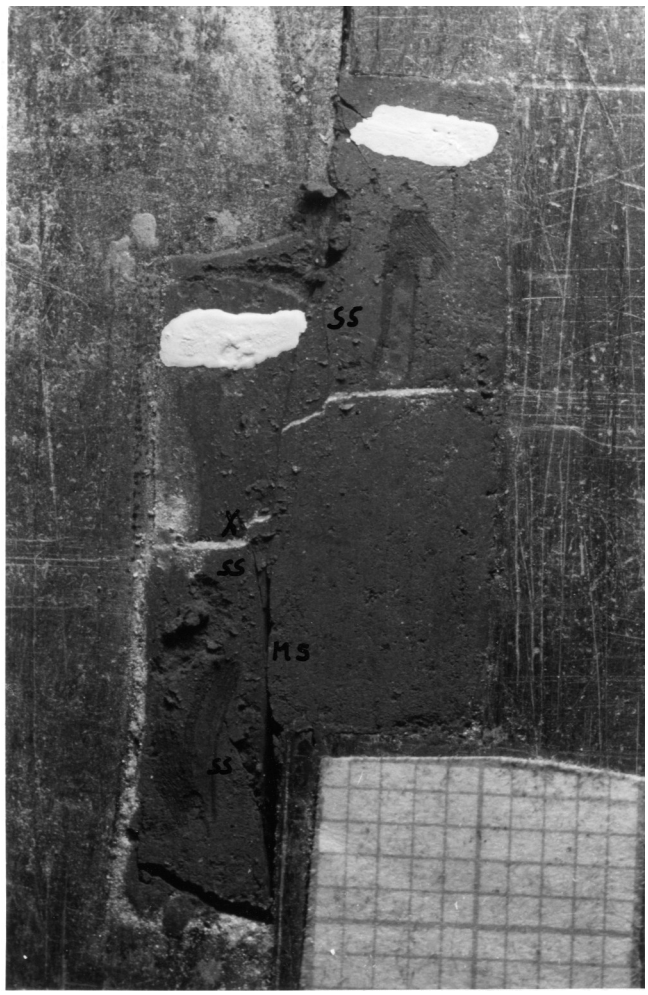

Figure 29. Main sliding surface, MS, and second-order slip planes, SS. 5.2 mm total displacement. At X, note the normal fault-like offset along one second-order slip plane. Marker grid is in mm. Experiment PS-056-R.

3.2.6.1. A model

In the experimentally deformed material, the ridge-in-groove type lineation developed only on surfaces which propagated through the intact, still cohesive clay, and not on surfaces separated prior to an experiment. The following observations were made: (i) more than one slip plane developed during an experiment, (ii) the marker lines on the outside of the samples bent, (iii) a strain modified fabric was recognized in the thin sections of the deformed pyrophyllitic clay samples, and (iv) striated slip planes in a C'-plane orientation were recognized in SEM-photomicrographs. According to the model proposed (figure 30) the ridge and groove formation occurs while the material still behaves plastically and is not related to frictional sliding.

Figure 28 showed voids present at the ends of the samples. Therefore, compaction must have occurred in the material next to the voids. Coincident with the experimental observations, C'-planes develop there first. The material closer to the middle of the sample can sustain shear strains longer, and the initiation of C'-planes occurs at a later time. For this reason, the heterogeneous strain distribution along the sample as observed in PS-066 and PS-067 has to be expected.

With further sliding the C'-planes cannot sustain the increasing shear strain anymore, and the C-plane, the main

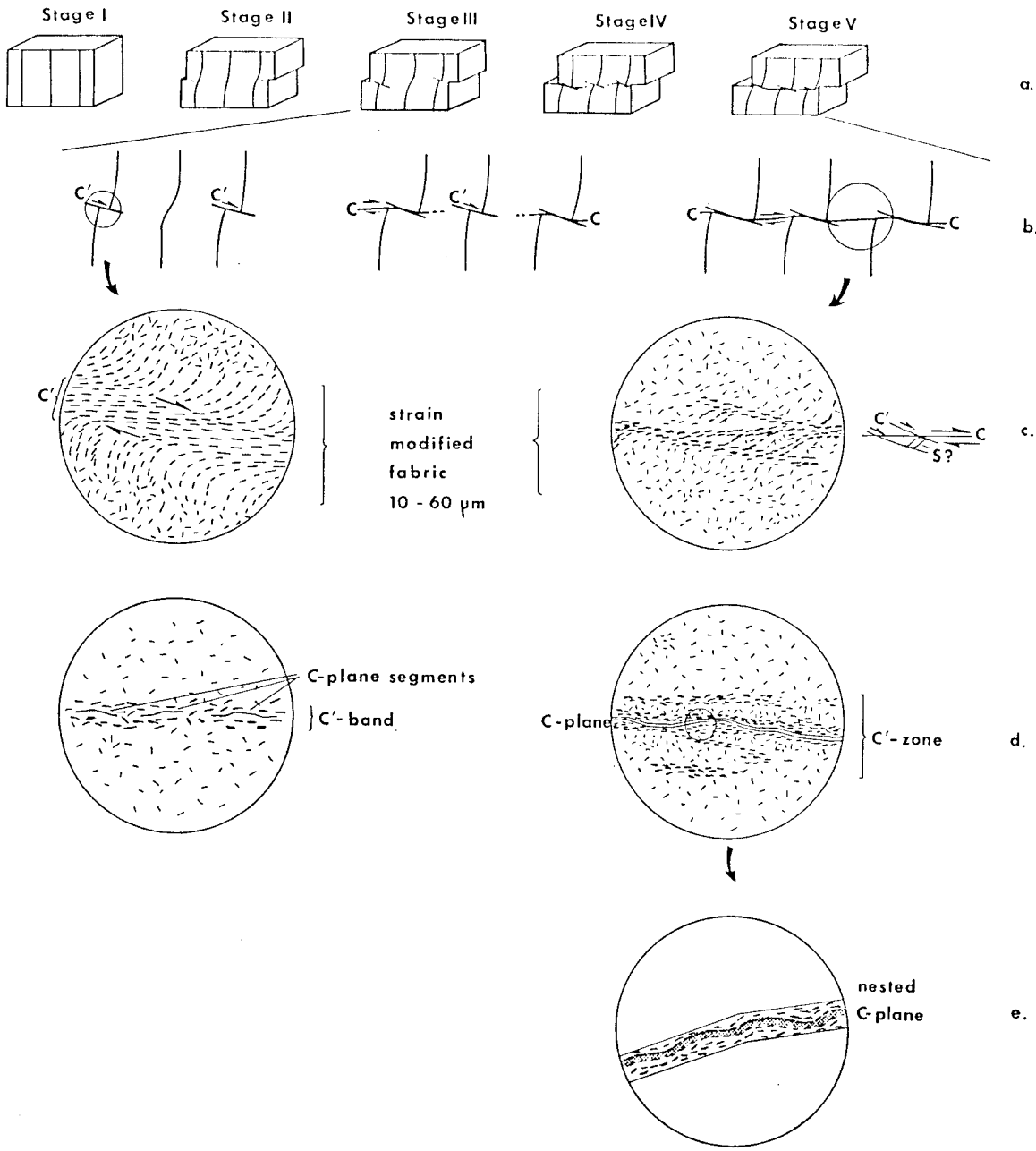

Figure 30. A model of the temporal sequence for the development of the slickenside of the ridge-in-groove type lineation (a). (b) Close-up of the stages III, IV, and V in (a) shows the marker line behavior. The arrows indicate at which planes sliding occurs. (c) View parallel to the sliding direction and perpendicular to the slickenside. At stage III shear bands and eventually S-planes developed, whereas at stage V shear bands, S-planes (?), and a C-plane are present. (d) View perpendicular to the lineation. At stage III a shear band with nucleated and propagating C-plane segments is present. At stage V a C'-zone is present as well as a fully developed C-plane within this zone. (e) Close-up of (d) showing the orientation of phyllosilicates next to minor ridges and grooves. Nesting occurs.

sliding surface, starts to propagate. It is suggested that this will occur preferentially at positions where the (001) planes of the phyllosilicates are more or less horizontal, and parallel to the bulk slip direction. This implies that the propagation of C-plane segments will start at different locations of high strain concentrations throughout the whole sample.

In a view perpendicular to the sliding direction, already nucleated C-plane segments are shown within a C'-band (figure 30d). The questions to answer are, how these C-plane segments propagate in a direction parallel to the slickenside and perpendicular to the slip direction, and how they finally link up to form a continuous, throughgoing C-plane. It is suggested that when C-plane segments propagating along slip-parallel (001) planes come to phyllosilicates whose (001) planes are inclined to the orientation of the propagating C-plane segment, the C-plane segment will propagate along the (001) planes of those inclined segments which offer the least resistance to sliding, and thus will change orientation. This will preferably take place on pyrophyllite flakes whose (001) planes are inclined the least to the slip plane but are still parallel to the slip vector. C-plane segments will propagate along these phyllosilicates within the C'-zone until either two propagating segments link up and form a lateral ramp or one propagating C-plane segment comes to phyllosilicates with a better orientation for

sliding, and changes direction again (fig. 30). Both cases explain the ridge and groove morphology on the final slip plane. Consequently, ridges and grooves are already present before a possible transition into frictional sliding conditions and the offset of the marker line occurs. This explains the "excess-length" property. At the stage where the marker line becomes offset, ridges and grooves were already present in the sample. Therefore, the "excess-length" property is expected in the context of this model.

However, the model still has one weak point: it explains the ridge and groove morphology perpendicular to the slip direction, but not necessarily why ridges and grooves propagate parallel to the slip vector. A possibility to explain this would be that the basal plane orientation of the phyllosilicates is more or less consistent in all of the C'-bands in the sample, and facilitates a slip-parallel propagation of a "ridge and groove shaped" C-plane. Grains, highly misoriented to the slip-parallel propagation direction might lead to an abrupt groove or ridge termination, or to the occasionally observed fact that ridges turn into grooves, and vice versa. This might also explain why some grooves and ridges of this type of lineation are shorter or longer than others. This idea could be checked by making serial thin sections perpendicular to the striations and recording the phyllosilicate orientation in the thin sections.

As shear strain increases further, a rotation of the

phyllosilicates into a strong preferred orientation of the (001) planes will become enhanced. A rotation is indicated by the strongly bent phyllosilicates with undulose extinction.

If the material is no longer able to accommodate the increasing shear strain by continued ductile deformation, then frictional sliding between the hangingwall and the footwall blocks will take place along the former C-plane.

Finally, this model can explain the nesting property between hangingwall and footwall blocks. After the cohesive forces between the phyllosilicates are broken, sliding occurs along the ridge and groove shaped former C-plane. Since less shear stress is necessary for slip to take place along the ridge and groove shaped surface than in the still intact material, further sliding will occur probably on the former C-plane and its ridge and groove shape will be preserved.

3.3. Twist experiments

The rotational experiments (Table IV) were carried out on solid pyrophyllite, and yielded frictional striations. They were performed to investigate the influence of displacement, normal stress, and slip-rate on the morphology of the striations and on the gouge material developed during an experiment.

In all of the experiments referred to below, the future sliding surfaces of the pyrophyllite blocks were polished with 600 and 1000 grits prior to the experiment.

In the cases where the amount of gouge material produced during an experiment was measured the gouge was removed from the sliding surface and weighed.

A dependence of the normal stress magnitudes on the three different types of pure Andersonian faults was pointed out by Sibson (1974). A simple Mohr circle construction (fig. 31) can be used to demonstrate this dependence. For pure Andersonian faults one of the principal stresses is always oriented perpendicular to the Earth's surface. This principal stress (σ_1 in the case of normal faults, σ_3 for reverse faults, and σ_2 for strike-slip faults) is identical to the lithostatic pressure at any given depth. The principal stresses for each fault type can be plotted on the horizontal axis of a Mohr diagram, and the three Mohr circles be drawn.

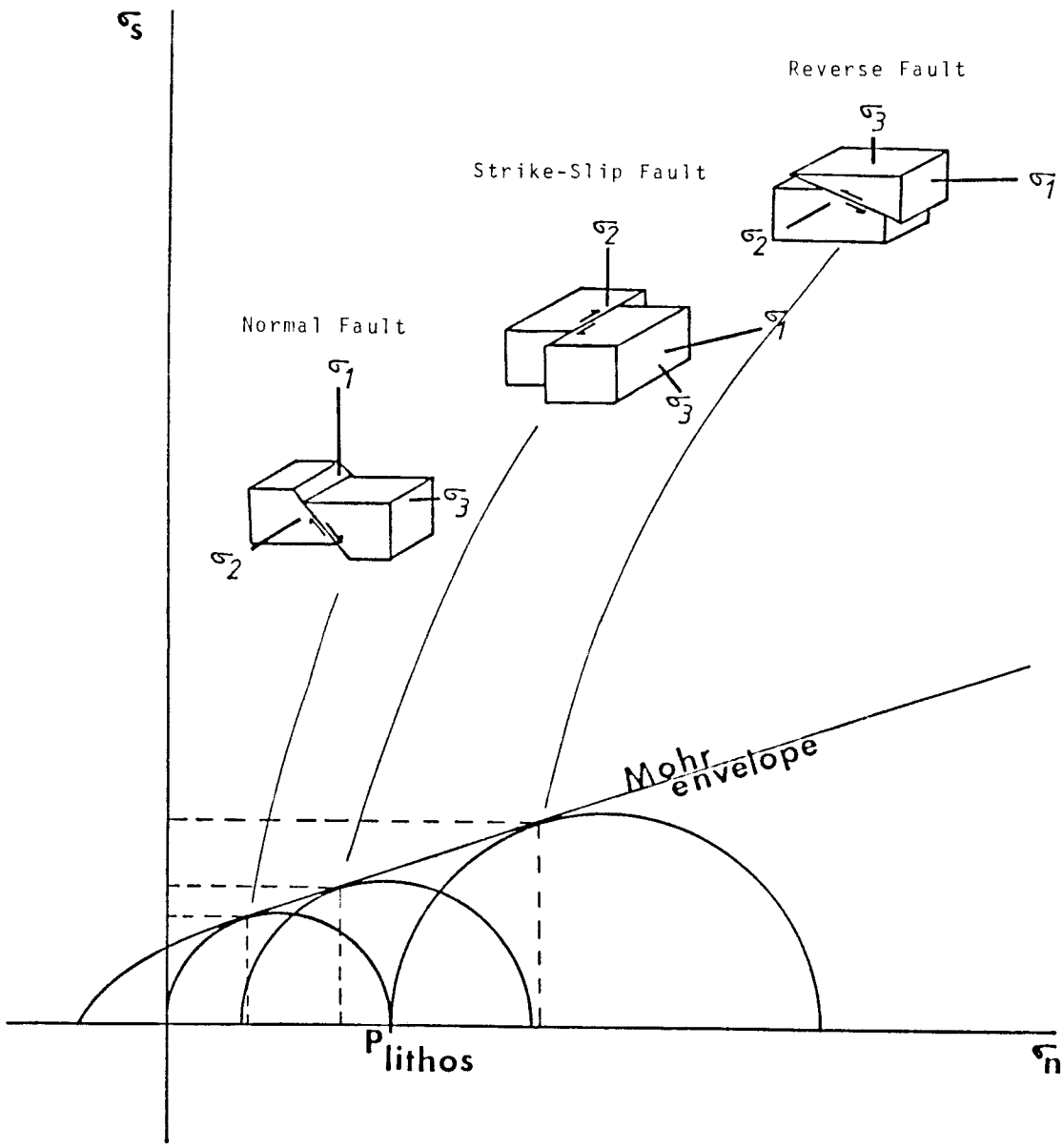

Figure 31. Mohr-circle construction showing the dependence of normal stress and shear stress magnitudes on the fault type. P_{lithos} is the lithostatic pressure.

Table IV. Experimental data obtained from twist experiments. (*) Maximum linear displacement at the sample rim.

Experiment	normal stress [bar]	[MPa]	displacement [°]	[mm]*
PS-017	224	22.4	?	?
PS-018	336	33.6	?	?
PS-019	224	22.4	?	?
PS-020	224	22.4	?	?
PS-023	112	11.2	?	?
PS-024	224	22.4	40	6.6
PS-025	336	33.6	5	0.8
PS-027	336	33.6	40	6.6
PS-029	403	40.3	60	10.0
PS-030	45	4.5	60	10.0
PS-031	90	9	55	9.1
PS-032	134	13.4	0	0
PS-032a	403	40.3	0	0
PS-033	134	13.4	10	1.7
PS-034	134	13.4	60	10.0
PS-035	179	17.9	47	7.8
PS-036	269	26.9	45	7.5
PS-037	269	26.9	51	8.5
PS-038	314	31.4	15	2.5
PS-039	314	31.4	20	4.2
PS-040	67	6.7	?	?
PS-040a	179	17.9	?	?

The magnitudes of the normal stresses acting on the fault planes are given by the tangential points of the Mohr circles and the Mohr envelope. It can be seen that σ_n (normal fault) $< \sigma_n$ (strike-slip fault) $< \sigma_n$ (reverse fault) for any given Mohr envelope with a positive slope, at a given depth. The shear stresses show the same pattern, σ_s (normal fault) $< \sigma_s$ (strike-slip fault) $< \sigma_s$ (reverse fault).

This explains that if there is any dependence of the geometry and morphology of fault plane striations on the normal stress, differences in the morphology of the striations would be expected to occur on normal, strike-slip, and reverse fault planes that were formed in the same lithology at the same depth, provided that the pore fluid pressure and slip rate were also identical at this depth.

3.3.1. Effects of displacement on surface features

At the same normal stress acting on the apparent area of contact, striations become more "evolved" and obvious with displacement. Figure 32a, PS-025, shows the appearance of a sliding surface after a rotation of 5^{o}; figure 32b, PS-027, shows a surface after 40^{o} rotation. Both experiments were carried out at the same normal stress of roughly 330 bars. The striations developed on PS-025 are very fine and shallow, and their morphological appearance does not seem to vary along the sliding surface, except that their length increases outwards. In experiment PS-027, not only are these fine striations present, but also broader and deeper grooves. The grooves occur mainly closer to the margin of the pyrophyllite block than to its center. Most of the grooves have irregular and indefinite margins. The same feature as observed in PS-027 was also present in several other experiments (PS-024, PS-029, PS-031, PS-034, PS-035). All of these experiments were rotated more than 40^{o} and revealed a "striation gradient" along the sliding surface. Experiments carried out with small displacement only (PS-025, PS-033, PS-038) do not have this gradient. By striation gradient I mean that striations close to the center are very fine and shallow scratches with very sharp edges, whereas striations closer to the marginal region of the slip surface are broader and deeper, and have less sharply defined margins than those

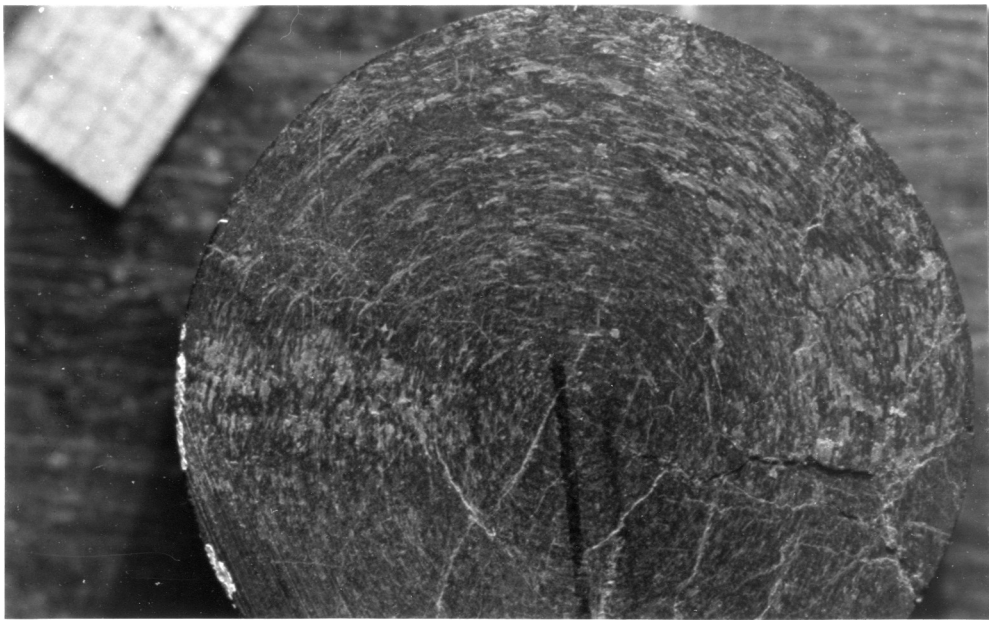

a

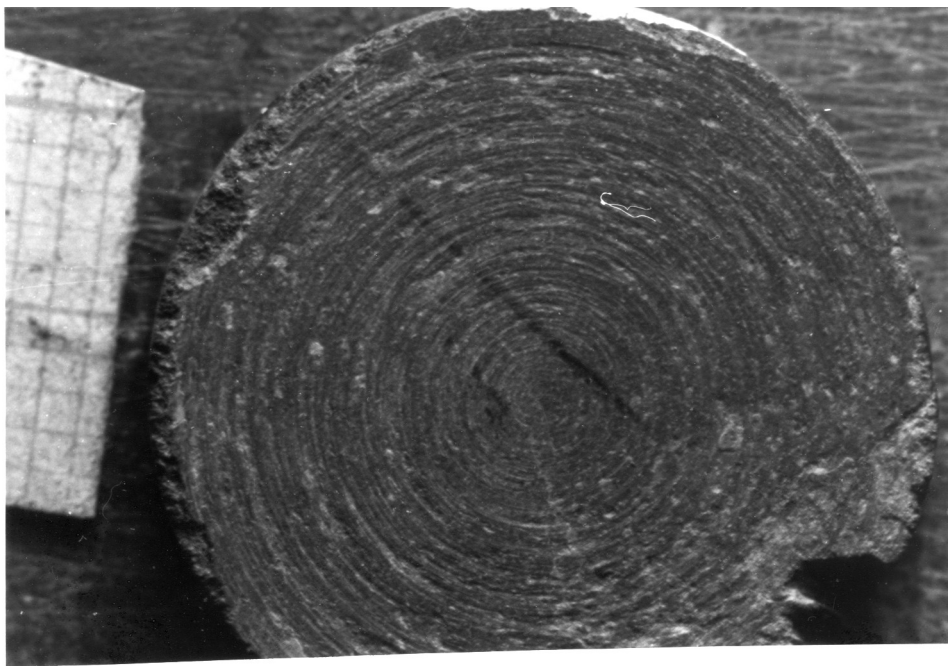

b

Figure 32. Surface appearance of PS-025 (a), and PS-027 (b) after rotations of 5^{o} and 40^{o}, respectively. The opposite blocks moved counterclockwise. Marker grid is in mm.

closer to the center. These grooves have sometimes striated bottoms. Such a striation gradient can be seen in figure 32b; whereas figure 32a shows a surface without an obvious change in the morphological appearance of the striations.

Polishing, regardless of the displacement, is not obvious on these surfaces. Especially near the marginal region, where the maximum displacement occurred and therefore polishing was to be expected, only grooves and fine striations are present.

3.3.2. Effects of normal stress on surface features

The striation gradient seems not to be influenced by the magnitude of the normal stress. The experiments PS-029, PS-030, PS-034 (all with a 60^{o} rotation), and PS-031 (55^{o} rotation) were carried out at different normal stresses, 403 bars, 45 bars, 134 bars, and 90 bars, respectively. In all of these experiments an outward transition from fine striations to broad grooves is obvious. The appearance of the striations and grooves, however, seems to vary with different normal stress magnitudes.

During PS-031 (90 bars) very fine, sometimes shiny striations developed as well as a few grooves. Patches of compacted and striated, shiny gouge material were present. PS-034 (134 bars) gave more or less the same result, except that more gouge material developed. The fine striations seemed to be more narrowly spaced than those in PS-031. Small

steps facing the movement of the opposite block developed in experiment PS-034. The appearance of the sliding surface produced during experiment PS-029 (403 bars) differed dramatically from the other two experiments. This surface is heavily fractured, and prominent steps on secondary, striated slip planes (R- shears ?) developed (figure 33). The steps oppose the movement of the opposite block. The surface became more deeply eroded and many more grooves were present than in the other experiments (figure 34).

3.3.3. Effects of slip-rate on surface features

Experiments PS-036 (45^{o} rotation) and PS-037 (51^{o} rotation) were carried out in order to obtain some insight into whether the slip-rate, under otherwise constant conditions, influences the morphological character of the slip plane.

PS-037 was carried out at a significantly higher slip-rate (approximately 100^{o} per second versus 5^{o} per second as in PS-036). In the case of slow twisting, PS-036, very fine and continuous striations developed. A weak striation gradient is present. The surface has a shiny luster and patches of striated, adhesive-type gouge (c.f. section 3.3.4.) occur. As seen in figure 35, the surface appearance is distinctly different from that of the high slip-rate experiment. The surface is not shiny, it is much more deeply

Figure 33. Steps facing the movement of the opposite block. Movement of the opposite block was counterclockwise. Marker grid in mm. Experiment PS-029.

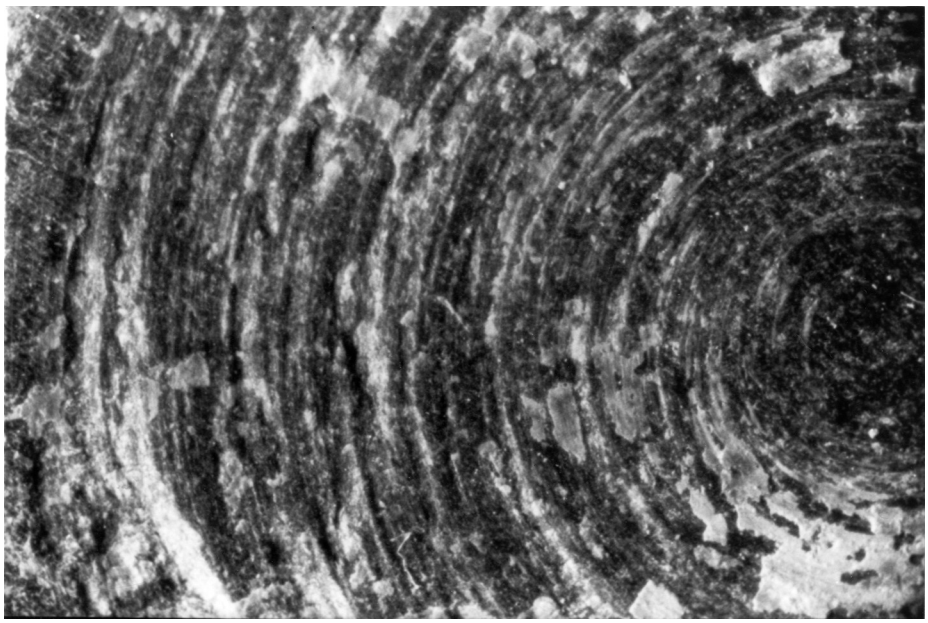

Figure 34. Surface appearance of PS-029 showing deeply excavated grooves. The opposite block moved counterclockwise. The field of view is 9 mm wide.

a

b

Figure 35. Sliding surfaces of (a) PS-036 (45° rotation), and (b) PS-037 (51° rotation). The slip-rate was approximately 20 times lower in (a) than in (b). The areas labeled AG on figure 35a show the adhesive type of gouge material. The opposite blocks moved counterclockwise. Specimens are 3/4 inch in diameter.

excavated, and broad grooves with striated bottoms occur. The groove edges are less sharply defined than those of the striations from PS-036 and cause the very rough surface appearance. More gouge material was produced, however, almost entirely of the abrasional type (see section 3.3.4.) only.

The same pattern, although less clearly seen, was obtained by the low slip-rate experiment PS-038, and the high slip-rate experiment PS-039. Due to these qualitative results, we intend to build a more sophisticated experimental set-up to investigate this apparent slip-rate sensitivity further.

3.3.4. Effects of slip displacement and normal stress on gouge material

At least two different types of gouge could be distinguished on the greyish sliding surface: (1) dull-looking gouge which consists of comminuted, loose grains of probably pure abrasional origin, and (2) light, shiny patches and flakes of compacted, mutually adhering individual grains. The first type occurred mainly to the margins of the samples, whereas the second type did not develop at a preferred location on the sliding surface. A good example of the first type of gouge was obtained in the experiments PS-040 and PS-040a, as shown in figure 36. The deeply eroded pyrophyllite surface is almost entirely covered with abrasive

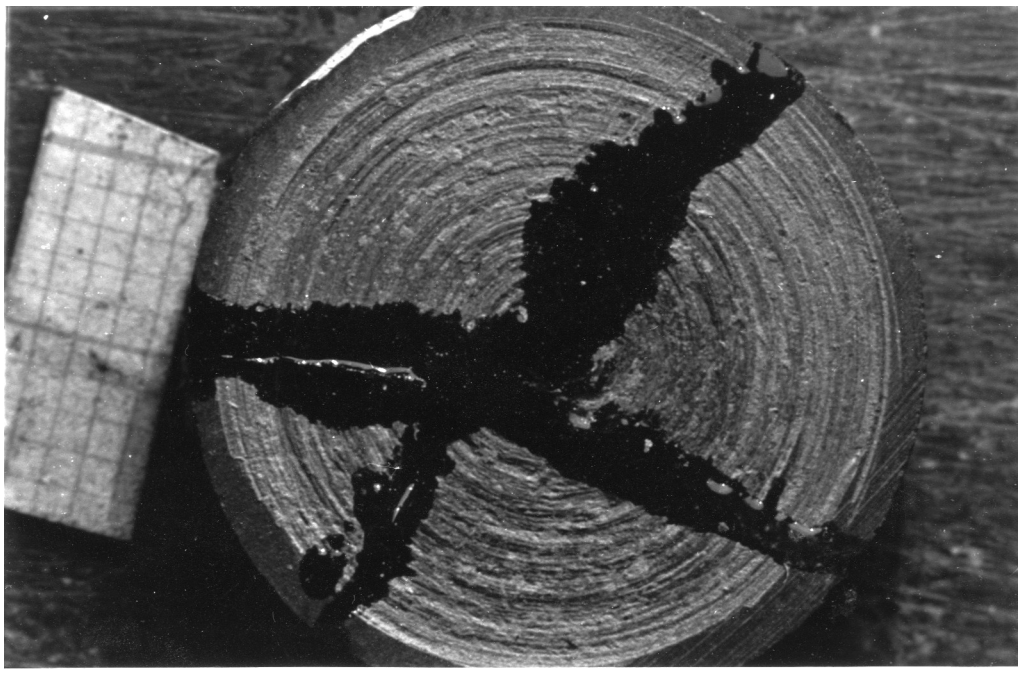

Figure 36. Abrasive gouge produced during shearing of pyrophyllite against sandpaper (60 grit) in experiment PS-040a. Movement of the sandpaper was counterclockwise. Marker grid is in mm. Black regions are epoxy.

gouge material. In these two experiments, pyrophyllite was slid past sandpaper (60 grit). No compaction of the gouge material occurred. As observed during the experiments, low normal stresses favour the formation of the first type of gouge, which will be called "abrasive gouge". High normal stresses lead to the formation of the second type of gouge, called "adhesive gouge". This type is itself occasionally striated.

Displacement is likely to be one factor that controls the amount of gouge material produced during sliding. This displacement dependence is indicated by the experiments PS-033 and PS-034, both carried out at the same normal stress. During experiment PS-034, with 60° rotation, approximately 12 times as much gouge material was produced as during the 10° rotation experiment of PS-033. The numerical value itself might be obscured by the fact that the contact area was smaller during PS-033 than in PS-034. This was caused probably by a different surface finish of the samples. The degree of mutual contact between the two sliding surfaces is indicated roughly by the part of the previously smooth surface that became striated and/or eroded.

A possible influence of normal stress on the amount of gouge material is indicated in figure 37. Due to the lack of sufficient data and the slightly different amounts of rotation, only the general trend of this graph will be discussed. At low normal stresses there is a rapid increase

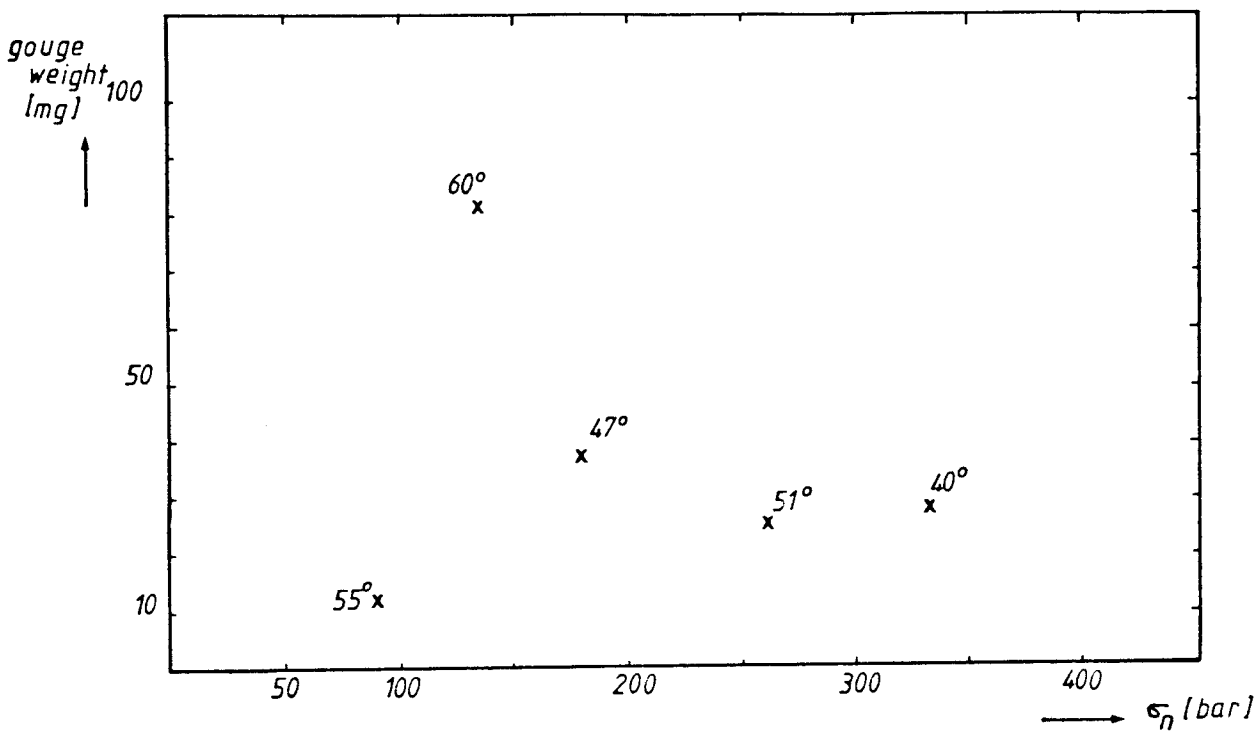

Figure 37. Gouge weight versus normal stress. Numbers in degree indicate the amount of rotation.

in the amount of the gouge material produced occurs. After an apparent peak at intermediate stresses, a reversed trend can be recognized. Further experiments in the 40^{o}-60^{o} range at 140 bars are necessary to prove or disprove this apparent peak at intermediate normal stresses. Figure 38b shows Sasada's (1984) wear versus sliding speed or load graph, which coincides with the trend recognized in figure 37. Even though, Sasada did not mention under which experimental conditions this graph was obtained, I assume that it shows the dependence of the amount of wear produced on sliding speed or load at constant sliding displacement. Furthermore, I assume that his wear versus sliding distance graph (figure 38a) was obtained at constant speed.

In connection with the gouge material, it was noted that the luster of a surface became enhanced where compacted gouge material was present on this surface.

3.3.5. Sense-of-shear indicators

Useful sense-of-shear indicators were found to be grooves with their ploughing tool still at the down-slip end, curled-up tips of striated adhesive gouge material, tapering-out striations, and steps facing the movement of the opposite block. Curled-up tips of adhesive gouge material sometimes face either way: either with or against the movement of the opposite block. But in 60-70% of observed

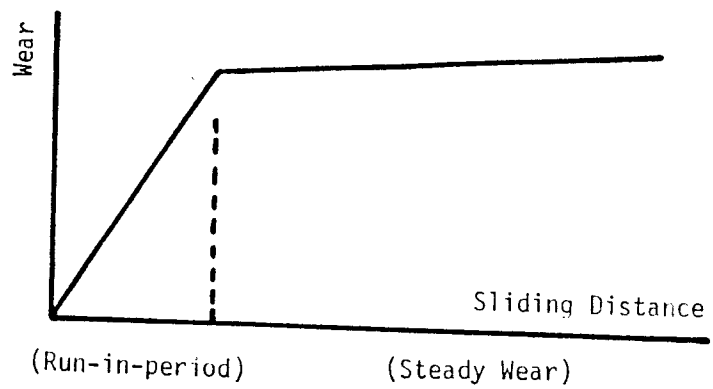

a.

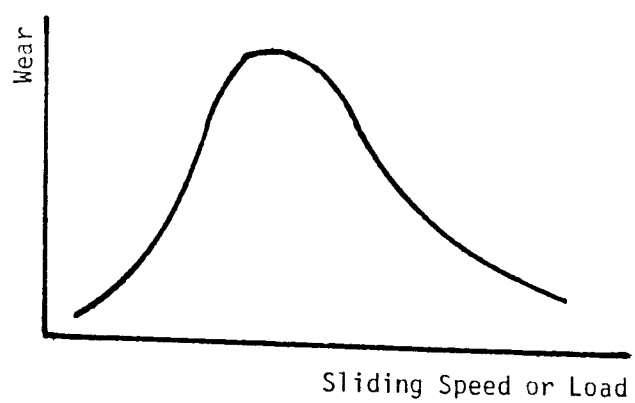

b.

Figure 38. (a) Wear versus sliding distance, (b) wear versus sliding speed or load. Redrawn from Sasada (1984, figures 2 and 3).

cases, the tips point in the direction opposite to the movement direction of the opposite block. Figure 39 shows these sense of shear indicators.

3.3.6. Discussion

Striations "evolve" with displacement. Low displacements yielded fine and shallow scratches, whereas broader and deeper striations and grooves developed at higher displacements. This is expected as long as striations and grooves are formed by a frictionally dominated asperity ploughing mechanism. But, as pointed out during the description of the ridge-in-groove type above it is not necessarily characteristic for such a mechanism.

A striation gradient becomes established after a certain amount of displacement, but seems to be independent of the magnitude of the normal stress. The origin of such a gradient is likely to depend on linear displacement, shear strain, shear strain-rate, or on some combination of these parameters. Further experiments where the parameters mentioned above can be controlled better, and the rotation is not carried out by hand with a pipe-wrench, might provide more insight into the formation of this striation gradient and its dependence on these parameters.

At high normal stresses, the surface becomes more deeply eroded than at low normal stresses, and grooves rather than

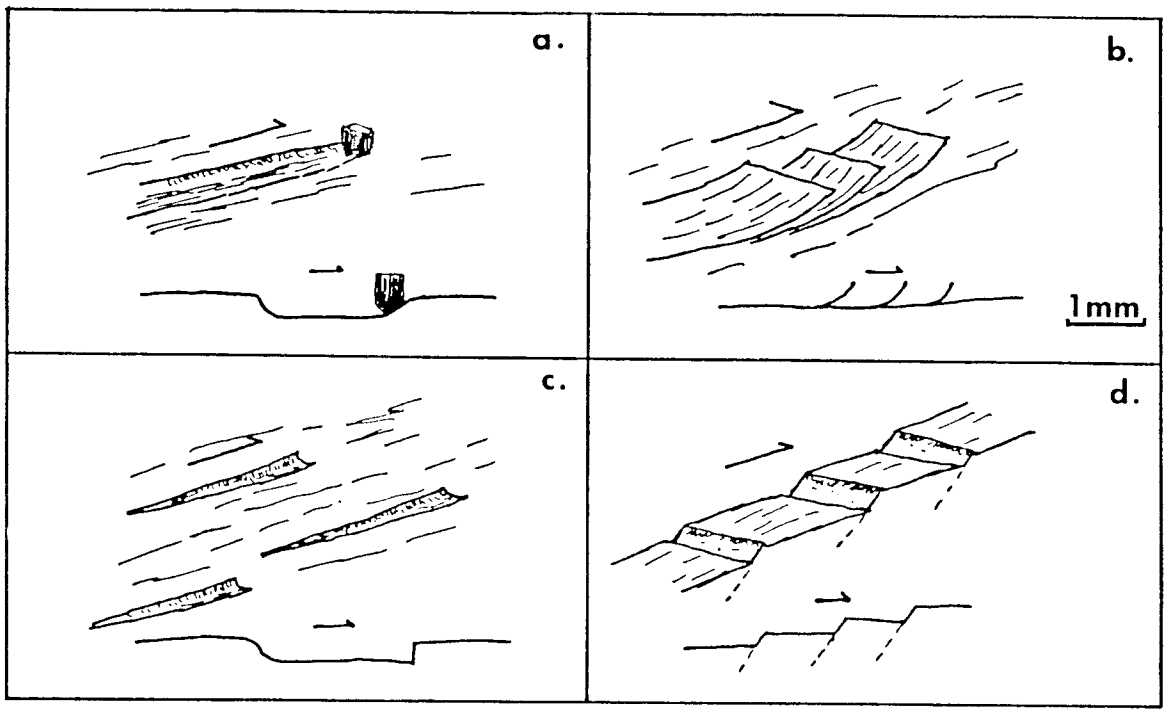

Figure 39. Sense of shear indicators in plane view, and parallel to the slip direction and perpendicular to the slickenside. (a) Grooves with the ploughing tool at one end, (b) curled-up tips of gouge material, (c) tapering-out striations, and (d) steps facing the movement of the opposite block.

striations are present. A similar pattern can be observed when the surfaces of the high slip-rate and the more shiny surfaces of the low slip-rate experiments are compared.

The different appearance of the abrasive and adhesive gouge might be related to different normal stress magnitudes on the sliding surface. Since there are no perfectly smooth surfaces, the initial contact between two surfaces will be restricted to a few points. At least two different types of processes, depending on the normal stress magnitude, can be envisaged. With the onset of sliding, and at low normal stress conditions, scratching will occur at the contact points and produces abrasive gouge material. At higher normal stress magnitudes, the initially abraded debris material becomes compacted into flakes. These compacted patches of gouge are sheared off with continued sliding. This could lead to the formation of the curled-up gouge material flakes as described above. In some experiments, for example during PS-034 (134 bar), both adhesive and abrasive gouge developed. The occurrence of the two types of gouge material might be indicative of transitional normal stress conditions. At even higher normal stresses another type of "gouge" can develop. This was shown by the experiments of Friedman et al. (1974), where local welding occured at sufficiently high normal stresses at the contact points between the two sliding surfaces. It should be noted, that this last process does not necessarily require shearing for the formation of gouge

material, as do the two other cases. The formation of gouge without shearing was not observed during experiments PS-032 and PS-032a.

The amount of gouge material produced is likely to be controlled by at least two parameters: the amount of displacement and the magnitude of normal stress. The displacement influence can be explained as follows. During the first sliding increments, asperities score into the surface. During further sliding they become worn down, and abraded gouge material is generated. This explains how a large amount of gouge material will be produced after a few increments of sliding. With ongoing sliding, fewer asperities will be present due to the increase in contact area, and therefore less gouge material will develop. This is a well-known feature to tribologists (tribology is the study of friction, lubrication, and wear). For example, Sasada's (1984) wear versus sliding distance graph (figure 38a) shows a steep increase in wear material produced at low sliding distances, and a steady-state behaviour at intermediate and higher displacements. He calls the first sliding increments during which large wear particles are created the "run-in period", and the later sliding increments during which fine wear particles are produced the "steady-wear period".

If the normal stress controls the amount of gouge material produced the following explanation is possible. At low normal stresses, dominantly brittle processes are active

and are responsible for the high amount of gouge produced. At higher normal stresses, a transition into a more ductile behaviour of the material is likely to occur and thus, less fault gouge material will be produced. This idea is probably basically right, but it certainly cannot be proved with these few data.

In these short term experiments, precipitational or dissolutional processes can be ruled out as a mechanism responsible for the formation of the striations observed. Furthermore, trails or spurs were not present, and nesting of the sliding surfaces could not be demonstrated. It can not be ruled out that nesting occured within the gouge material. However, I could not prove or disprove this possibility, since no "hangingwall or footwall gouge parts" belonging together could be identified with absolute certainty.

It is concluded that the striations on the pyrophyllite surfaces observed in these experiments were frictional in origin.

One last remark on these experiments. They led to some ideas about the formation of fault gouge material, and the parameters possibly controlling the amount of gouge material produced. But they were not really useful, or even succesful, in answering the questions about the origin and significance of slickensides and their striations, especially with reference to the ridge-in-groove type lineation. By using better observation techniques such as scanning electron

microscopy, for example, better results and more information might be obtained about the significance of the striations produced in this type of experiment.

4. Investigations of naturally formed slickensides and slickenlines

In the introductory part of this thesis I wrote that slickensides and slickenlines might some day be used to infer slip magnitudes, slip rates, mode of sliding, depths of formation, etc., on fault planes and fold surfaces. In order to achieve this goal it is necessary to describe first the morphological and microstructural features of slickensided surfaces.

The ideal approach would be to describe these features in an environment where lithology and structural history are well known. In addition to knowledge about lithology, it is very important to know the slip rates and magnitudes, the orientations and magnitudes of the effective principal stresses, the age and depth of formation, etc., which lead to the formation of a slickenside. If all of these parameters were known, it would be feasible to do analytical comparative studies between slickensides at different locations where only one of the above-mentioned parameters varied. Such a comparative study would greatly improve our current understanding about the conditions of slickenside formation, and would be well suited for unravelling the sensitivity of slickensides and slickenlines to the parameters above.

However, in order to carry out such a study, suitable outcrops have to be found. This was the basic problem

involved with the work presented here. In none of the studied outcrops and quarries in West Germany or in New England could the desired ideal conditions be encountered.

However, localities can in principle be found where only one parameter is likely to have varied. For example, a fold hinge or a fault set with different displacements on the faults are probably good locations to study the effects of displacement on the morphology and microstructure of slickensides. Outcrops with different types of faults of the same age and more or less the same amount of displacement would be well suited to study an influence of the fault type on slickensides.

In a railroad cut near Glenmont, N.Y., the orientations of three different types of slickensides (slickensides with a phyllosilicate coating, slickensides with fibrous quartz, and slickensides with a glossy surface appearance) and their striations were measured. Approximately 90 measurements were taken. At this location, no dependence between the slickenside type and their orientations could be found, but all three different types measured had more or less the same orientation. It is not known, however whether the three different slickenside types are of the same age, or formed at different times.

This leaves us with a general idea about future research, however at the present stage the work on naturally produced slickensides and slickenlines is still at its beginning.

In the following chapter, surface features, as well as microstructural observations made in thin sections, are discussed.

4.1. Description of surface features on hand samples

The slickensides were collected in various lithologies from different locations in West Germany and New England. The locations of the samples are given in Appendix B. Slickenside dimensions, profiles, and nesting are described in the following chapter.

4.1.1. Demonstration of nesting

Three alternative techniques to demonstrate nesting between two opposite walls can be used. Two methods were described by Means (1987), and a third technique was developed during this study (c.f. chapter 3.2.2.).

These methods were applied to an Ordovician shaly mudstone from Latham, N.Y. (new roadcuts on NY Route 7 just E of junction with NY Route 9). Figure 40a shows footwall and hangingwall surfaces of this shale. Nesting can be checked when a cast of one surface is made and compared with the other wall. If the two surfaces nest, the morphology on the cast and that on the opposite original surface will match closely. This is shown in figure 40b. The casting material,

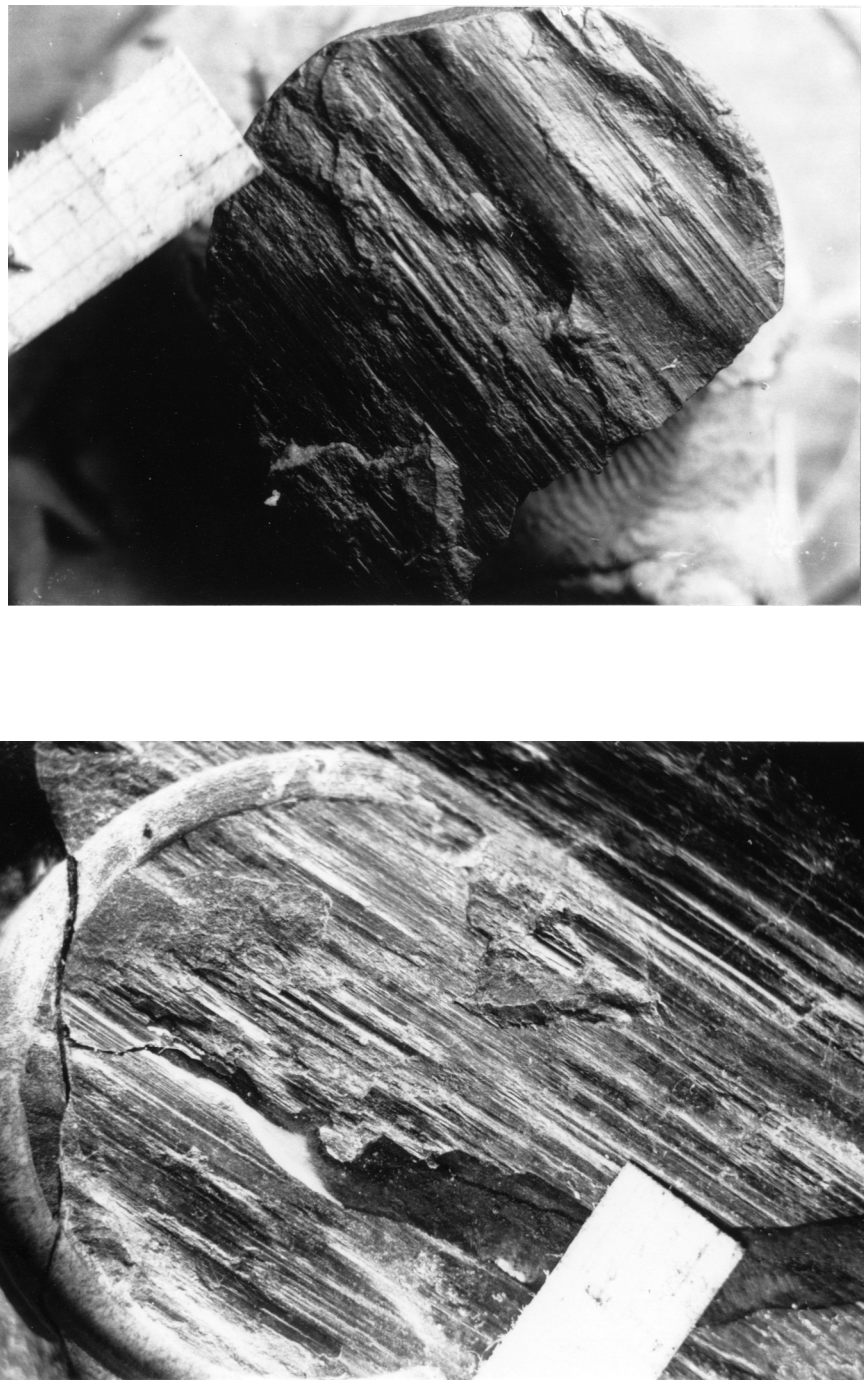

Figure 40a. Hangingwall (top) and footwall surfaces (bottom) of specimen L-1. Marker grid is in mm.

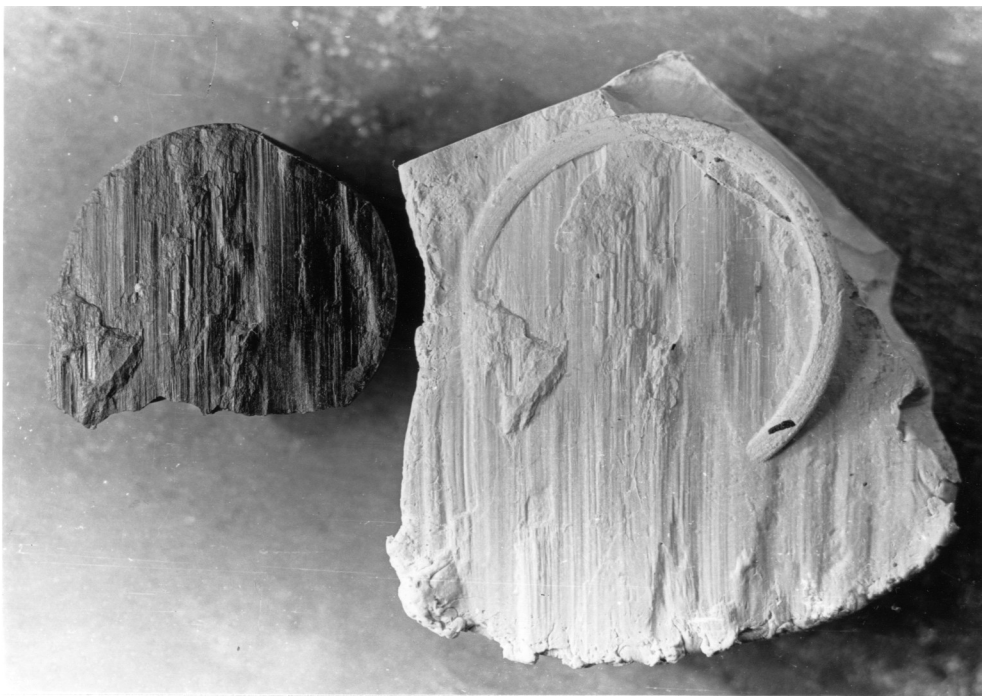

Figure 40b. Nesting is demonstrated by the close match of hangingwall surface and a cast of the footwall surface. Scale as indicated by the coin.

"K-Splint", was put into a beaker of boiling water, removed after it became plastic, and carefully pressed on the surface.

Mirror-images of the footwall and hangingwall surfaces can be obtained using the photographic method of Means (1987). Figure 41 shows a mirror symmetry of dark and bright stripes (Means, 1987; fig. 6) on a Latham sample.

The result of the reversed print technique explained above is shown in figure 42.

4.1.2. Profiles perpendicular to the sliding direction and angle measurements

The angles between the planar sliding segments, or facets, on a ridge-in-groove type lineated surface might be characteristic of one or even more of the parameters controlling sliding. For this reason, profiles were taken perpendicular to the sliding direction, and the angle between adjacent facets, the "interfacet angle", was measured.

The profiles were obtained in the following way. A thin layer of epoxy was applied onto the sliding surface. Next, a white ceramic cement ("Tile-Grout") layer approximately 5 mm in thickness was applied on this coated surface. This protected the slickensided surface during the cutting process. If the rock was very soft, a second ceramic piece was glued on the bottom of the specimen. This ensured that

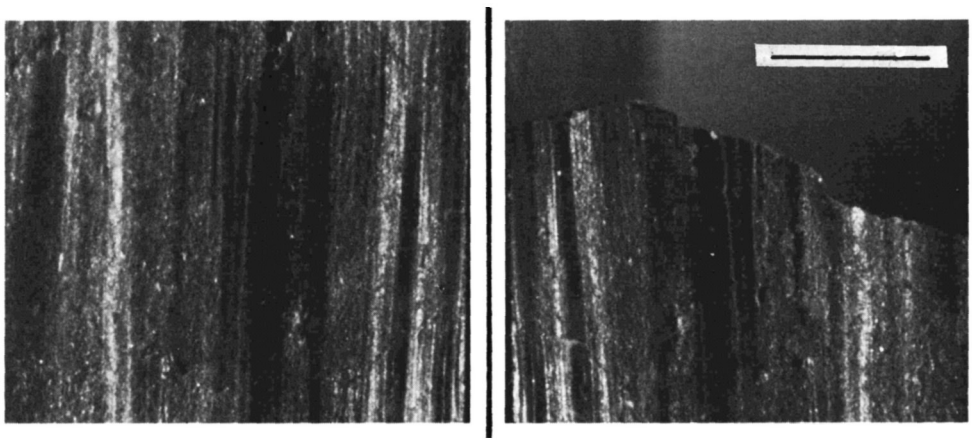

Figure 41. Demonstration of nesting by the mirror-image technique of Means. The specimen comes from the same location as the specimen in figure 40. Scale bar 1mm. From Means (1987, figure 6).

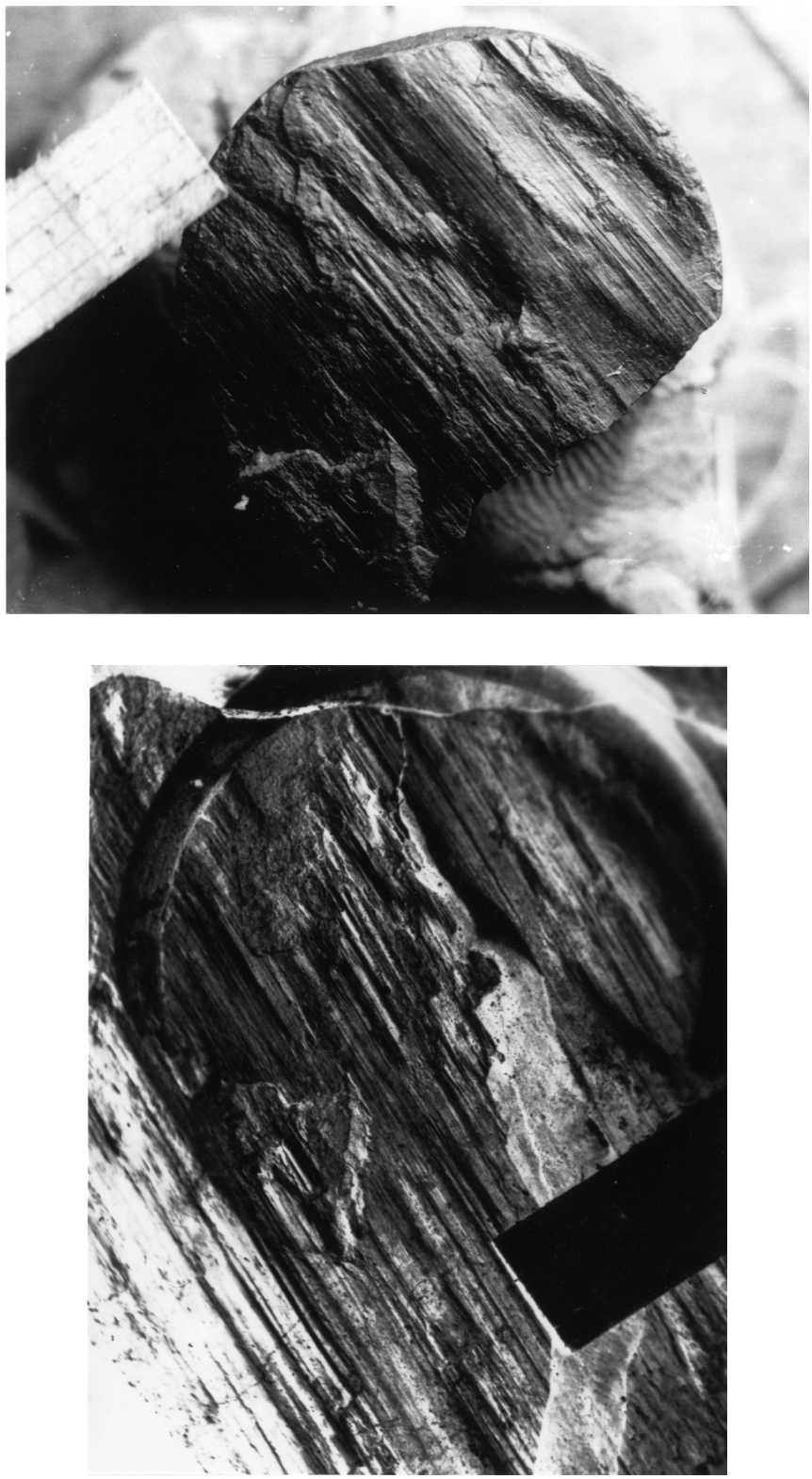

Figure 42. Demonstration of nesting using the reversed print technique. Same specimen as in figure 40. The specimen broke apart before the technique was applied and was glued together with epoxy. The epoxy causes the fuzzy appearance in the center of the reversed print.

the weak rock could be sliced into slabs. The prepared samples were allowed to dry at room temperature for 18-24 hours. Due to the dimensions of the sample chuck the maximum sample size was 3.5 cm long, 2.5 cm wide, and 2.0 cm high. The sample was sliced into slabs 0.635 mm thick using a low-speed saw (Buehler "Isomet"). The slabs obtained were then photographed, and the surface morphology was traced from the photographs.

Figure 43 shows two profile series from slickensides; figure 43a a hematitic fault rock breccia from Steep Rock, Ontario, SR-1, (this rock was obtained as a courtesy of H. Helmstedt, Queens University, Kingston, Ontario to W. Means); and figure 43b a fault rock breccia from Germantown, N.Y., GT-1. In both profile series a step- or cascade-like surface morphology is visible. The top and bottom segments of the ridges and grooves are made up of planar fault plane parallel segments that are mutually connected by planar segments inclined to the average fault plane, but yet parallel to the slip vector. The planar ridge and groove segments that cause the step-like, or faceted appearance of the whole fault surface are not expected in the context of the models traditionally used to explain the formation of slickenlines. In the figures 43b, V-shaped grooves are present in addition to the planar groove bottoms. These V-shaped grooves might be caused by asperities scoring the surface. If this interpretation is correct, it would imply that at least two

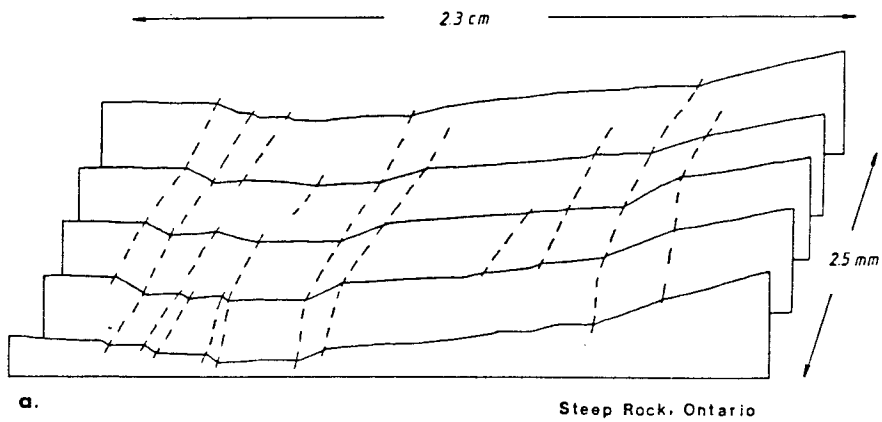

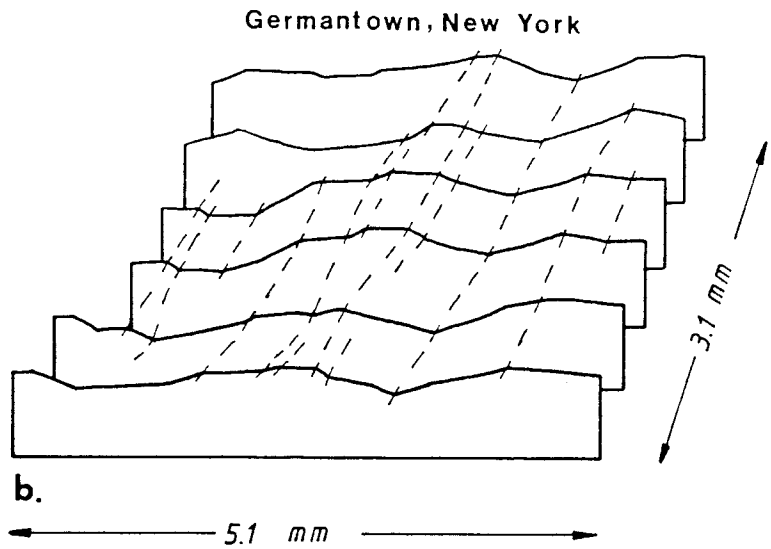

Figure 43. Profile series perpendicular to striation. (a) Specimen SR-1. (b) Specimen GT-1). Both profile series show fault surfaces made up of planar fault plane segments. The dashed lines connect the main inflection points. No vertical exaggeration.

different sliding processes were active on these surfaces. Nesting could not be proved for these samples, since the hangingwall blocks could not be collected. And, at the present stage we cannot be absolutely sure whether all faceted striations nest.

Interfacet angles were measured with a protractor on the profile series of the Steep Rock and Germantown samples.

The interfacet angle is the angle measured between two adjacent surface segments. The interfacet angle is indicated in the inserts of figures 44a and 44b. Figure 44a shows the distribution of the measured interfacet angles in the Steep Rock sample. A maximum can be recognized between 5^{o} and 20^{o}. More than 62% of all measured angles range between these values. In the case of the Germantown sample (figure 44b) the maximum is broader, and approximately 54% of all the data have values between 10^{o} and 30^{o}.

These angles might be diagnostic of displacement, slip rate, etc. At the current state of knowledge, and since the kinematic histories of these rocks are unknown, it is not possible to correlate these angles with the displacement, etc.

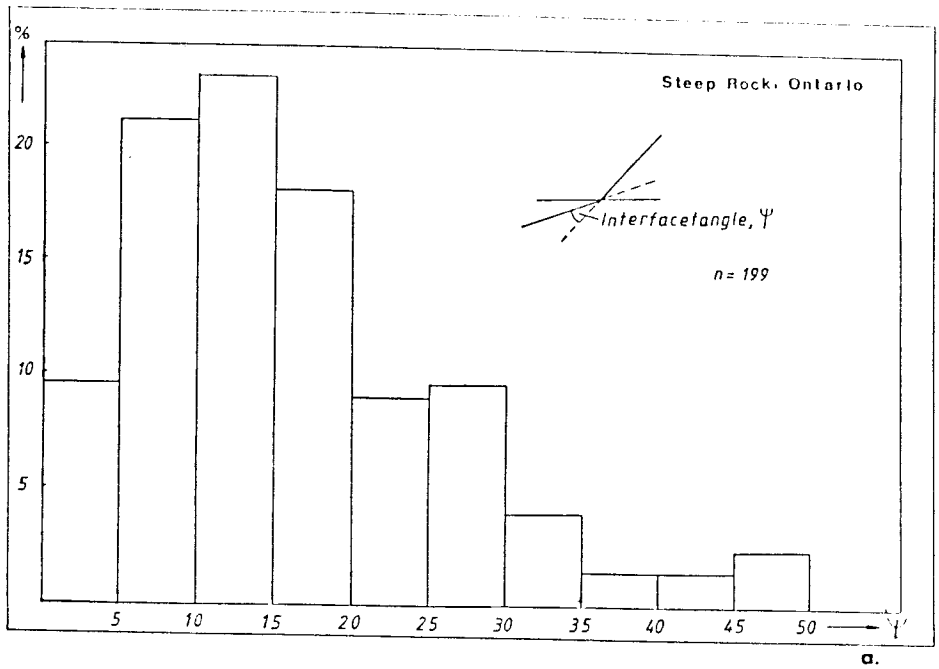

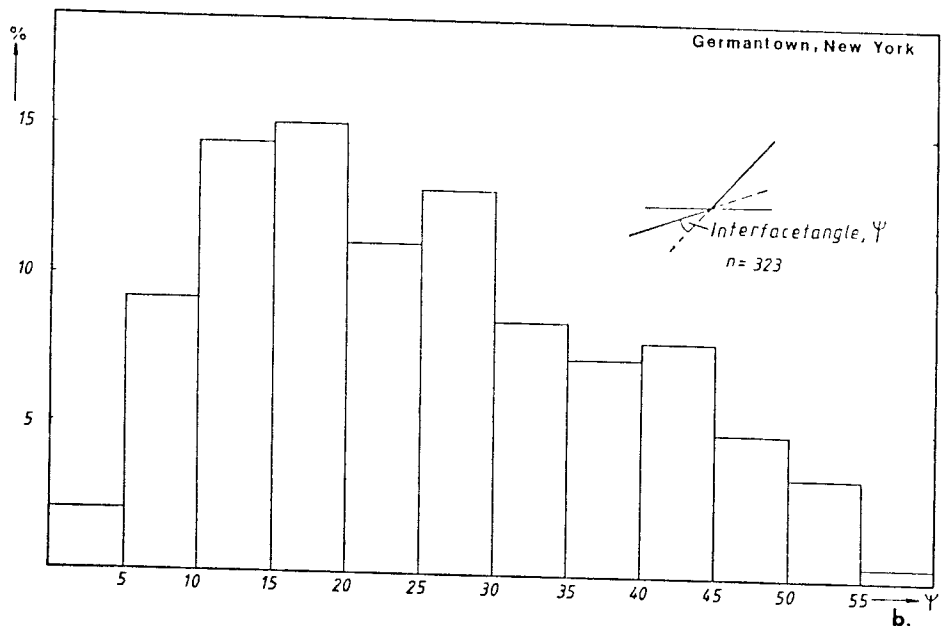

Figure 44. Histograms showing the distribution of the interfacet-angles for the specimens SR-1 (a), and GT-1 (b).

4.2. Observations in thin sections

A problem was encountered when thin sections of rocks with slickensided surfaces were made. Since during the standard thin section preparation technique the rock surface is in direct contact with the cutting and the grinding wheels, the slickensided surface and the subsurface structures were destroyed. Simple coating of the slickenside with an epoxy layer did not improve the quality of the final thin sections. For this reason, a slightly different technique for making thin sections was employed. The rock was cut into two pieces that were glued together, slickenside facing slickenside. This put the slickensides in the center of the slide and not at its margin, thus ensuring that the slickenside was not obliterated or destroyed during preparation.

The slickensides studied here do not include slickolites, slickensides containing debris streaks, and trails or spurs. These slickensides and slickenlines could not be collected. The latter lineations are mostly defined by soft material, which weathers very quickly, and therefore becomes eroded soon after the development of the slickenside lineation.

In thin sections, it was possible to distinguish different horizontal zones in the naturally deformed rocks. A near-surface zone of variable thickness containing the slickenside material is present, and overlies a zone of less

deformed host rock material, and further away from the sliding surface, a zone of undeformed host rock material. In the description below, the near surface zone will be referred to as the slickenside or S-zone, and the strain unmodified zone as the host rock or R-zone.

In the thin sections investigated the S-zone had a variable thickness up to 100 um. The lithic components observed in the S-zone include quartz; carbonates (mainly calcite); very fine grained brown and reddish brown material which could not be identified by means of optical microscopy; opaque, carbonaceous material; slivers of the host rock; and layer silicates.

4.2.1. Microstructural features

Unless indicated otherwise, all photomicrographs show a viewing plane parallel to the displacement direction and perpendicular to the slickenside. The sense of shear indicated refers always to the movement direction of the upper, removed block.

Extension veins perpendicular to the fault plane (fig. 45, US-5) were observed in several thin sections (US-5; B-3; GM-1a). These dilational openings are filled with vein quartz as in US-5 or with calcite (B-3). In sample SL-1a, cracks and tension gashes filled with calcite (fig. 46) were present. In this sample, the orientation of the filled tension gashes and

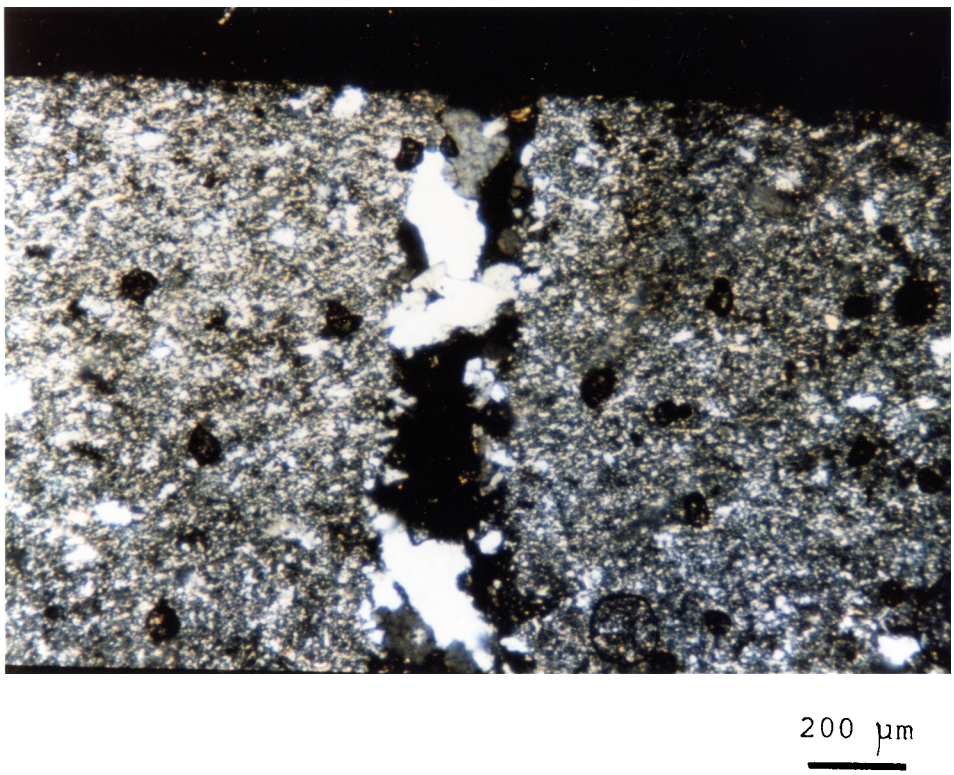

Figure 45. Extension vein filled with vein quartz. The sense of shear is unknown. Field of view is 2 mm wide, crossed polarizers. Specimen US-5.

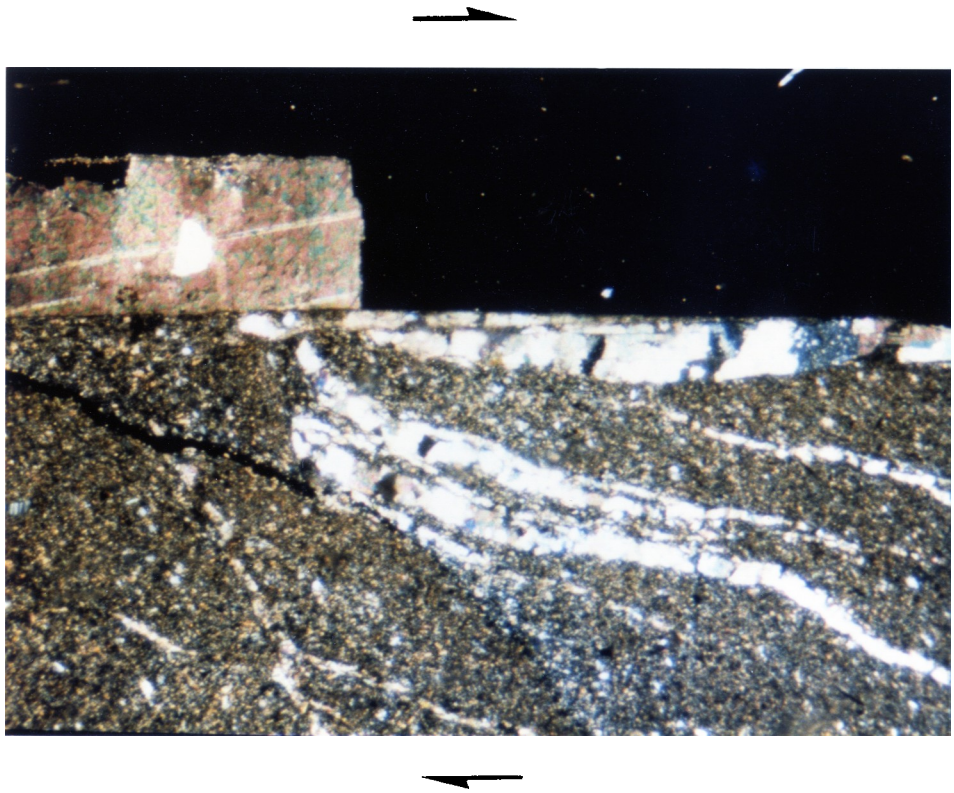

Figure 46. Calcite step and tension gashes filled with calcite and quartz. The sense of shear as inferred from these features is dextral. Field of view is 3.4 mm wide, crossed polarizers. Specimen SL-1a.

the calcite step are consistent with an overall dextral sense-of-shear.

Grain-shape preferred orientations could be frequently observed in the phyllosilicates of the outermost surface layer. Sigmoidally shaped chlorite is shown in figure 47 (GT-1a). Figure 48 (B-204) shows chlorite minerals with sub-parallel and low-angle orientations to the fault surface. Approximately 80-90 individual layers of chlorite are present in this thin section. The phyllosilicates can be deformed or undeformed (fig. 49, SR-1). The latter case indicates that no deformation took place after the crystallization or recrystallization (?) of the chlorites. Another example of a grain shape preferred orientation can be seen in the photomicrograph of the sample LCR-4a (fig. 50). The S-zone consists of the two phyllosilicate layers and the material between them, which is made up of quartz that has a considerably smaller grain size than the quartz grains in the R-zone, phyllosilicate flakes, and very dark, fine grained gouge (?) material. Phyllosilicate flakes between the two phyllosiicate layers define a S-shape foliation (see arrow). Across the S-zone, dark seams and phyllosilicates are present at an acute angle to the outermost surface layer. Their orientation corresponds to that of a shear band. This fabric indicates a sinistral sense of shear.

Sample B-202 shows an array of three normal faults running at an angle of approximately 45^{o} to the sliding

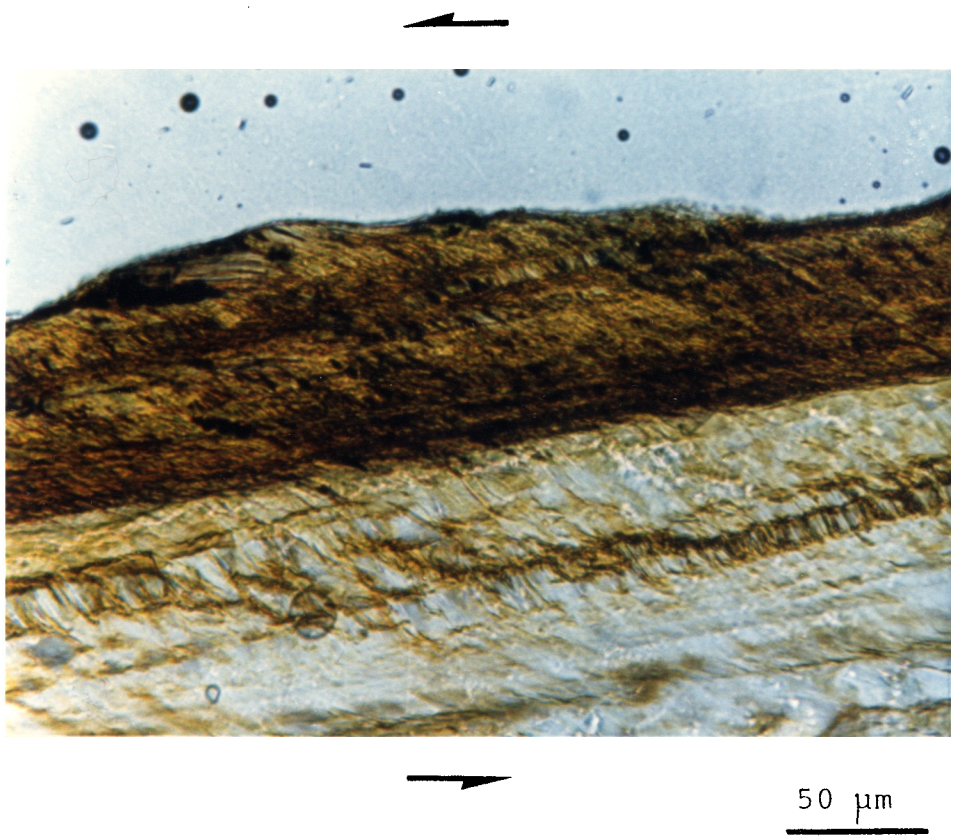

Figure 47. Sigmoidally shaped chlorites. A S-C foliation can be recognized. The sense of shear as inferred from the S-C foliation is sinistral. The difference in color is caused probably by a different iron content of the chlorites in the field of view (0.34 mm wide). Plane light, specimen GT-1a.

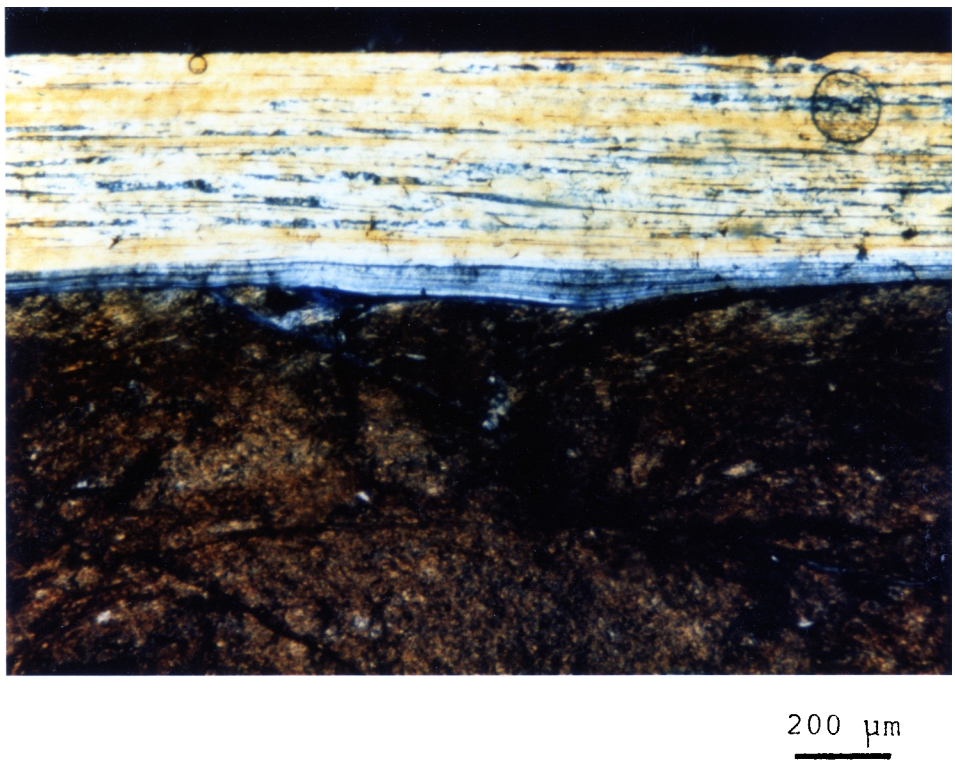

Figure 48. Chlorites oriented sub-parallel and at shallow angles to the fault plane. Sense of shear is unknown. Field of view is 2 mm wide, crossed polarizers. Specimen B-204.

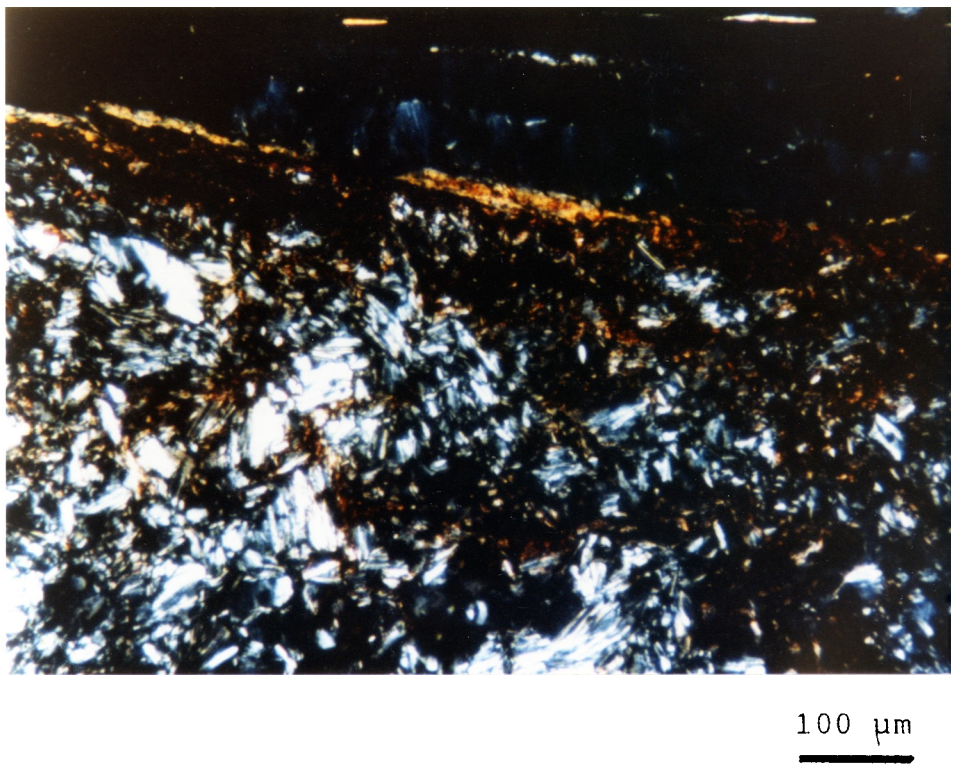

Figure 49. Undeformed chlorites in the outermost surface layer indicate a post-deformational deposition. Field of view is 0.86 mm wide, crossed polarizers. Specimen SR-1.

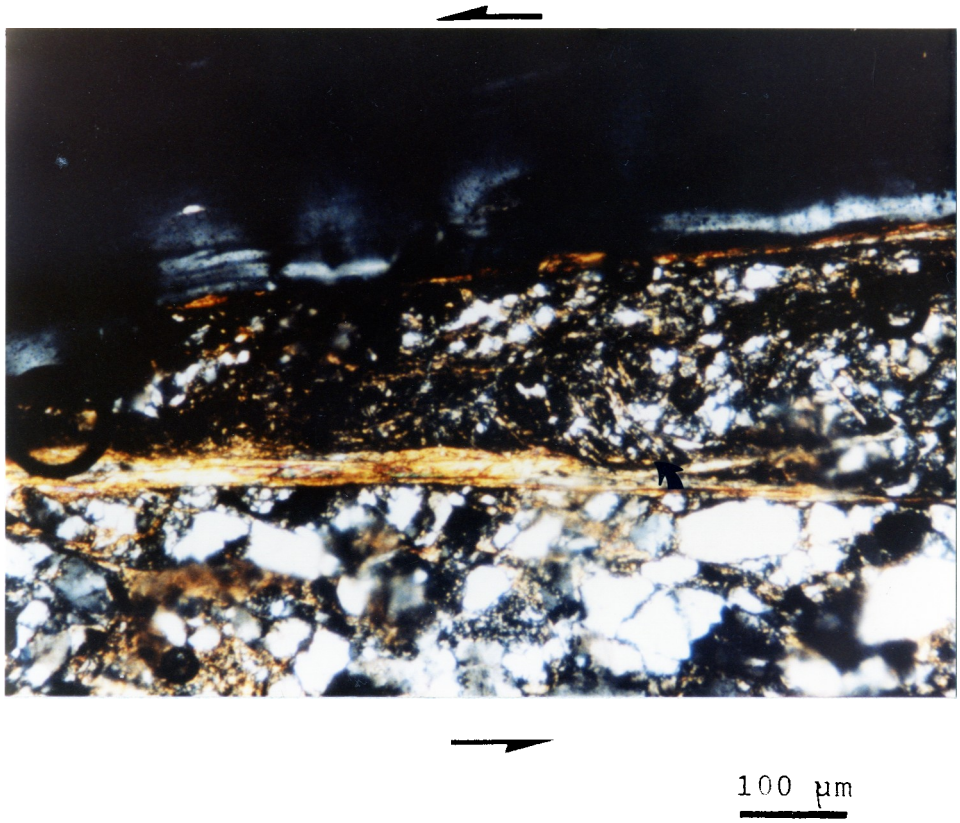

Figure 50. S- shaped foliation defined by the alignment of phyllosilicates (arrow) in the S-zone of specimen LCR-4a. In addition, dark bands and phyllosilicates occur in a shear band orientation in the S-zone. Sense of shear as inferred from the foliation is sinistral. Field of view is 0.86 mm wide, crossed polarizers.

surface (fig. 51). The normal fault character of these faults is indicated by the offset pattern of the top of the host rock material. The high birefringence of the chlorites is probably due to a high iron content (G. Putman, pers. comm.). The gaps between the chlorite layers and the host rock are filled with very fine grained material. These gaps appear to have formed as a response to the rotation of the normal fault blocks in the shale and filled with the fine grained material. These normal faults can be easily traced by their thin chlorite coating. Their orientation indicates a dextral sense of shear on the main fault plane when faulting occured. The presence of the fine grained material in the gaps indicates that the normal faulting event predates the deposition of the chlorites on the horizontal main fault surface. Under high magnification a sigmoidal shape of some of the chlorites in the outermost layer can be recognized. Their orientation indicates a dextral sense of shear. Thus, early deformation caused the normal faulting, followed by dextral shearing causing a rigid body rotation, and chlorite deposition on these small-scale fault planes. Subsequently, the fine grained material, which is likely to be fault gouge, fills the gaps produced by the rotation of the normal fault. At a later stage syndeformational (as indicated by the sigmoidal shape of the phyllosilicates) deposition of chlorite occurs on the main fault plane. In the hand sample, the surface is shiny.

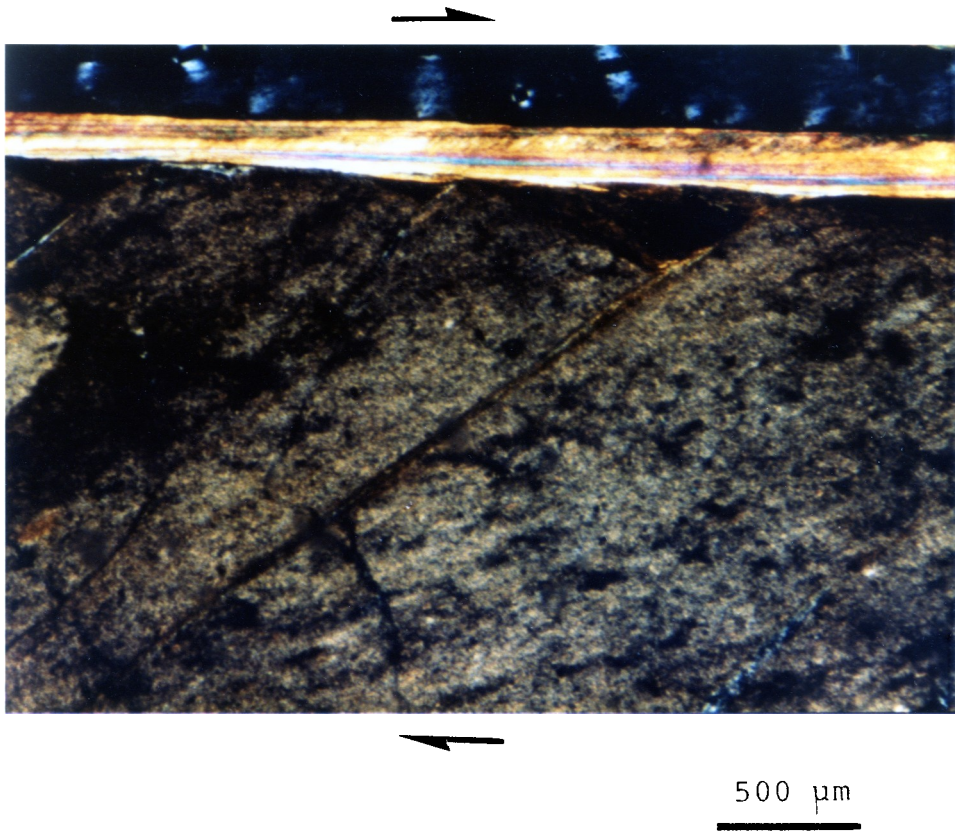

Figure 51. Normal faulting in specimen B-202 indicates a dextral sense of shear at the time of faulting. Field of view is 3.4 mm wide, crossed polarizers.

Normal faults, as indicated by the offset dark inclusion trails, within chlorites of the S-zone were observed in the thin section of sample GT-1a (fig. 52). The fault pattern indicates a sinistral sense of shear at the time the chlorites were faulted.

Deflected "bands" of dark brownish material occur at the R- and S-zone interface. They may represent bedding planes, an earlier cleavage, or selvage seams. As seen in figure 53 (GT-1a), these planes make a shallow angle with the fault plane and become more closely spaced closer to the surface. At the contact between the chlorite layer and the host rock, these bands are deflected into an orientation subparallel to the surface. Two independent sense of shear indicators are visible in this photomicrograph. The prominent quartz step on top of the surface indicates a sinistral sense of shear, which is also supported by the listric normal faulting in the S-zone of this rock (fig. 52). If the steps at the layer silicate - host rock interface are interpreted in terms of the traditional smoothness-principle, then the facing direction of the steps coincides well with a sinistral shear. It is proposed, that the deflection of the dark seams as seen in the photomicrograph of this rock can be used as a criterion for the sense of shear. The thin section is interpreted in the following way: sinistral shearing caused the deflection of the dark seams and produced the steps on the top of the host rock. Contemporaneously, chlorite and

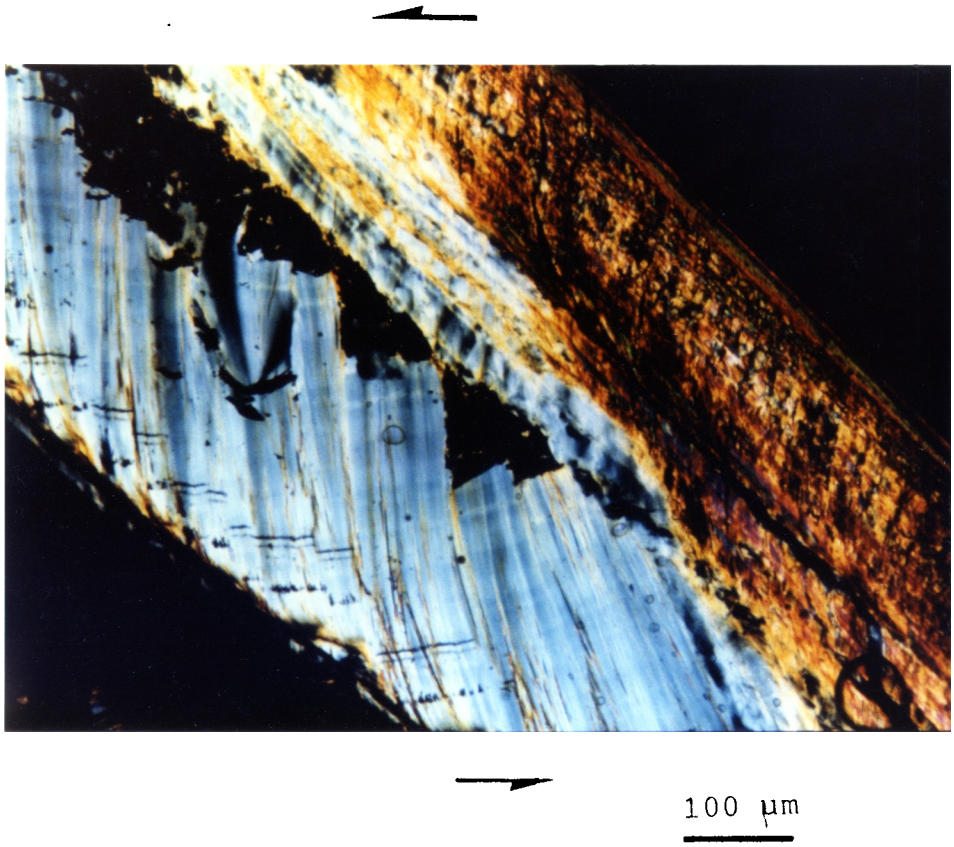

Figure 52. Normal faulting in chlorite with the blue birefringence. Sense of shear is sinistral at this time. Field of view is 0.86 mm wide, crossed polarizers. Specimen GT-1a.

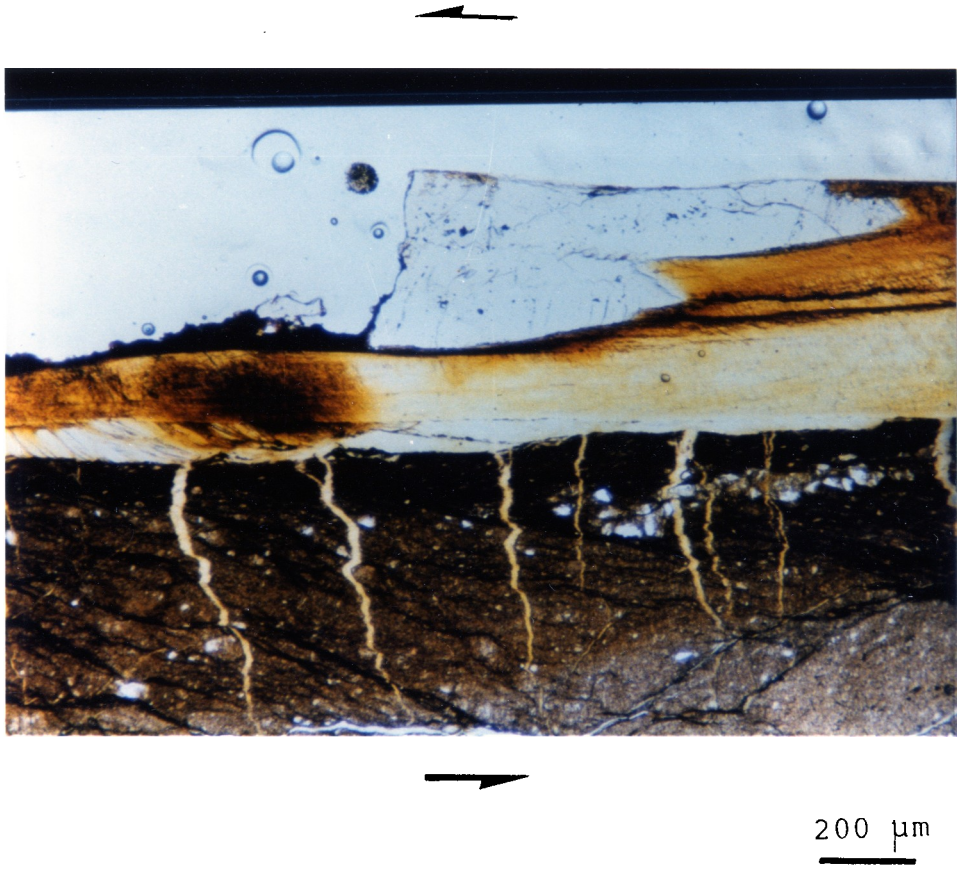

Figure 53. Deflection of brownish bands at the R- and S-zone interface. The quartz step indicates a sinistral sense of shear. This coincides with the step facing at the host rock / layer silicate interface as long as the steps are interpreted in terms of the "smoothness-principle". Note the sinistral offset of the chlorite veins in the host rock. Field of view is 2 mm wide, plane light. Same specimen as in figure 52.

quartz precipitated out of a fluid phase infiltrating the fault surface, and penetrated partly into the host rock. Further sinistral shearing caused the listric normal faulting (fig. 52) and the slight offset of the chlorite veins extending sub-perpendicular to the surface.

Figure 54 (GT-4) shows a sub-surface zone of en-echelon shaped dark seams. Below the band, coarse vein quartz is present, whereas above the band, only fine grained, recrystallized quartz occurs. A transition in grain size occurs across this band. The sliding surface is marked by the brownish material on top of the recrystallized quartz. A structure very similiar in appearance is shown in the photomicrocraph of US-1a (fig. 55). A "horse-like" structure can be seen in the S-zone. The term "horse" is employed here to emphasize that the calcite minerals present are completely surrounded by a thin layer of chlorite. The sense of shear is unknown for both samples.

Intracrystalline fractures could be seen in a few cases. Figure 56 (HK-1) shows a large, heavily fractured quartz grain. The much smaller quartz grains closer to the sliding surface have very irregular and ragged grain boundaries, and show undulose extinction. The appearance of the quartz grains next to the sliding contact is probably caused by high shear strain concentrations in the upper part of the S-zone. Presumably, further away from the fault surface the shear strain was less, and the large quartz grain accomodated the

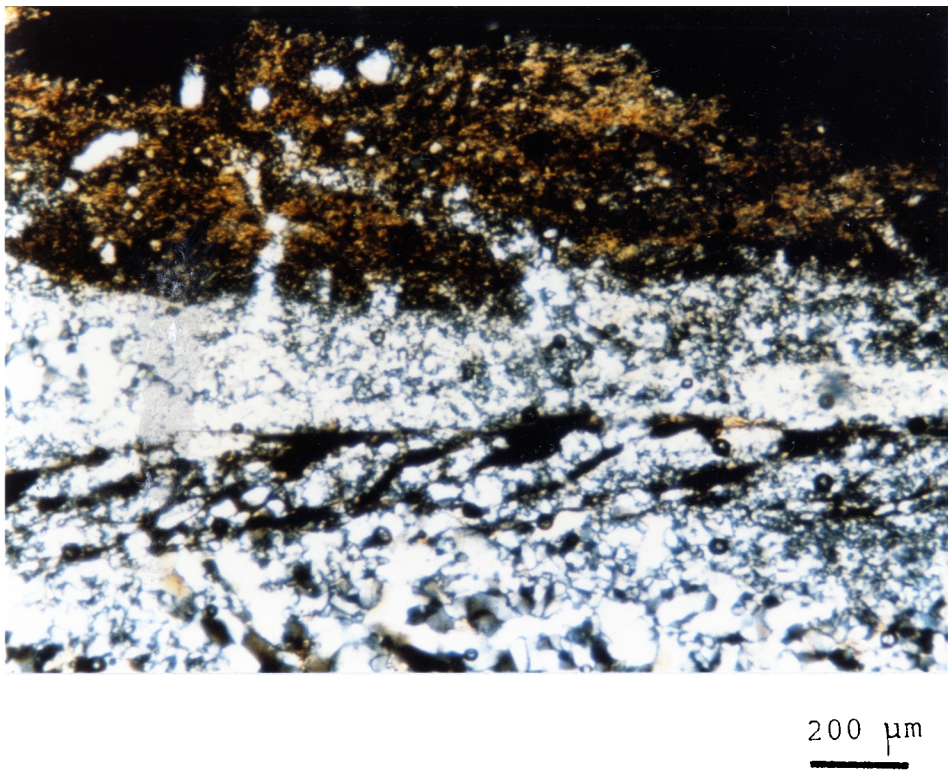

Figure 54. En-echelon array of dark seams in sample GT-4. A transition in grain size occurs across this array. Sense of shear is unknown. Field of view is 2 mm wide, crossed polarizers.

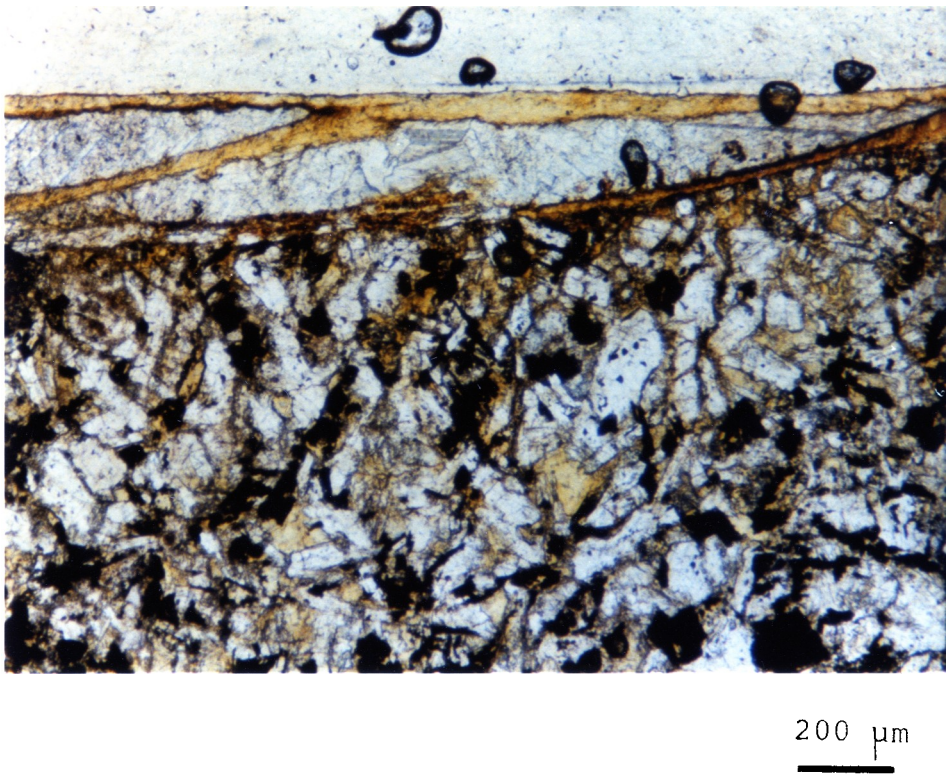

Figure 55. Twinned calcite embedded completely in chlorite seams. Sense of shear is unknown. Field of view is 2 mm wide, plane light. Specimen US-1a.

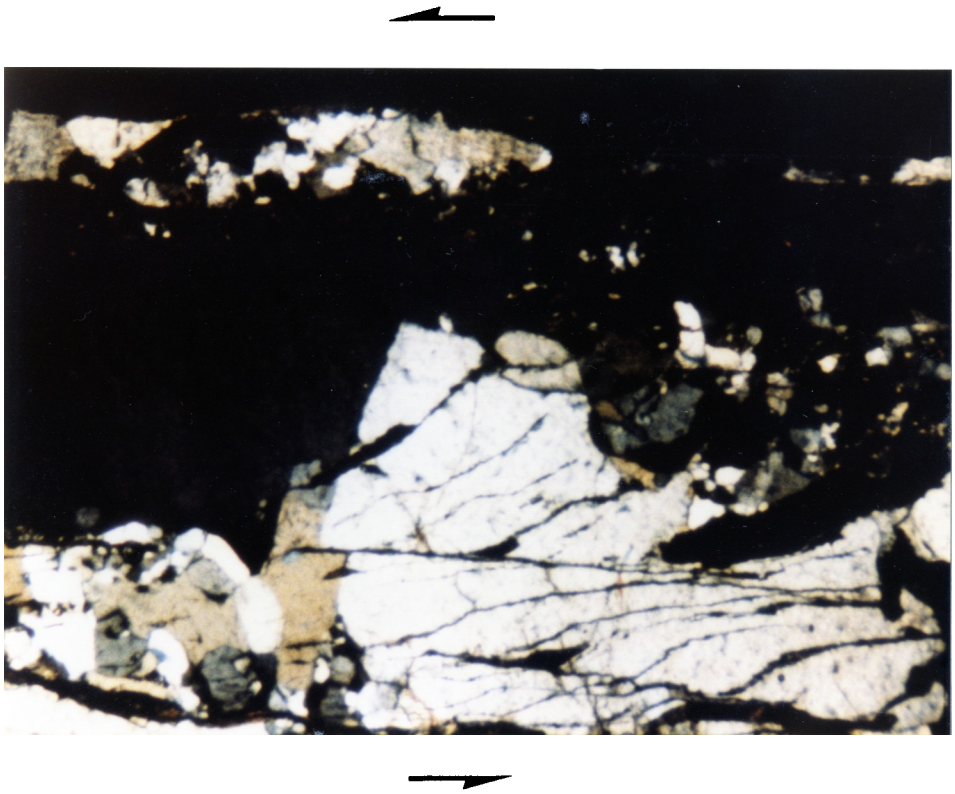

Figure 56. Heavily fractured large quartz grain overlain by smaller quartz with undulose extinctions and irregular grain boundary shapes. The sense of shear as inferred from the fracture pattern is sinistral. Field of view is 3.4 mm wide, crossed polarizers. Specimen HK-1.

strain by brittle deformation.

Other structures observed include broken fragments of host rock material within the S-zone, host rock "fish" (fig. 57, CPA-1) in slickenveins, truncation of quartz grains by an overlying zone of dark material, and twinned and untwinned calcite crystals (fig. 57).

The structural features observed are listed below.

General features

- The S-zone has a variable thickness up to 100 um.
- Filled and unfilled tension gashes occur in the S- and R-zone.
- Normal faulting can occur in both zones.
- Dark bands (bedding or cleavage planes) become deflected at the S- and R-zone interface.
- Phyllosilicates can align in S- and C-plane, and in shear band orientation.
- Extension veins can occur perpendicular to the sliding surface.
- A grain shape preferred orientation is present in the S-zone.
- "Horses" and host rock "fish" can occur in the S-zone.

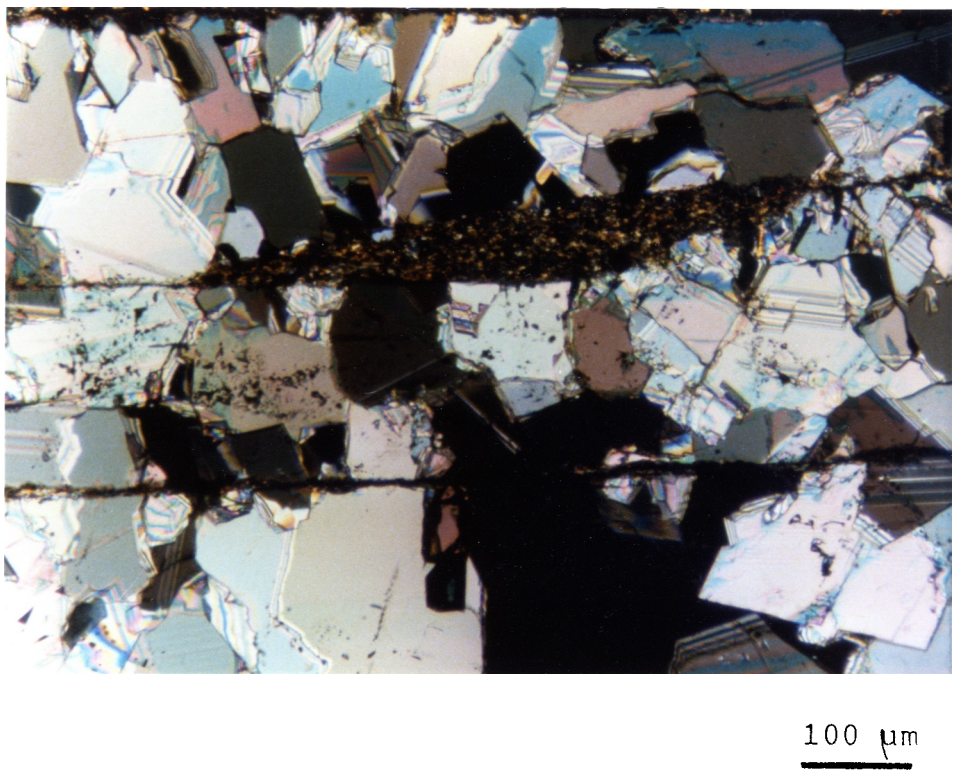

Figure 57. Host rock fish in slickenvein. Sense of shear is unknown. The similarity to mica-fish is obvious. If the host rock fish is interpreted like mica fish, the sense of shear would be dextral. Recrystallized, and twinned and untwinned calcite is present. The field of view is 0.86 mm wide, crossed polarizers. Specimen CPA-1.

Structural features in quartz crystals

- Quartz crystals or aggregates of any grain size can occur in the S-zone.
- Quartz can be strain-free or strained (ragged grain boundaries, undulose extinction).
- Recrystallization of quartz can occur next to the fault plane.
- Intragranular fracturing can occur.
- Intergrowth with other minerals (especially chlorite and calcite) was observed.

Structural features in layer silicates

- Chlorite crystals in the S-zone are mostly fibrous.
- Chloritic S-zones can consist of up to 80-90 individual layers of chlorite.
- Phyllosilicates can define a strong crystal shape preferred orientation in the S-zone. The phyllosilicate orientation can be at high angles, shallow angles, or sub-parallel to the fault surface. Furthermore, a sigmoidal shaped preferred orientation can occur.
- Sometimes a less prominent grain shape preferred orientation of phyllosilicates occurs in the R-zone.

I do not intend to claim that all of the microstructural features described above can occur in a slickenside zone only, and need necessarily be related to the formation of a slickenside. However, features such as the preferred orientations of phyllosilicates in the slickenside zone are very likely to be genetically related to the formation of a slickenside. This is supported by the observed fabric change in the experimentally deformed pyrophyllitic clay where planes with S- (?), C-, and C'-plane orientations developed, and nesting was present. Some of these fabric elements were also observed in naturally produced slickensides (e.g. GT-1, LCR-4a). However, there is no direct evidence for nesting in these two rocks due to the missing hangingwall blocks of the samples. Therefore, we cannot be sure whether these fabric elements are characteristic of nested surfaces. Future research might find an answer to this question.

In addition to the sense of shear criteria commonly used, such as fiber steps, slickolites, ploughing tools at one end of a groove, etc. (fig. 58a), the following microstructural features, might represent useful sense of shear indicators for slickensides: preferred orientations of phyllosilicates in the S-zone, deflected bedding or cleavage planes, and host rock fish in the S-zone (fig. 58b). Another possible sense of shear indicator is the position of maximum light reflection as discussed below.

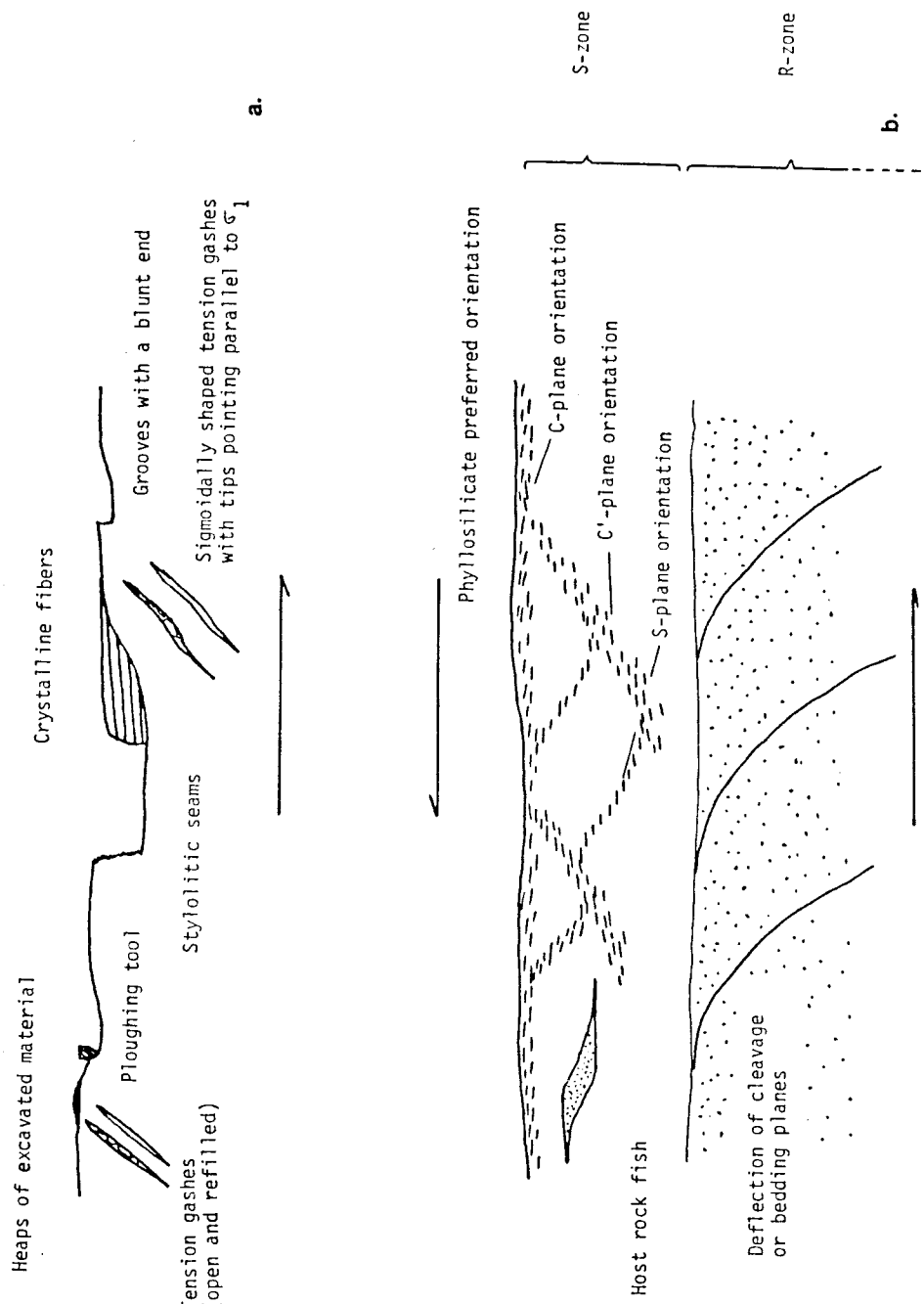

Figure 58. (a) Some shear criteria commonly used on fault surfaces, and (b) microstructural features proposed to infer the sense of shear in a slickenside zone.

4.2.2. Shiny slickensides - Polishing or mineral alignment

Sometimes, slickensided surfaces have a shiny appearance with a sub-metallic or even metallic luster under reflected light. Both polishing and mineral alignment can be used to explain why the slickensides are shiny. With a purely abrasive polishing process, truncated mineral grains would be expected at the sliding surface. This was never observed in thin sections. Instead, all the shiny slickensides I investigated, although none of them was mirror-like, had a surface coated with either carbonaceous material (fig. 59, view perpendicular to sliding direction and slickenside, BV-1) or with phyllosilicates (fig. 60, B-302). My shiniest hand sample (fig. 61) has an outermost surface layer of opaque, carbonaceous (vitrinite ?) material. The other shiny samples had a phyllosilicate coating of variable thickness.

I first expected that the surface shine might be a function of the thickness of the layer silicate coating. This hypothesis was tested by simple reflection measurements. The following technique was used. In the darkroom, the sample was mounted horizontally on a goniometer stage and illuminated with white light at an angle of 45°. Striated specimens were oriented so that their striations were parallel to the horizontal projection of the incident and the reflected light on the goniometer stage. The intensity of the light source

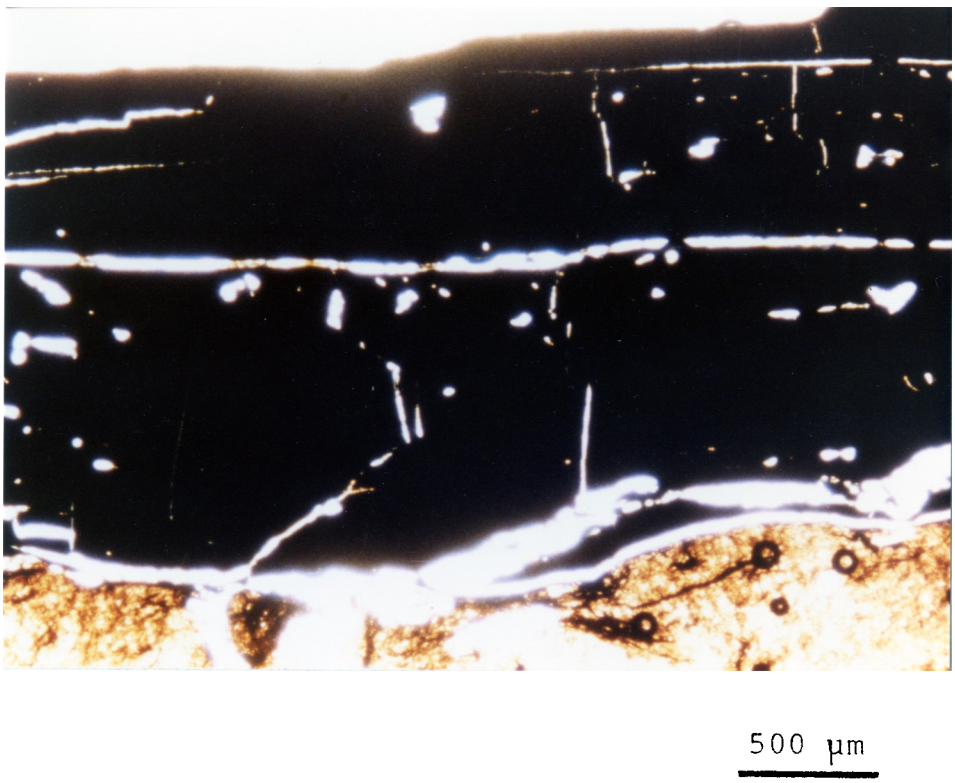

Figure 59. Opaque, carbonaceous material at the fault surface of specimen BV-1. The sense of shear is unknown. The field of view is 3.4 mm wide. View perpendicular to striations, plane light.

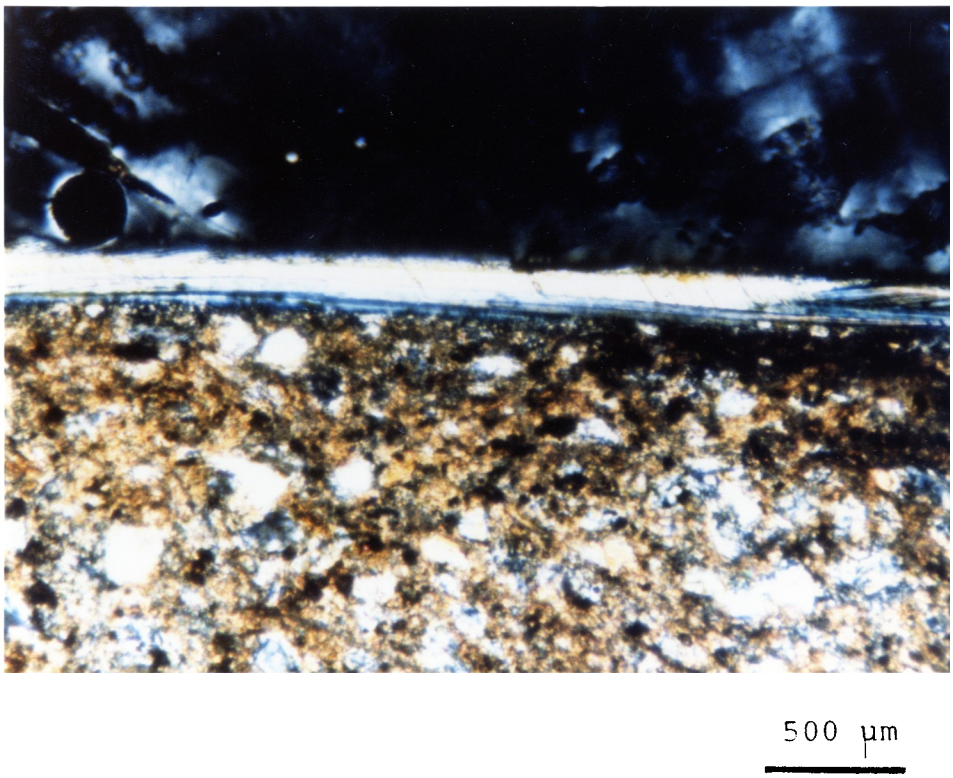

Figure 60. Phyllosilicate layers on shiny slickenside. Small tension gashes are present in the chlorite layers. Field of view is 3.4 mm wide, crossed polarizers. Specimen B-302.

Figure 61. Shiny slickenside. Dimensions of the specimen are 3 cm by 3.8 cm. Specimen BV-1.

was measured with an exposure meter. The exposure meter was attached over the shiny slickenside in an orientation parallel to the normal to the goniometer stage. Then, the sample was tilted about the horizontal axis of the stage that was perpendicular to the striations. The intensity of the reflected light was measured in 10^{o} intervals, using the exposure meter.

The ratio of the intensity of the light source and the intensity of the light reflected from the slickensided surface was calculated for the position where the sample was at maximum reflection. This number is called "maximum relative intensity". In the samples measured this value ranged between 0.45 and 0.55, and appeared to be more or less independent of the thickness of the phyllosilicate layers.

The samples reflected the most at angles of approximately 25^{o} to 35^{o} to the light source. In thin sections of shiny slickensides, phyllosilicates were present at a shallow angle to the sliding surface (figures 48 and 60). It is suggested that a preferred orientation of phyllosilicates is responsible for the maximum light reflection at one angle, and thus for the surface shine of these slickensides. If shearing causes the preferred orientation of phyllosilicates, then this dependence between preferred orientation and maximum light reflection might lead to a new sense of shear indicator on shiny slickensides. This technique proposed could be used in the field as well as in a laboratory. Figure

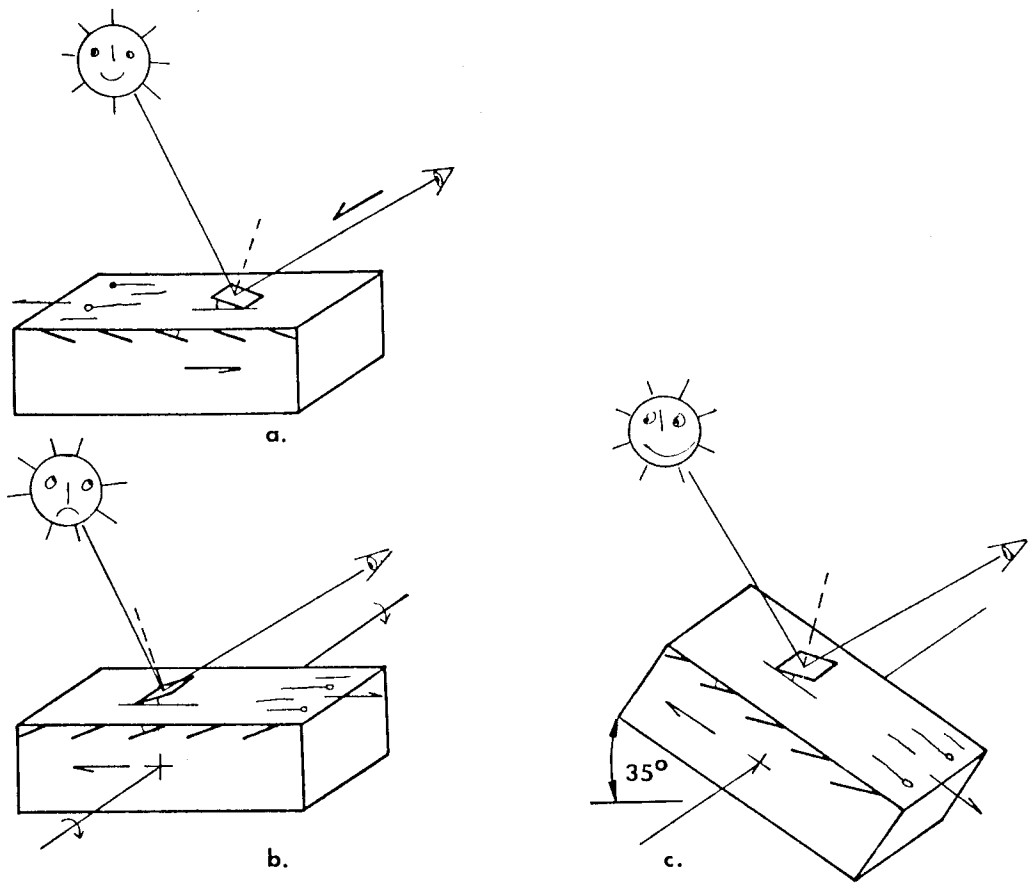

Figure 62. Proposed sense of shear criterion. (a) Phyllosilicates inclined to the slickensided surface reflect light most at the position indicated. (b) At the same position as in (a), the specimen reflects light light less brightly when rotated 180°. (c) In order to receive maximum brightness, the rotated specimen has to be tilted with the angle indicated. The sense of shear is given by the direction of the sight-line from the viewer's eye to the surface, at the position of minimum tilt (figure 62a).

62 explains this technique. A specimen must be oriented so that the viewer looks down onto the slickensided surface and along the striations. The specimen must be tilted until it reflects most (figure 62a). This will occur when the normal to the basal planes of the phyllosilicates bisects the angle between the viewer's eye and the sun (or the vertical axis of a microscope). Next, the specimen has to be rotated by 180^{o} (figure 62b) and tilted until maximum reflection occurs (figure 62c). The sense of shear can be inferred at the position of minimum tilt or dip (figure 62a), by the sight line from the eye of the viewer to the phyllosilicates. This shear criterion is similar to S. Reynold's "fish-flash" in quartzo-feldspathic rocks (Simpson, 1986), but could be used in a wider variety of rocks.

4.3. Definition and classification problems

Throughout this thesis the terms slickenside and slickenline were used in a broad sense. The whole spectrum of different slickenside markings ranging from slickenveins, where vein fillings are essential to abrasive scratches were included. Through the usage of these terms in such a broad sense, the whole range of fault or fold surface features produced during shearing on these surfaces is covered.

During the study of the thin sections it became clear that slickensides are penetrative features, as indicated by

the strain-modified sub-surface fabric. For this reason, the S-zone and R-zone terminology was introduced. Figure 63 shows a simplified profile across a slickenside. The deformed host rock and the exotic material, which includes the material precipitated out of infiltrating fluids, define the S-zone, and the undeformed host rock represents the R-zone. This sketch indicates that a further refinement of the S- and R-zone terminology is feasible. For example, the S-zone can be subdivided into a S_1-zone, the layer which consists mainly of exotic material, and into a S_2-zone, the deformed host rock area. Further subdivisions might well be possible. Those might depend on the presence or absence of dominantly ductile or brittle processes in the S-layer. For example, whether recrystallization took place, whether subgrain formation occurred, whether a strong crystal shape or crystallographic preferred orientation is present, whether material precipitated out of a fluid phase penetrated the R-zone, etc. Such a terminology might lead to a future slickenside classification based on fabric elements.

Combining the penetrative character of slickensides with the broad usage of the term slickenside the following definition is proposed: a slickenside is a "strain-modified zone of variable thickness at a fault plane, whose surface displays any kind of markings produced during shearing on this surface". At least in my opinion this has the advantage that it defines a slickenside without any genetic conno-

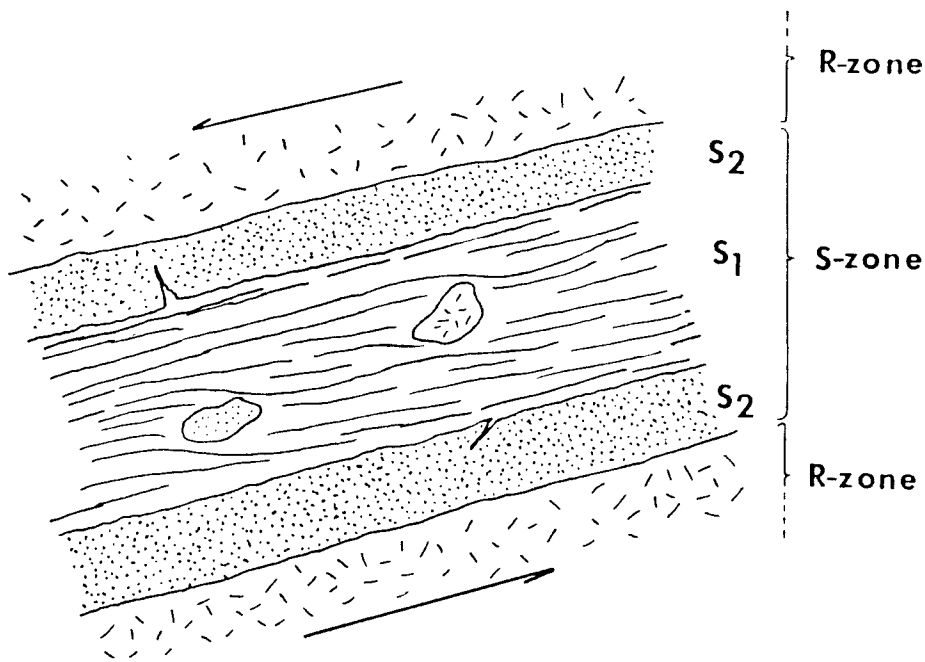

Figure 63. Nomenclature proposed for slickensides. S is the strain-modified slickenside zone, R the the undeformed host rock zone. S_1 indicates the layer of exotic material, S_2 the strain-modified host rock zone.

tations as implied by the terms "friction" or "polished". A slickenside of this type might be called a "slickenside sensu lato" whereas a slickenside fitting the traditional definition, "polished and smoothly striated surface that results from friction along a fault plane", Gary et al. (1977, p.665), might be called a "slickenside sensu stricto".

Slickensides can be described in terms of their morphology, or by means of the processes responsible for the formation of a specific type of slickenside. Slickensides can be categorized by means of descriptive morphological features such as slickensides with linear markings and those without linear markings, or the presence or absence of fluid related features, for example crystalline fibers versus scratches. If these two criteria are combined, four classes of slickensides are obtained: (1) slickensides with linear markings, but without fluid related features, (2) slickensides with linear markings and fluid related features, (3) slickensides without linear markings and fluid related features, and (4) slickensides without linear markings, but with fluid related features. Scratches, spurs, trails, and posssibly the ridge-in-groove type lineation belong to class (1); crystalline fibers to class (2). Class (3) includes steps in material which did not precipitate out of a fluid, and shiny surfaces whose shine is produced by abrasive polishing. Class (4) includes steps in material that precipitated out of a fluid phase, slickenveins and shiny surfaces, as long as the

surface shine is caused by material that precipitated out of a fluid phase. Even though these classes are based on descriptive scheme, using only non-mechanistic terms, overlaps occur between the classes (3) and (4) when steps and shiny surfaces are categorized. Only the introduction of terms with a genetic connotation, such as shine caused by abrasive polishing etc. avoids this overlap. This leads to a classification using genetic and non-genetic terms, which is not fully satisfying.

It can be attempted to categorize slickensides in terms of the processes believed to be responsible for their formation. Slickensides produced by brittle processes could be distinguished from slickensides produced under more ductile conditions. The latter group would possibly include the ridge-in-groove type lineation, since the experiments described in this work as well as the wax-shearing experiments of Means (1986, 1987) suggest that ductile processes are involved, at least partly, in the formation of this type of striation. Such categories might be further subdivided when the scale of observation is included, for example, whether the deformation was localized on a grain-scale or whether it occurred on a larger scale throughout the entire slickenside without a localized, small-scale strain concentration.

Through future work it might become feasible to establish "slickenside mechanism maps" for different types of rocks.

Such a hypothetical deformation mechanism map is shown in figure 64 plotting slip rate versus depth. This map shows fields of slickenside markings produced by frictional sliding processes, slickenside markings formed under solution transfer conditions, and slickenside markings produced under more ductile conditions. Transitions between the individual fields are likely to occur. If it were possible to develop such maps it would be a great step towards the interpretation of slickensides in terms of processes and conditions of their formation.

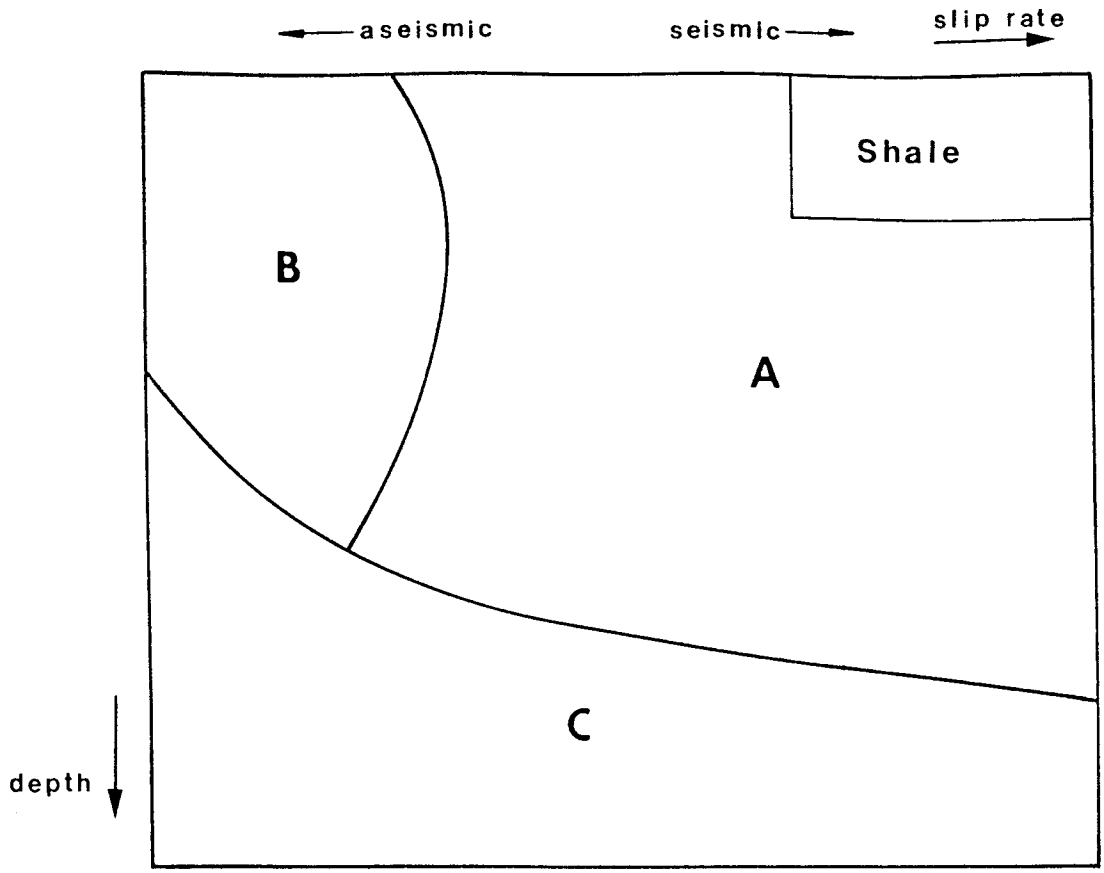

Figure 64. Hypothetical slickenside mechanism map for a given lithology. Field A includes all slickenside markings produced by frictional sliding (scratches, striations, etc.), field B markings formed by pressure solution slip (crystalline fibers, slickenveins, slickolites), and field C features formed at more ductile conditions (ridge-in-groove type lineation).

5. References

Angelier, J. (1979): Determination of the mean principal stresses for a given fault population. Tectonophysics, 56: T17-T26.

Billings, M.P. (1954): Structural geology. 2nd edition. Prentice Hall (Englewood Cliffs, N.J.).

Bretz, J.H. (1940): Solution cavities in the Joliet limestone of northeastern Illinois. J. Geol., 50: 675-811.

Bretz, J.H. (1950): Origin of the filled sink-structures and circle deposits of Missouri. Geol. Soc. Am. Bull., 61: 789-834.

Burg, J.P. and Ponce de Leon, M.I. (1985): Pressure-solution structures in a granite. J. Struct. Geol., 7: 431-436.

Chamberlin, T.C. (1888): Rock scorings of the great ice age invasion. U.S. Geol. Surv., Seventh Ann. Report: 218-224.

Coulson, J.H. (1970): The effects of surface roughness on the shear strength of joints in rock. Tech. Rep. MRD-2-70, Mo. River Div., Corps of Eng., Omaha, Nebr.

Deer, W.A., Howie, R.A. and Zussman, J. (1976): An introduction to the rock-forming minerals. 9th edition. Longman (London).

Durney, D.W. and Ramsay, J.G. (1973): Incremental strain measured by syntectonic crystal growth. In: Gravity and tectonics (DeJong, K.A. and Scholten, R., eds.): 67-96.

John Wiley and Sons (New York).

Dzulynski, S. and Kotlarczyk, J. (1965): Tectoglyphs on slickensided surfaces. Bull. l'Acad. Polonaise des Sci., ser. geol. et geogr., 17: 149-154.

Elliot, D. (1976): The energy balance and deformation mechanisms of thrust sheets. Phil. Trans. R. Soc. London, A283: 289-312.

Embleton, C. and King, C.A.M. (1975): Glacial geomorphology, vol. 1. 2nd edition. Edward Arnolds (London).

Engelder, J.T. (1974): Microscopic wear-grooves on slickensides: indicators of paleoseismicity. J. Geophys. Res., 79: 4387-4392.

Engelder, J.T. (1978): Aspects of asperity-surface interaction and surface damage of rocks during experimental frictional sliding. Pageoph., 116: 705-716.

Etchecopar, A., Vasseur, G. and Daignieres, M. (1981): An inverse problem in microtectonics for the determination of stress tensors from fault striation analysis. J. Struct. Geol., 3: 51-65.

Fleuty, M.J. (1975): Slickensides and slickenlines. Geol. Mag., 112: 319-322.

Friedman, M., Logan, J.M. and Rigert, J.A. (1974): Glass indurated quartz gouge in sliding-friction experiments on sandstone. Bull. Geol. Soc. Am., 85: 937-942.

Gary, M., McAfee, R.Jr. and Wolf, C.L., eds. (1977): Glossary of geology. American Geological Institute (Washington,

D.C.).

Gay, N.C. (1970): The formation of step structures on slickensided surfaces. J. Geol., 78: 244-258.

Harris, S.E.Jr. (1943): Friction cracks and the direction of glacial movement. J. Geol., 51: 523-532.

Hobbs, B.E., Means, W.D. and Williams, P.F. (1976): An outline of structural geology. John Wiley and Sons (New York).

Hurlbut, C.S.Jr. and Klein, C. (1977): Manual of mineralogy. 19th edition. John Wiley and Sons (New York).

LaFountain, L.J., Swain, M.V. and Jackson, R.E. (1975): Origin of macroscopic wear grooves generated during frictional sliding experiments. Int. J. Rock Mech. Min. Sci., 11: 235-249.

Lindström, M. (1975): Steps facing against the slip direction: a model. Geol. Mag., 111: 71-75.

MacClintock, P. (1953): Crescentic crack, crescentic gouge, friction crack, and glacier movement. J. Geol., 61: 186.

Mattauer, M. (1973): Les deformations des materiaux l'ecorce terrestre. Hermann (Paris).

Means, W.D. (1986): A newly recognized type of slickenside striation (abs.). Geol. Soc. Am. Ann. Meet., Program with Abstracts, 18: 691-692.

Means, W.D. (1987): A newly-recognized type of slickenside striation. subm. to J. Struct. Geol.

Means, W.D. and Rogers, J. (1964): Orientation of

pyrophyllite synthesized in slowly strained materials. Nature, 204: 244-246.

Moore, G.W. (1980): Slickensides in deep sea cores near the Japan trench, Leg 57, Deep Sea Drilling Project. In: Initial reports of the Deep Sea Drilling Project 56-57, part 2 (Lee, M. and Stout, L.N., eds.): 1107-1115. U.S. Geol. Surv. (Menlo Park, CA).

Norris, D.K. and Barron, K. (1969): Structural analysis of features on natural and artificial faults. In: Proceedings, Conference on research in tectonics (Baer, A.J. and Norris, D.K., eds.). Can. Geol. Surv. Paper, 68-52: 136-167.

Paterson, M.S. (1958): Experimental deformation and faulting in Wombeyan marble. Geol. Soc. Am. Bull., 69: 465-476.

Petit, J.-P., Proust, F. and Tapponier, P. (1983): Criteries de sens de mouvement sur les miroirs de failles en roches non calcaires. Bull. Soc. Geol. France., 25: 589-608.

Petit, J.-P. and Laville, E. (1986): Morphology and microstructures of "hydroplastic slickensides" in sandstone. Geol. Soc. London, Spec. Publ., Deformation mechanisms in sediments and sedimentary rocks (in press).

Platt, J.P. (1979): Extensional crenulation cleavage. J. Struct. Geol., 1: 95-96.

Platt, J.P. and Vissers, R.L.M. (1980): Extensional

structures in anisotropic rocks. J. Struct. Geol., 2: 397-410.

Preston, F.W. (1921): The structure of abraded glass surfaces. Opt. Soc. London Trans., 23: 141-146.

Riecker, R.E. (1965): Fault plane features, an alternative explanation. J. Sed. Petrol., 35: 746-748.

Rispoli, R. and Vasseur, G. (1983): Variation with depth of the stress tensor anisotropy inferred from microfault analysis. Tectonophysics, 93: 169-184.

Sasada, T. (1984): Wear research in Japan: trends and future directions. Wear, 100: 561-577.

Sibson, R.H. (1974): Frictional constraints on thrust, wrench and normal faults. Nature, 249: 542-544.

Sibson, R.H. (1986): Earthquakes and rock deformation in crustal fault zones. Ann. Rev. Earth Planet. Sci., 14: 149-175.

Simpson, C. (1986): The determination of movement sense in mylonites. J. Geol. Education (in press).

Suppe, J. (1985): Principles of structural geology. Prentice-Hall (Englewood Cliffs, N.J.).

Tchalenko, J.S. (1970): Similarities between shear zones of different magnitudes. Geol. Soc. Am. Bull., 81: 1625-1640.

Tjia, H.D. (1964): Slickensides and fault movement. Geol. Soc. Am. Bull., 75: 683-686.

Tjia, H.D. (1967): Sense of fault displacement. Geologie

Mijnbouw, 46: 392-396.

Tjia, H.D. (1968): Fault-plane markings. 23rd Int. Geol. Cong., Czechoslovakia, Proc., 13: 279-284.

Tjia, H.D. (1972): Fault movement, reoriented stress field and subsidiary structures. Pacific Geol., 5: 49-70.

Willis, B. and Willis, R. (1934): Geologic structures. 3rd edition. Mc-Graw Hill (New York).

Yaalon, D.H. and Kalmar, D. (1978): Dynamics of cracking and swelling clay soils, displacement of skeletal grains, optimum depth of slickesides, and rate of intra-pedonic turbation. Earth Surf. Proc., 3: 31-42.

6. Appendixes

6.1. Appendix A - Program "Triacom"

The program was written for a Hewlett Packard CV-41 calculator. It calculates the three principal stresses, the differential stress, the normal and the shear stresses. All stresses are calculated in bars. The program also calculates the longitudinal strain, the strain rate (in seconds^{-1}), and the dynamic coefficient of friction for a triaxial compression test.

The program calculates the stresses as explained below. The confining pressure, CP, is calculated as the ratio of the force reading as the wax extrusion out of the ports started, and the cross-sectional area of the wax and specimen. The confining pressure equals σ_2, and σ_3. In order to calculate σ_1, the following equations were combined and solved for σ_1:

$$A_{spec} = V_o/l_i$$

$$A_{wax} = A_{total} - A_{spec}$$

$$F_{wax} = CP \times A_{wax}$$

$$F_{spec} = F_{total} - F_{wax}$$

$$\sigma_1 = F_{spec}/A_{spec}$$

where A_{total}, A_{spec}, and A_{wax} are the cross-sectional areas of the piston, specimen, and wax, respectively. F_{total}, F_{spec}, and F_{wax} are the total force read from the force gauge acting on the specimen and the wax, the force acting on the

specimen, and the force acting on the wax only. V_o and l_i are the volume of the specimen, and its length at the time i. During deformation, a constant volume of the specimen has to be assumed. Normal and shear stresses were calculated using the following equations, $\sigma_n = (\sigma_1 + \sigma_3)/2 + (\sigma_1 - \sigma_3)/2 \times \cos 2\theta$, and $\sigma_s = (\sigma_1 - \sigma_3)/2 \times \sin 2\theta$, where θ is the angle measured counterclockwise from the σ_1-direction (assumed to be vertical) to the normal to the fault plane. The program calculates this angle using the dimensions EB, FD, and BD (figure 65). The longitudinal strain is the ratio of the length of the deformed to the undeformed specimen, and the dynamic coefficient of friction is calculated as the ratio of shear stress to normal stress on the fault plane.

The time when the upper platen hit the specimen has to be calculated. This can be done when the difference between the initial and final lengths of the specimen is subtracted from the final gauge displacement reading. This is the displacement of the piston when it hit the specimen. During each run, displacement, force, and time were recorded. Thus, the displacement value obtained above corresponds to the time when the upper piston hit the specimen.

The following are variables incorporated into the calculation. Figure 65 explains the meaning of the symbols AB, etc. Unless otherwise indicated all variables are in inches.

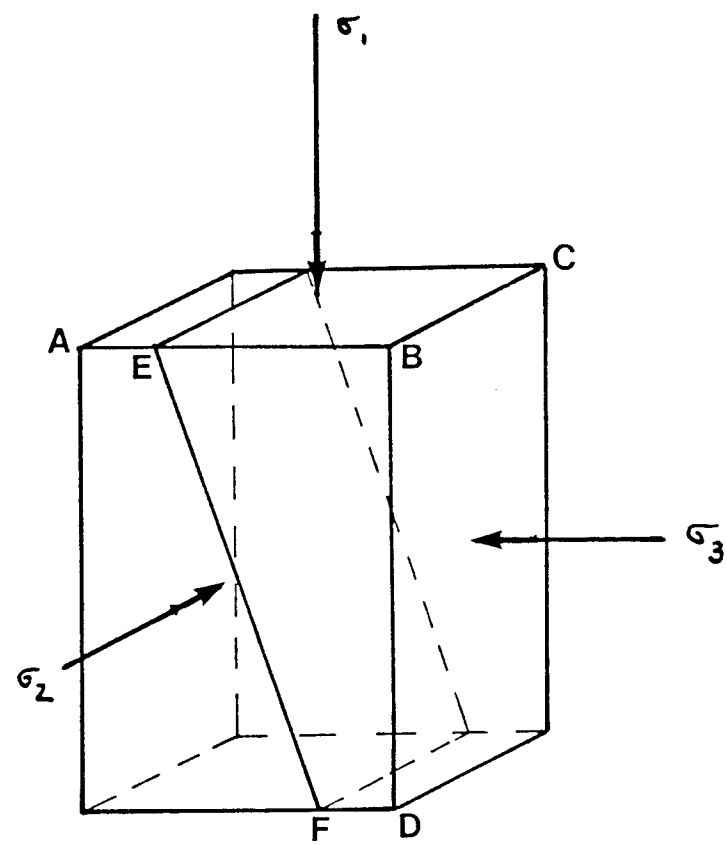

Figure 65. Sketch of sample dimensions explaining the use of the symbols for the program "Triacom".

STO 00 Time when the upper platen hit the specimen (in minutes)

STO 01 BD, the initial length of the specimen

STO 02 AB

STO 03 BC

STO 04 EB

STO 05 FD

STO 06 Final displacement from the displacement gauge

STO 07 Cross-sectional area of the piston; $(0.75"/2)^2 \times \pi$ (in square inches)

STO 08 Final length of the specimen

STO 09 28.7 (factor by which the force gauge readings have to be multiplied to convert them into pounds per square inches)

STO 10 6.895×10^{-2} (factor converting pounds per square inch into bars)

STO 11 Total force when extrusion started (in force-gauge units)

The program prompts for "Time ?", Force T ?", and "Displ. ?" referring to the time after hit (in minutes), the total force from the force-gauge (in force-gauge units), and the displacement from the displacement gauge (in inches). Based on these data, the program will calculate the stresses, strain, strain rate etc. The program is given in figure 66.

```
01*LBL "TRIACOM"
    02 RCL 02
    03 RCL 03
    04 *
    05 STO 15
    06 RCL 01
    07 FRX
    08 *
    09 STO 16
    10 RCL 07
    11 RCL 15
    12 -
    13 STO 17
    14 RCL 04
    15 RCL 05
    16 -
    17 1/X
    18 RCL 01
    19 *
    20 ATAN
    21 CHS
    22 180
    23 +
    24 STO 18
    25 RCL 11
    26 RCL 09
    27 *
    28 RCL 07
    29 /
    30 RCL 10
    31 *
    32 STO 19

    33*LBL 01
    34 "TIME "
    35 PROMPT
    36 RCL 00
    37 -
    38 STO 12
    39 RCL
 40 "FORCE I "
    41 PROMPT
    42 FRX
    43 RCL 09
    44 *
    45 STO 13
    46 FRX
 47 "DISPL "
    48 PROMPT
    49 STO 14
    50 FRX
    51 ADV
    52 RCL 06
    53 RCL 08
    54 +
    55 RCL 14
    56 -
    57 STO 20
    58 RCL 11
    59 RCL 09
    60 *
    61 STO 31
    62 CHS
    63 RCL 13
    64 +
    65 RCL 07
    66 *
    67 RCL 20
    68 *
    69 RCL 31
    70 RCL 16
    71 *
    72 +
    73 RCL 07
    74 RCL 16
    75 *
    76 /
    77 RCL 10
    78 *
    79 STO 21
 80 "SIGMA 1 ="
    81 ARCL X
    82 AVIEW
    83 RCL 19
 84 "SIGMA 2 ="
    85 ARCL X
    86 AVIEW
    87 RCL 19
 88 "SIGMA 3 ="
    89 ARCL X
    90 AVIEW
    91 RCL 21
    92 RCL 19
    93 -
    94 STO 22
 95 "DIFF STR ="
    96 ARCL X
    97 AVIEW
    98 RCL 20
    99 RCL 01
   100 /
   101 1
   102 -
   103 CHS
   104 STO 23
   105 100
   106 *
   107 STO 24
 108 "STRAIN ="
   109 ARCL X
   110 AVIEW
   111 RCL 12
   112 60
   113 *
   114 1/X
   115 RCL 23
   116 *
   117 STO 25
118 "STR RATE ="
   119 ARCL X
   120 AVIEW
   121 RCL 18
   122 2
   123 *
   124 STO 26
   125 COS
   126 RCL 22
   127 Z
   128 /
   129 STO 27
   130 *
   131 RCL 31
   132 RCL 19
   133 +
   134 2
   135 /
   136 +
   137 STO 28
   138 "SN ="
   139 ARCL X
   140 AVIEW
   141 RCL 26
   142 SIN
   143 RCL 27
   144 *
   145 STO 29
   146 "CS ="
   147 ARCL X
   148 AVIEW
   149 RCL 29
   150 "X/Q?"
   151 CHS
   152 RCL 28
   153 -
   154 STO 30
155 "FRI COEF ="
   156 ARCL X
   157 AVIEW
   158 ADV
   159 ADV
   160 GTO 01

   162 END
```

Figure 66. Program "Triacom".

6.2. Appendix B - Sample locations

Sample number	Location	Rock type
B-1	Glenmont, N.Y.	Shale
B-3	Glenmont, N.Y.	Shale
B-5	Glenmont, N.Y.	Shale
B-201	Glenmont, N.Y.	Shale
B-202	Glenmont, N.Y.	Shale
B-204	Glenmont, N.Y.	Shale
B-302	Glenmont, N.Y.	Shale
BV-1	Bear Valley Coal Mine, near Shamokin, P.A.	Coal
CPA-1	Clifton Park, N.Y.	Limestone
GT-1a	Germantown, N.Y.	Fault breccia
GT-4	Germantown, N.Y.	Fault breccia
HK-1	Hell's Kitchen, near Troy, N.Y.	Shale
L-1	Latham, N.Y.	Shale
LCR-4	Laurel Creek Reservoir, near Potter Mills, P.A.	Sandstone
SL-1	Schodack Landing, N.Y.	Shale
SR-1	Steep Rock, Ont., Canada	Fault breccia
US-1a	Untersteinach, FRG	Diabase
US-5	Untersteinach, FRG	Diabase
US-7a	Untersteinach, FRG	Diabase